Minimum-Weight Design of Symmetrically Laminated Composite Plates for Postbuckling Performance under In-plane Compression Loads

by

Dong Ku Shin

Dissertation submitted to the Faculty of the
Virginia Polytechnic Institute and State University
in partial fulfillment of the requirements for the degree of
Doctor of Philosophy
in
Engineering Mechanics

APPROVED:

Zafer Gürdal, Co-Chairman

O. Hayden Griffin, Jr., Co-Chairman

Raphael T. Haftka

Liviu Librescu

J. N. Reddy

September 10, 1990

Blacksburg, Virginia

Minimum-Weight Design of Symmetrically Laminated Composite Plates for Postbuckling Performance under In-plane Compression Loads

by

Dong Ku Shin

Committee Co-chairmen; Zafer Gürdal and O. Hayden Griffin, Jr.

Engineering Mechanics

(ABSTRACT)

A postbuckling analysis procedure for simply-supported, symmetrically laminated, rectangular, generally orthotropic plates under uniaxial compression based on a Marguerre-type energy method was developed. The analysis assumes the out-of-plane displacement to be represented by using a truncated Fourier sine series. The unknown coefficients of the displacement function were obtained from a system of nonlinear algebraic equations by using the principle of minimum potential energy. The number of terms that are to be retained in the out-of-plane displacement function to obtain an accurate response was studied and identified for a wide range of generally orthotropic plates. In the postbuckling load range, plates are also allowed to change their buckled form. The magnitudes of the total potential energy for possible different deformed shapes of a plate were compared to determine the actual deformed shape. The effect of bending-twisting coupling terms on the postbuckling behavior of anisotropic laminates was also investigated. Several postbuckling problems for isotropic, orthotropic, and anisotropic plates were considered and the results obtained by the present approach were compared with available literature results and finite element solutions to demonstrate the present analysis procedure.

The analysis procedure developed was, then, applied to minimum-weight design of laminated plates for postbuckling performance. Laminate failure load used in the postbuckling regime was calculated based on a maximum strain failure criterion. The failure criterion was demonstrated to predict the failure load reasonably well when compared with available test results. Weight comparison between the plates designed against buckling and the ones designed for the postbuckling strength was made to quantitatively evaluate the weight savings achieved for plates that are allowed to buckle. The design variables were assumed to be the layer thicknesses with specified fiber orientations and assumed to take only discrete values. A simple approach based on the penalty method was proposed to achieve the discrete-valued designs. In addition to the regular penalty terms for constraint violation, the proposed approach introduces penalty terms to reflect the requirement that the design variables take discrete values. A variable magnitude penalty term in the form of a sine function was implemented with the extended interior penalty method of the optimization package NEWSUMT-A. The proposed discrete optimization technique was applied to the classical truss and laminated composite plate design problems to demonstrate the performance of the procedure.

DEDICATION

The author wishes to dedicate this work

to his wife, Eunjean, and son, Manseop.

Acknowledgements

The author wishes to express his sincere appreciation to his co-advisors, Drs. Z. Gürdal and O. H. Griffin, Jr., for their guidance and support during the course of this efforts. He is also grateful to Drs. R. T. Haftka, L. Librescu and J. N. Reddy for their time spent serving on his advisory committee. Their standards improved this dissertation.

Most of the research reported in this dissertation was supported by Newport News Shipbuilding and Dry Dock Company at Hampton, Virginia. The support is gratefully acknowledged.

The author is sincerely grateful to his parents and his brother back in Korea for their continuous concern, encouragement and support. Their common values toward life have influenced the author in many positive ways.

The author would like to express his deepest appreciation to his wife and best friend, Eunjean, for her patience, love and the many sacrifices she has made during this endeavor, and to his son, Manseop, for making life so much more pleasant and enriched during the last three years of this work by his arrival. Without their presence, this work cannot be accomplished.

Table of Contents

List of Illustrations

List of Tables

Nomenclature

a, b	length of plate in x-, and y-directions, respectively
t	total thickness of plate
t_{ply}	ply thickness
k	number of half waves in deformed plate
Φ	stress function
u, v	in-plane displacements in x- and y-directions, respectively
w	out-of-plane displacement
w_0	initial deflection
ϕ_x	rotation about y-axis
ϕ_y	rotation about x-axis
Δ_x, Δ_y	end-shortening in x- and y-directions, respectively
$\varepsilon_x^0, \varepsilon_y^0$	mid-plane strains in x- and y-directions, respectively
γ_{xy}^0	mid-plane shearing strain in xy-plane
$\varepsilon_x, \varepsilon_y$	total strains in x- and y-directions, respectively
γ_{xy}	total shearing strain in xy-plane
Δ_x, Δ_y	end-shortening in x- and y-directions, respectively
Δ_{xcr}	critical end-shortening in x-direction
ε_{11}	strain component in fiber direction
ε_{22}	strain component in the normal to fiber direction
γ_{12}	shearing strain in principal material direction
$\varepsilon_{11}^{cu}, \varepsilon_{11}^{tu}$	ultimate compressive and tensile strains in fiber direction, respectively
$\varepsilon_{22}^{cu}, \varepsilon_{22}^{tu}$	ultimate compressive and tensile strains in the direction perpendicular to fiber direction, respectively

γ_{12}^{u}	ultimate shearing strain in principal material direction
Δ_{xcr}	critical end-shortening in x-direction
σ_x, σ_y	normal stresses in x- and y-directions, respectively
τ_{xy}	shearing stress in xy-plane
N_x, N_y	resultant in-plane forces per unit length in x- and y-directions, respectively
N_{xy}	resultant shearing force per unit length in xy-plane
$\hat{N}_x$, $\hat{N}_y$	average in-plane edge load per unit length in x- and y-directions, respectively
$\hat{N}_{xcr}$	buckling load per unit length in x-direction
$\overline{Q}_{ij}$	transformed reduced stiffnesses
A_{ij}, D_{ij}	extensional and bending stiffnesses, respectively
A^*_{ij}	components of extensional compliance matrix
$\tilde{U}$	strain energy per unit volume
$\overline{U}$	strain energy per unit area
U	strain energy of entire plate
Π	total potential energy of entire plate
W_{mn}	arbitrary parameters in the assumed deflection
W_0	amplitude of initial deflection
X	design variable vector
x_i	design variables
d_{ij}	prescribed discrete values
r	penalty multiplier for constraint violation
s	penalty multiplier for discrete values
$F(X)$	objective function
$\Phi(X, r)$	pseudo-objective function
$\Psi(X, r, s)$	modified pseudo-objective function
$g_j(X)$	constraint function

$p^*(g_j)$	penalty function for constraint violation
$\phi_d^i(X)$	penalty function for non-discrete design variables
ε_c	convergence criterion activating discrete optimization
ε_d	convergence criterion terminating discrete optimization
N_D	design load per unit length
N_f	failure load per unit length

CHAPTER I

INTRODUCTION

1.1 Motivation

In conventional aircraft and aerospace applications it has been a common practice to design plate and shell structures such as fuselage and stabilizer panels to buckle at load levels below their design ultimate load, thus exploiting the postbuckling strength of these structural components. Although advanced composites have a significant advantage over metals in specific stiffness and strength, composite structures, if designed to be buckling resistant, may be heavier than their metallic counterparts that are allowed to operate in the postbuckling load regime. While thick isotropic or composite plates under in-plane load generally fail at load levels below or in the vicinity of their buckling load, failure of thin flexible plates generally occurs far beyond the buckling load. If a plate fails far before its buckling load is achieved, potentially its weight can be reduced by reducing its thickness, thus its weight, without jeopardizing its load carrying capability. If, on the other hand, the thickness of the plate is too small, then the plate starts experiencing out-of-plane deformations upon loading. This type of deformation results in softening of the plate in the applied load direction. However, if the edges of the plate are properly supported, this softening does not cause the plate to lose its load carrying capability. Such plates are referred to have postbuckling strength. To compete on a weight-efficiency basis, therefore, thin composite panels must be designed to function under postbuckling conditions.

Designing fiber reinforced composite plates for postbuckling strength via rigorous optimization techniques, however, is a challenging problem because of the necessity to use costly nonlinear analysis which usually requires an iterative type of solution for a single analysis. To the author's knowledge, investigations on the optimum design of laminated or even isotropic plates for postbuckling strength have been very limited in the literature, although considerable effort has been made in the area of optimum design of laminated plates for buckling strength. One of the objectives of the present study is to provide guidelines for the application of employing optimization techniques when laminated plates are designed to serve in the postbuckling load regime. In particular, emphasis is placed on demonstrating the relative additional weight savings for various design loads and laminate stacking sequences, by comparing the weight of plates designed for buckling strength with those designed for postbuckling strength.

In carrying out the optimization, it is important to select an efficient postbuckling analysis procedure. Although the finite element method is a powerful tool for many structural analysis problems, nonlinear nature of the postbuckling response makes use of a finite element code undesirable due to excessive computing time required. Furthermore, it is known that the postbuckling analysis by the finite element method experiences difficulty in convergence near a bifurcation point because of sharp changes in plate response. These difficulties associated with the finite element method can be avoided if an inexpensive but reliable postbuckling analysis procedure is employed for the optimization. An effort to develop such an analysis procedure is made in the present study.

In many of the previous analytical investigations on the postbuckling behavior of laminated plates, unknown displacements and/or stress functions were assumed in the

form of series functions, such as a Fourier series. One of the important issues involved in using series functions for the unknown variables is the determination of number of terms to be retained to obtain an accurate answer. For the case of isotropic plates when, for instance, the Fourier series is used as the unknown variables, it has been shown that use of only the first few terms results in very accurate solutions. Unfortunately, no convergence study on the use of different numbers of terms is available in the literature covering a wide range of plate aspect ratios and degrees of plate orthotropy. In the present study, the Fourier sine series is used to represent the deformed plate shape, and the number of terms required to obtain an accurate solution is identified for various generally orthotropic plates.

A plate subject to in-plane compressive load beyond buckling can undergo changes in its buckled form. After buckle pattern change, the postbuckling stiffness of laminates is degraded, and ignoring mode change may result in non-conservative estimation of the load carrying capability. To obtain an accurate analysis of thin plates in a wide postbuckling range, changes in buckling mode must be taken into account. As will be discussed in the literature review, previous investigations of this phenomenon are very limited and based on an ad-hoc approach. The general notion in dealing with this phenomenon is to use an increased number of terms for the displacement series to capture the mode change in the postbuckling load regime. In the present study, a systematic approach based on energy consideration which does not necessarily require the use of many terms in displacement functions is proposed.

In the context of the present optimum design study, the design variables such as the thickness of a given ply orientation can only take discrete values since they are made up of individual layers that consist of integer multiples of a single ply thickness. Such

problems generally require the use of an integer programming algorithm. In the present study, a simple approach based on the penalty method is proposed to solve both the continuous and discrete optimization without using the costly integer programming technique after obtaining the continuous optimum.

1.2 Literature Review and Present Study

In this section, previous investigations on postbuckling analysis, buckle pattern change, optimum design of laminated plates, and optimization with discrete design variables are discussed, along with a brief introduction of the present approaches to these topics.

1.2.1 Postbuckling Analysis

It is well known that, unlike a simple column, a rectangular isotropic or anisotropic plate supported on all sides is capable of carrying considerable load beyond its buckling load. Compared to a plate designed to carry a specific design load without buckling, plates designed to buckle are more flexible and, therefore, weigh less. Because of the potential weight savings, behavior of plates beyond the critical buckling load is of great practical interest. Since von Karman [1] developed the basic differential equations for a plate undergoing large deflections, the geometrically nonlinear elastic stability analysis has usually been formulated in either of two ways.

One of the procedures, introduced by Levy [2], treats the out-of-plane displacement and stress function as independent variables. In this approach, a system of nonlinear algebraic equations for the independent variables is obtained by substitution of the assumed deflection and the stress function into the large deflection equations of von

Karman. Levy [2] assumed the deflection and stress function as a Fourier series and obtained a converged solution by retaining six terms of the series for a simply supported square plate. This approach has been used in Refs. [3-10] for investigation of the postbuckling behavior of orthotropic and anisotropic plates. Yusuff [3] studied the postbuckling behavior of square orthotropic plates with and without imperfections, and presented three resulting nonlinear algebraic equations for the coefficients of the assumed deflection. He used only the first three terms of a sine series for the out-of-plane displacement. Prabhakara and Chia [4] investigated the postbuckling behavior of a simply supported, orthotropic plate subjected to biaxial compression. They assumed the out-of-plane deflection and the stress function to be in the form of a double Fourier series and free-vibration beam functions, respectively. In their subsequent paper [5], by using a similar approach that was in Ref. [4], they presented extensive results for the postbuckling behavior of clamped and simply supported, unsymmetrically laminated, angle-ply plates and clamped, unsymmetrically laminated, cross-ply plates. They reported that the converged solution is obtained by using as many as nine terms for the assumed deflection and stress function. Another investigation on the large deflection of an orthotropic plate subjected to the combined action of edge compression and out-of-plane load was performed by the same authors in Ref. [6], where the solution is obtained in the form of the first nine terms of free-vibration beam functions for both transverse deflection and stress function.

Chandra [7] presented an approximate solution for a simply supported, unsymmetric cross-ply plate by assuming the deflection as a single term sine function. Harris [8] investigated the initial postbuckling behavior of angle-ply laminates by assuming a simple sine form of deflection and stress function. The emphasis in his investigation was focused on the stiffness of laminates before and after the critical buckling load. Zhang

and Matthews [9] investigated postbuckling of simply-supported, symmetrically laminated plates under pure shear, and combined compressive and shear loading. The out-of-plane displacement and stress function were assumed as Fourier sine series and free-vibration beam functions, respectively. In their subsequent paper [10], the postbuckling behavior of flat and curved panels of unsymmetrically laminated composite materials under in-plane shear and compression is presented by a method similar to that of Ref. [10].

The other conventional approach is based on the principle of virtual work or the energy method, in which the in-plane and out-of-plane displacements are assumed to be independent variables. Marguerre [11] and Timoshenko [12] applied an energy method in their studies of postbuckling analysis of isotropic plates. Using the Marguerre-type energy method, Banks [13] obtained an approximate solution for the postbuckling behavior of orthotropic panels, simply supported on the loaded edges and elastically restrained on the unloaded edges. He assumed the out-of-plane displacement as a one-term sinusoidal function in the loading direction. An analysis procedure developed for use in the design of symmetric stiffened laminated plates subjected to biaxial compression and shear was presented by Dickson *et al.* [14]. They used the in-plane and out-of-plane displacements developed by Koiter [15] for long isotropic plates. Feng [16] investigated the postbuckling behavior of a laminated anisotropic plate subject to biaxial compression and shear loads with simply supported, fixed, or mixed boundary conditions. Both the out-of-plane displacements for simply supported boundary conditions and the in-plane displacements for all boundary conditions are expressed as a double trigonometric series, while the out-of-plane displacements for fixed boundary conditions are assumed to be free-vibration beam functions. In Ref. [17], Stein studied the postbuckling response of simply supported and clamped, long rectangular

orthotropic plates covering a wide range of plate dimensions and material properties. By assuming unknown displacements to be in the form of trigonometric functions in the loading direction, he derived a system of ordinary nonlinear differential equations to replace the partial differential equations of plate theory based on the principle of virtual work. Stein, in Ref. [18], presented the postbuckling behavior of long orthotropic plates in combined shear and compression by a method similar to the one used in Ref. [17]. The coefficients for the assumed displacements are determined by the Ritz method (Refs. [11-14, 16]) or by solving the nonlinear equations derived from the principle of virtual work (Refs. [17,18]). In general, for all the analysis procedures where a series is used for the independent variables the degree of accuracy in the postbuckling solution depends upon the number of terms used in the series.

In the present study, the general approach is essentially the one proposed by Marguerre [11] for isotropic plates. In Ref. [11], by using only the first three terms of the Fourier series for the out-of-plane displacement, Marguerre obtained a solution which was later proven to be in excellent agreement with Levy's converged solution [2] for an isotropic square plate. While most investigators who used the principle of virtual work [12,14,16-18] assumed both the in-plane and out-of-plane displacements to be independent variables, Marguerre, in Ref. [11], treated only the out-of-plane displacement as the independent variable. He then obtained an expression for the stress function from the compatibility equation of von Karman. By writing the potential energy of the buckled plate in terms of the assumed out-of-plane displacement and the stress function, a system of nonlinear algebraic equations for the unknown coefficients in the deflection was obtained from the principle of minimum potential energy. Marguerre's energy method eliminates some possible sources of error by excluding the assumption on the in-plane displacements, which can lead to error due to the inevitable

arbitrariness of these variables. Moreover, exclusion of the coefficients of the in-plane displacements from the set of unknown variables results in a smaller system of nonlinear equations that needs to be solved. In the present study, the Marguerre-type energy method is extended to specially orthotropic plates. A Fourier sine series is used as the assumed form of deflection to represent the shape beyond the buckling load. The convergence of postbuckling solutions for orthotropic and angle-ply laminates is examined by using different numbers of sine terms in the assumed out-of-plane displacement series.

The basic assumptions and restrictions of the present study for the postbuckling analysis of a composite plate are,

1) The plate is initially perfectly flat without imperfections.
2) The plate is simply supported at all four sides.
3) The in-plane normal displacements are constant along the plate edges.
4) All four edges are free of shear stresses.
5) The plate is thin relative to its length and width, and transverse shear is ignored.
6) The laminate is symmetric, so bending-extensional coupling does not exist.
7) The plate behaves elastically during the entire range of loading.
8) The extension-twisting coupling terms, A_{16} and A_{26}, are ignored, and the laminate is specially orthotropic or can be considered as specially orthotropic (D_{16} and $D_{26} \ll D_{66}$).

1.2.2 Buckle Pattern Change

Another aspect of the present work is the study of the change of postbuckling mode shape from the initial postbuckling shape, as the plate is loaded deeper into the postbuckling regime. The phenomenon of buckle pattern change for thin plates in the

postbuckling load regime is often encountered in experiments [19-24]. In the usual postbuckling analysis, however, the buckled form of plates is generally assumed to remain unchanged, and little effort has been made on investigation of the phenomenon of buckle pattern change. Thus, there is a need to develop a systematic approach to account for this phenomenon. An early discussion of the phenomenon of buckle pattern change was presented by Stein [25] for a three-bar-column model subjected to axial compressive load. In his subsequent paper [21], he considered buckle pattern change for postbuckling analysis of isotropic plates with various aspect ratios. He obtained the load end-shortening curves for successive modes of postbuckling deformation and superposed them. The broken continuous curve that forms the lower bound envelope is then assumed to be load end-shortening curve for the panel and the actual buckled shape is taken to be the one which corresponds to a certain section of that curve. Other investigations, as in Refs. [17, 26-27], where the mode changes of plates are allowed during compressive loading, used the procedure proposed by Stein. In the most recent version of the STAGS [28] computer code, referred to as STAGS-TP, the capability to account for the change in buckle pattern during postbuckling response is included, as indicated in Refs. [20, 29].

The proposed approach is different from the previous investigations in the sense that the energy state is examined for several successive mode shapes of a plate, which were analyzed simultaneously. The magnitudes of the total potential energy are compared for the possible modes, and the mode which has the minimum value of the total potential energy is assumed to represent the actual buckled shape. The effects of panel aspect ratio, laminate stacking sequence, and fiber orientation as well as in-plane boundary conditions on the mode shifting phenomenon are discussed.

1.2.3 Optimum Design of Laminated Plates

The freedom to tailor the stiffness and strength of laminated fiber-reinforced composites has stimulated interest in optimization procedures for the design of efficient laminated composite plates for many applications. The minimum weight design of laminated plates has been reported in Refs. [30-39], where the thicknesses of individual layers with pre-assigned fiber orientations and/or fiber orientations are treated as design variables. Schmit and Farshi [30] presented a method for minimum weight design of symmetric laminates subject to multiple in-plane loading conditions with strength and stiffness constraints. The maximum strain failure criterion was used to evaluate the strength requirement, and minimization was carried out by the method of inscribed hyperspheres, in which only critical and near-critical constraints are considered at each stage of optimization. Using a procedure similar to the one presented in Ref. [30], Schmit and Farshi added a constraint on the buckling load in their subsequent paper [31]. Khot *et al.*, in Ref. [32], considered minimum weight design of plate elements under in-plane and/or out-of-plane loading conditions with strength and displacement constraints. The constraint on the strength of laminates was calculated based on the Tsai-Hill failure criterion.

Minimum-mass design of composite wings with constraints on buckling, strength, and displacement was investigated by Starnes and Haftka in Ref. [33]. Wing segments were analyzed by the finite element method, and SUMT technique in conjunction with constraint approximations was used for optimization. Rao and Singh [34], using the SUMT technique, presented minimum-weight design of cross-ply laminates with constraints on natural frequency, buckling load, and displacement. Calculation of the constraints was based on analytical expressions derived from generally orthotropic

plate theory. Stroud and Anderson in Ref. [35] presented a computer program, denoted PASCO, for analyzing and sizing uniaxially stiffened composite panels under various in-plane and out-of-plane loading conditions as well as temperature loadings. PASCO is capable of including such design requirements as buckling, material strength, stiffness, and vibration frequency during the optimization process, and the thicknesses of individual layers and their orientation can be used as design variables as well as the dimensions of the plate segments that made up of the stiffened panel. PASCO uses a mathematical programming algorithm based on the method of feasible directions algorithm CONMIN [40] for optimization.

Maximization of eigenvalues that correspond to either buckling load or natural frequency of laminated plates has been studied in Refs. [41-46]. Fiber angles [41-44] or layer thicknesses [45,46] were treated as design variables. Hirano [41,42] used Powell's conjugate direction technique [47] for optimization, and simple formulas for the buckling analysis of plates under axial compression [41] or pure shear [42]. Any other behavioral constraints were not imposed in his studies. Shin *et al.*, in Ref. [45], using a homotopy method [48], investigated maximization of the buckling load for plates under uniaxial compression. While keeping the total thickness of laminates constant, they treated the relative thicknesses of layers as design variables. Buckling analysis was performed by using a finite element method. The maximization of the fundamental frequency of simply supported and clamped laminated plates without constraints was studied by Bert in Refs. [43] and [44], respectively. Mesquita and Kamat [46] studied the maximization of fundamental frequencies of stiffened laminated plates subject to frequency separation constraints and an upper bound on weight. In their study, the design variables were the number of plies and stiffener areas, which are integer and continuous variables, respectively. By taking the fiber

directions as design variables, Chao *et al.* [49] combined the buckling and failure load as an objective function. The buckling load was calculated by the Ritz method, and the Tsai-Hill criterion was used to monitor the stress state of a plate under in-plane load. Tauchert and Adibhatla considered maximum stiffness [50] and maximum bending strength [51] designs for plates subject to out-of-plane loads. The design variables were assumed to be fiber angles and/or layer thicknesses.

In an attempt to incorporate postbuckling analysis into a design cycle, Dickson and Biggers developed a minimum-weight design computer program, POSTOP [52], intended for the preliminary design of metal or composite panels with open-section stiffeners subjected to combined biaxial compression, shear and normal pressure loading. The postbuckling analysis of the skin portion of a panel is based on the shear field theory developed by Koiter [15]. The unknown parameters involved in the out-of-plane displacement is obtained by applying the Rayleigh-Ritz method. Sizing is performed by CONMIN [40] optimization program. The maximum strain or Tsai-Hill failure criterion is used to monitor the failure of the skin portion of a panel. The design study based on numerical examples, however, is not included in Ref. [52].

The analytical basis of all these previous efforts, except the last one mentioned above, for optimum design of laminated plates was the linear plate theory which allows only small deformations of a plate. In the case of plates under in-plane loads where strength constraints based on Tsai-Hill or maximum strain failure criterion are considered, the required stresses and strains are calculated from the basic force-deformation relations of classical lamination theory by decoupling membrane and bending behavior. If a plate is under in-plane tensile load or it is thick relative to its width, linear plate theory can be applied for the calculation of strength

requirements since bending action of the plate does not exist or is negligibly small. A thin plate subject to an in-plane compressive load beyond buckling, however, can sustain a load level several times higher than its buckling load without failure, and is concurrently subjected to a large bending action. To take full advantage of this additional load-carrying capability, it is desirable to design such a thin plate to serve in the postbuckling load range. Because of large deformations in thin plates, the geometrically nonlinear plate theory must be applied in the analysis. To the author's knowledge, investigations on the optimum design of composite plates subjected to postbuckling load are not available in the literature except the work by Dickson and Biggers in Ref. [52]. In the present study, minimum-weight design of laminated thin plates which fail at the load level beyond their buckling load is investigated. In addition, minimum weight design of laminates with buckling constraints is considered. The weight of a plate designed for the postbuckling strength is compared with that of buckling strength design to demonstrate the weight savings. The failure load of laminates in the postbuckling regime is calculated by using the maximum strain failure criterion. Previously, this criterion was successfully used in predicting the failure load of graphite-epoxy plates under postbuckling load by Arnold *et al.* in Ref. [53]. To further justify the use of this criterion, the failure load of various graphite-epoxy plates under postbuckling load is compared with available test results by Starnes *et al.* [54].

1.2.4 Optimization with Discrete Design Variables

The design variables used in the present study are the thicknesses of plies with pre-selected fiber orientations. In the context of the optimum laminated plate design, such design variables can only take discrete values since plies with different orientations are essentially made up of integer multiples of a single layer of

pre-impregnated tape. The use of design variables that accept only discrete values appear in other optimization problems. For many practical applications, the designer must choose the design variables from a list of commonly available values. The design variables such as cross-sectional areas of trusses, thicknesses of plates and membranes also fall into this category. However, most available optimization techniques have been developed under the implicit assumption that the design variables are continuous-valued. The most common way of achieving a design with discrete-valued design variables is to round-off the optimum values of the design variables, obtained by assuming them to be continuous variables, to the nearest acceptable discrete value. Although the idea is simple, for problems with a large number of design variables selection of the discrete values without violating the design constraints can pose serious difficulties. More systematic approaches such as a Branch and Bound method and a Lagrangian relaxation method are proposed in the research environment.

The main framework for Branch and Bound (B & B) method was introduced by Land and Doig [55] to solve integer linear programming (ILP) problems. The Branch and Bound method forms new subproblems, called candidates, after obtaining the continuous optimum. These candidates exclude the infeasible (non-discrete) regions by branching, and bounds are used to rapidly discard many of the possible candidates, due to the convexity of the problem, without analyzing them. Reinschmidt [56] used the B & B method for plastic design of frames by posing the problem as an ILP problem. Garfinkel and Nemhauser [57] extended this method to the minimization of convex nonlinear problems. John *et al.* [58] merged the Branch and Bound algorithm with sequential linear programming (SLP) for the discrete optimal design of trusses. Mesquita and Kamat [46] employed some efficiency measures to improve Darkin's Branch and Bound algorithm [59] in solving a nonlinear mixed integer programming

(NMIP) problem. Olsen and Vanderplaats [60] proposed a method, denoted Sequential Linear Discrete Programming (SLDP), which is essentially an extension of the Sequential Linear Programming (SLP) method. The solution in Ref. [60] is found by using two different software packages, one for continuous optimization and the other for integer programming. Use of two different packages, however, can be inconvenient for the practicing engineer. Also, integer programming problems are difficult to handle.

Schmit and Fluery [61] proposed a method in which the original structural optimization problem is replaced by a sequence of convex and separable approximate subproblems. Each subproblem was solved using Lagrange relaxation, and the dual function was maximized using a subgradient method. The subproblem is convex in the continuous sense. When discrete variables are introduced, however, the problem is no longer convex and there is no guarantee that the dual methods will yield the globally optimum solution to the discrete problem. Sizing type problems with discrete variables are solved successfully by this method. The efficiency of the dynamic round-off, Branch and Bound, and Lagrangian relaxation method for various discrete optimization problems is investigated by Ringertz [62].

The present study introduces a simple approach to minimization problems with discrete design variables by modifying the penalty function approach of converting the constrained problems into sequential unconstrained minimization technique (SUMT) problems [63]. In general, the penalty approach is used for converting a constrained optimization problem into a sequence of unconstrained problems. The objective function for the unconstrained problem at each step of the sequential optimization includes terms that introduce penalty depending on the degree of constraint violation.

In addition to the penalty terms for constraint violation, the proposed approach introduces penalty terms to reflect the requirement that the design variables take discrete values. A variable magnitude penalty term in the form of a sine function is introduced and implemented with the extended interior penalty method of the optimization package NEWSUMT-A [64]. The present approach is applied to classical truss and laminated composite plate design problems to demonstrate the performance of the procedure.

1.2.5 Present Design Study

In the present study, minimum-weight design of simply-supported, symmetrically laminated, thin, rectangular, generally orthotropic plates for buckling and postbuckling strength is investigated. The postbuckling analysis is based on a Marguerre-type energy method extended to generally orthotropic plates with a special consideration of the mode change in the postbuckling load regime. The failure load of laminates is calculated by the maximum strain failure criterion based on the in-plane strains. Design variables are individual layer thicknesses with specified fiber orientations and assumed to take only discrete values corresponding to multiples of the lamina thickness. The proposed optimization technique is applied to the design of rectangular laminates made up of 0, ± 45, 90 degree laminae with various aspect ratios.

Formulation of the postbuckling analysis of laminated plates based on the modified Marguerre solution is presented in Chapter II. Results of postbuckling response of generally orthotropic plates are presented to demonstrate the analysis procedure. The phenomenon of buckle pattern change is discussed in Chapter III. The procedure

developed for the implementation of the buckle pattern change is proposed. The failure criterion used for the determination of postbuckling strength is introduced in Chapter IV. The validation of the failure criterion is demonstrated by comparing predicted strengths with experimentally determined ones. The procedure developed for discrete valued optimization is presented in Chapter V. The optimization with discrete valued design is achieved by introducing additional penalty terms, in the form of a sine function, to the regular pseudo-objective function of sequential unconstrained minimization technique (SUMT). In Chapter VI, the formulation and implementation of minimum-weight plate design problems are presented. Also included in Chapter VI is the design study of square and long rectangular quasi-isotropic laminates for postbuckling performance. Based on the results presented, conclusion of the present study is drawn in Chapter VII.

CHAPTER II

FORMULATION FOR POSTBUCKLING ANALYSIS OF LAMINATED PLATES

2.1 Assumption of Out-of-plane Displacement

The large deflection equations governing the postbuckling behavior of orthotropic plates are an extension of the well-known von Karman equations for thin isotropic plates of uniform thickness. The development of these equations is given by Timoshenko [12], and the extension for orthotropic analysis by Lekhnitskii [65]. Ignoring anisotropic extension-shearing terms (A^*_{16} and A^*_{26}), the compatibility equation can be expressed as

$$A^*_{22}\Phi_{,xxxx} + (2A^*_{12} + A^*_{66})\Phi_{,xxyy} + A^*_{11}\Phi_{,yyyy} = w_{,xy}{}^2 - w_{,xx}w_{,yy} \tag{2.1}$$

where A_{ij}* are the components of the extensional compliance matrix, and the stress function, Φ, is related to the mid-plane stress resultants per unit length by

$$N_x = \Phi_{,yy} \quad , \quad N_y = \Phi_{,xx} \quad , \quad N_{xy} = -\Phi_{,xy} \tag{2.2}$$

such that the in-plane equilibrium equations are automatically satisfied.

An important step in the Rayleigh-Ritz energy method is the selection of the assumed deformed shape. For a simply supported rectangular panel with the coordinate convention shown in Fig. (1), the out-of-plane displacement, w, is assumed to be

$$w = \sum_{m=1,3,..}^{\infty} \sum_{n=1,3,..}^{\infty} W_{mn} \sin\frac{k(m\pi x)}{a} \sin\frac{n\pi y}{b} \tag{2.3}$$

where the integer, k, represents the number of half waves in the loading direction corresponding to the buckling mode obtained from the linear buckling analysis. Since it was observed in an extensive numerical study on the selection of the out-of-plane displacement that the critical mode of a plate is always obtained to be in the form of a single half wave in the y-direction, regardless of plate aspect ratios or laminate stacking sequences, the deflection function (2.3) includes only the odd number of terms in the y-direction. Thus the first term in the series expansion of the assumed deflection always represents the buckling mode of a given plate. If the critical mode of the plate is represented by (k) half waves in the loading direction, extensive numerical study indicated that the contribution of the (k)-th half waves is most significant to the postbuckling mode shape, while there is no contribution from modes that have less than (k) half waves. By introducing the integer, k, the deformed shape in the postbuckling regime is represented as a superposition of the (k)-th mode and the modes with more than (k) half waves. If a plate in the initial postbuckling regime buckles into many half waves, this feature becomes very useful since the assumed deflection function eliminates the unnecessary terms which are associated with modes less than (k) half waves. The use of additional parameter k also makes it possible to use only the odd values of the parameter m. Depending on the values of k the value of the product $k \cdot m$ can either be even or odd. Thus, the assumed form of deflection (2.3) minimizes the number of nonlinear algebraic equations to be solved in the postbuckling analysis, and is applicable to rectangular plates of any aspect ratio that deform into any number of half sine waves.

The expression (2.3) does not fulfill the natural boundary conditions of zero bending moments along the plate sides if the bending-twisting coupling terms, D_{16} and D_{26}, exist. The Rayleigh-Ritz method, however, is an approximate procedure and requires

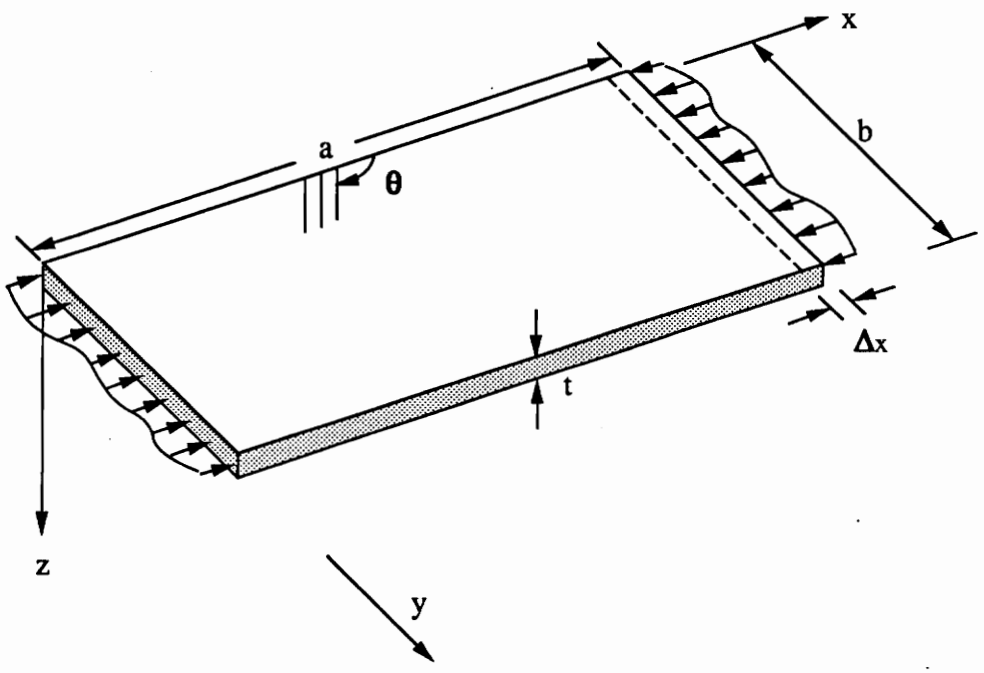

Fig. 1 Rectangular plate under uniaxial compression

that the assumed deflection satisfy only the geometrical boundary conditions. Thus, the assumed deflection can be applied to laminates for which D_{16} and D_{26} are not zero. Effects of ignoring these anisotropic terms on the accuracy of the solution for plate deflections as a function of the magnitude of D_{16} and D_{26} will be demonstrated later in the Numerical Examples section.

2.2 Derivation of Stress Function

Using the assumed deflection (2.3), the stress function for a rectangular panel can be obtained from the compatibility Eqn. (2.1). The solution of the fourth-order partial differential equation for the stress function, Φ, consists of a complementary and a particular part. Using the assumption that the edges are shear free, a complementary solution can be obtained as

$$\Phi_c = -\frac{1}{2}(\hat{N}_y x^2 + \hat{N}_x y^2) \tag{2.4}$$

where, for the time being, $\hat{N}_x$ and $\hat{N}_y$ are unknown load-dependent constants. By introducing the deflection (2.3) into the right-hand-side of the compatibility Eqn. (2.1), a particular solution can be calculated as

$$\Phi_p = \sum_{p=0,2,..}^{\infty} \sum_{q=0,2,..}^{\infty} b_{pq} \cos\frac{k(p\pi x)}{a} \cos\frac{q\pi y}{b} \tag{2.5}$$

In the above particular solution, the coefficients b_{pq} are

$$b_{pq} = \frac{\sum_{n=1}^{9} B_n}{4\left[p^4 \frac{b^2}{a^2} A^*_{22} + p^2 q^2 (2A^*_{12} + A^*_{66}) + q^4 \frac{a^2}{b^2} A^*_{11}\right]} \tag{2.6}$$

where B_n are functions of undetermined load-dependent parameters W_{mn}, and are given in Appendix A.

Then, the complete solution of Eqn. (2.1) can be written as

$$\Phi = -\frac{1}{2}(\hat{N}_y x^2 + \hat{N}_x y^2) + \sum_{p=0,2,..}^{\infty} \sum_{q=0,2,..}^{\infty} b_{pq} \cos\frac{k(p\pi x)}{a} \cos\frac{q\pi y}{b} \tag{2.7}$$

In the above expression (2.7), the load-dependent constants $\hat{N}_x$ and $\hat{N}_y$ are to be determined next.

2.3 Load End-shortening Relation

From classical lamination theory, ignoring the extension-twisting terms (A_{16} and A_{26}), the in-plane strains for symmetrically laminated plates are related to in-plane stress resultants by

$$\begin{aligned} \varepsilon_x^0 &= A^*_{11} N_x + A^*_{12} N_y \\ \varepsilon_y^0 &= A^*_{12} N_x + A^*_{22} N_y \\ \gamma_{xy}^0 &= A^*_{66} N_{xy} \end{aligned} \tag{2.8}$$

The in-plane strains can be also written in terms of mid-plane displacements from the definition of the nonlinear strain-displacement relations of von Karman as

$$\begin{aligned} \varepsilon_x^0 &= u_{,x} + \frac{1}{2} w_{,x}^2 \\ \varepsilon_y^0 &= v_{,y} + \frac{1}{2} w_{,y}^2 \\ \gamma_{xy}^0 &= u_{,y} + v_{,x} + w_{,x} w_{,y} \end{aligned} \tag{2.9}$$

Introducing the definition of the stress function (2.2) into the relations (2.8) and using the strain-displacement relations (2.9), the infinitesimal strains $u_{,x}$ and $v_{,y}$ in the x- and y-directions, respectively, can be written as

$$u_{,x} = [A^*_{11}\Phi_{,yy} + A^*_{12}\Phi_{,xx} - \frac{1}{2} w_{,x}{}^2] \tag{2.10}$$

$$v_{,y} = [A^*_{12}\Phi_{,yy} + A^*_{22}\Phi_{,xx} - \frac{1}{2} w_{,y}{}^2]$$

By integration of expression (2.10) over the length and width of the plate, the in-plane edge displacements, Δ_x and Δ_y, in the x- and y-direction can be obtained as

$$\Delta_x = -\int_0^a u_{,x}\, dx = -\int_0^a [A^*_{11}\Phi_{,yy} + A^*_{12}\Phi_{,xx} - \frac{1}{2} w_{,x}{}^2]dx \tag{2.11}$$

$$\Delta_y = -\int_0^b v_{,y}\, dy = -\int_0^b [A^*_{12}\Phi_{,yy} + A^*_{22}\Phi_{,xx} - \frac{1}{2} w_{,y}{}^2]dy$$

Substituting the assumed out-of-plane displacement, w, and the stress function, Φ, into the expressions (2.11), the edge displacements are obtained in terms of the constants, $\hat{N}_x$ and $\hat{N}_y$, and unknown parameters in the deflection, W_{mn}, as

$$\Delta_x = a\,[\,A^*_{11}\hat{N}_x + A^*_{12}\hat{N}_y + \frac{k^2\pi^2}{8a^2} \sum_{m=1,3,..}^{\infty} \sum_{n=1,3,..}^{\infty} m^2 W_{mn}^2] \tag{2.12}$$

$$\Delta_y = b\,[\,A^*_{12}\hat{N}_x + A^*_{22}\hat{N}_y + \frac{\pi^2}{8b^2} \sum_{m=1,3,..}^{\infty} \sum_{n=1,3,..}^{\infty} n^2 W_{mn}^2]$$

The above relations permit expression of the unknown constants, $\hat{N}_x$ and $\hat{N}_y$, in terms of the applied end-shortenings and unknown parameters in the deflection, as

$$\hat{N}_x = A_{11}\frac{\Delta_x}{a} + A_{12}\frac{\Delta_y}{b} - \frac{\pi^2}{8} \sum_{m=1,3,..}^{\infty} \sum_{n=1,3,..}^{\infty} [\frac{m^2k^2}{a^2} A_{11} + \frac{n^2}{b^2} A_{12}]W_{mn}^2 \tag{2.13}$$

$$\hat{N}_y = A_{12}\frac{\Delta_x}{a} + A_{22}\frac{\Delta_y}{b} - \frac{\pi^2}{8} \sum_{m=1,3,..}^{\infty} \sum_{n=1,3,..}^{\infty} [\frac{m^2k^2}{a^2} A_{12} + \frac{n^2}{b^2} A_{22}]W_{mn}^2$$

The physical meaning of the constants $\hat{N}_x$ and $\hat{N}_y$ can be explained by integrating the in-plane normal loads along the sides, i.e.,

$$\frac{1}{b}\int_0^b N_x dy = \frac{1}{b}\int_0^b \Phi_{,yy} dy = -\hat{N}_x \tag{2.14}$$

$$\frac{1}{a}\int_0^a N_y dx = \frac{1}{a}\int_0^a \Phi_{,xx} dx = -\hat{N}_y$$

It can be deduced from the above expressions that the constants, $\hat{N}_x$ and $\hat{N}_y$, are the average in-plane loads along the edges, acting in the x- and y-direction, respectively, corresponding to end-shortening Δ_x and Δ_y. Thus, the expression (2.13) represents the load versus end-shortening relationship where W_{mn} 's are load dependent unknown displacement parameters.

2.4 Derivation of Total Potential Energy

The next step in Marguerre's energy method is to determine the load-dependent unknown parameters W_{mn} in the expression of the out-of-plane displacement. Derivation of the nonlinear system of equations for the calculation of these parameters is based on the principle of minimum potential energy.

The strain energy per unit volume, $\tilde{U}$, for the k-th layer can be written as

$$\tilde{U}^{(k)} = \frac{1}{2}\left[\sigma_x \varepsilon_x + \sigma_y \varepsilon_y + \tau_{xy}\gamma_{xy}\right]^{(k)} \tag{2.15}$$

From the plane-stress constitutive relations, the stresses in the k-th layer can be expressed as

$$\begin{Bmatrix} \sigma_x \\ \sigma_y \\ \tau_{xy} \end{Bmatrix}^{(k)} = \begin{bmatrix} \overline{Q}_{11} \overline{Q}_{12} \overline{Q}_{16} \\ \overline{Q}_{12} \overline{Q}_{22} \overline{Q}_{26} \\ \overline{Q}_{16} \overline{Q}_{26} \overline{Q}_{66} \end{bmatrix}^{(k)} \begin{Bmatrix} \varepsilon_x \\ \varepsilon_y \\ \gamma_{xy} \end{Bmatrix}^{(k)} \tag{2.16}$$

where the $\overline{Q}_{ij}$'s are the transformed reduced stiffnesses given in Ref. [66]. Substituting the stress-strain relations (2.16) into the strain energy (2.15), another form of the strain energy can be obtained as

$$\tilde{U}^{(k)} = \frac{1}{2} [\overline{Q}_{11} \varepsilon_x^2 + 2\overline{Q}_{12} \varepsilon_x \varepsilon_y + \overline{Q}_{22} \varepsilon_y^2 + 2(\overline{Q}_{16} \gamma_{xy} \varepsilon_x + \overline{Q}_{26} \gamma_{xy} \varepsilon_y) + \overline{Q}_{66} \gamma_{xy}^2]^{(k)} \tag{2.17}$$

Under the Kirchhoff assumption, the strain components can be written in terms of the mid-plane strains and curvatures as

$$\begin{Bmatrix} \varepsilon_x \\ \varepsilon_y \\ \gamma_{xy} \end{Bmatrix} = \begin{Bmatrix} \varepsilon_x^0 \\ \varepsilon_y^0 \\ \gamma_{xy}^0 \end{Bmatrix} + z \begin{Bmatrix} \kappa_x \\ \kappa_y \\ \kappa_{xy} \end{Bmatrix} \tag{2.18}$$

where $\kappa_x = -w_{,xx}$, $\kappa_y = -w_{,yy}$, and $\kappa_{xy} = -2w_{,xy}$.

By substituting the relations (2.18) into the expression (2.17) and integrating through the thickness, the strain energy per unit area, $\overline{U}$, can be obtained as

$$\overline{U} = \frac{1}{2} \sum_{k=1}^{n} \int_{-t/2}^{t/2} \tilde{U}^{(k)} dz \tag{2.19}$$

or

$$\begin{aligned} \overline{U} = \frac{1}{2} \sum_{k=1}^{n} \int_{-t/2}^{t/2} \{ & \overline{Q}_{11}^{(k)} (\varepsilon_x^0 - z w_{,xx})^2 + 2\overline{Q}_{12}^{(k)} (\varepsilon_x^0 - z w_{,xx})(\varepsilon_y^0 - z w_{,yy}) + \overline{Q}_{22}^{(k)} (\varepsilon_y^0 - z w_{,yy})^2 \\ & + \overline{Q}_{66}^{(k)} (\gamma_{xy}^0 - 2z w_{,xy})^2 + 2[\overline{Q}_{16}^{(k)} (\varepsilon_x^0 - z w_{,xx}) + \overline{Q}_{26}^{(k)} (\varepsilon_y^0 - z w_{,yy})](\gamma_{xy}^0 - 2z w_{,xy}) \} dz \end{aligned} \tag{2.20}$$

where n is number of layers and t is total plate thickness. If the definitions of the extensional stiffnesses, A_{ij}, and bending stiffnesses, D_{ij}, in classical lamination theory are introduced, the strain energy (2.20) per unit area for symmetric laminates can be expressed as

$$\overline{U} = \frac{1}{2}[A_{11}(\varepsilon_x^0)^2 + 2A_{12}\varepsilon_x^0\varepsilon_y^0 + A_{22}(\varepsilon_y^0)^2 + A_{66}(\gamma_{xy}^0)^2] \tag{2.21}$$

$$+\frac{1}{2}[D_{11}w_{,xx}{}^2 + 2D_{12}w_{,xx}w_{,yy} + D_{22}w_{,yy}{}^2 + 4D_{16}w_{,xx}w_{,xy} + 4D_{26}w_{,yy}w_{,xy} + 4D_{66}w_{,xy}{}^2]$$

If the definition for the stress function (2.2) is substituted in the mid-plane strains (2.8), the strain energy for the entire plate, U, can be finally expressed, in terms of the stress function and out-of-plane displacement, as

$$U = \frac{1}{2}\int_0^a\int_0^b [\,(A^*_{11}\Phi_{,yy}{}^2 + 2A^*_{12}\Phi_{,xx}\Phi_{,yy} + A^*_{22}\Phi_{,xx}{}^2 + A^*_{66}\Phi_{,xy}{}^2) \tag{2.22}$$

$$+ (D_{11}w_{,xx}{}^2 + 2D_{12}w_{,xx}w_{,yy} + D_{22}w_{,yy}{}^2 + 4D_{16}w_{,xx}w_{,xy} + 4D_{26}w_{,yy}w_{,xy} + 4D_{66}w_{,xy}{}^2)\,]dxdy$$

The unknown coefficients in the assumed deflection can be determined from the principle of minimum potential energy. The total potential energy consists of the strain energy due to bending and stretching and the work done by the external forces. In the present study, the sides of the plate are assumed to be uniformly displaced to specified levels (displacement controlled). Consequently, the external forces contribute no work on the sides since the first variation of the predetermined displacement along the loaded sides is zero. Therefore, the total potential energy, Π, reduces to the strain energy itself, i.e.,

$$\Pi = U \tag{2.23}$$

By substituting the stress function Φ of expression (2.7) and assumed out-of-plane displacement w (2.3) into the expression (2.22) and performing the integration on the entire surface of the plate, the total potential energy can be obtained as a function of the average in-plane load and unknown parameters W_{mn} as

$$\Pi = \frac{ab}{2}\,[\,A^*_{11}\hat{N}_x^{\,2} + 2A^*_{12}\hat{N}_x\hat{N}_y + A^*_{22}\hat{N}_y^{\,2}\,] + \frac{\pi^4 ab}{8}\,\{[\,\frac{k^4 D_{11}}{a^4}\sum_{m=1,3,..}^{\infty}\sum_{n=1,3,..}^{\infty} m^4 W_{mn}^2$$

$$+ \frac{2k^2(D_{12}+2D_{66})}{a^2b^2}\sum_{m=1,3,..}^{\infty}\sum_{n=1,3,..}^{\infty} m^2n^2W_{mn}^2 + \frac{D_{22}}{b^4}\sum_{m=1,3,..}^{\infty}\sum_{n=1,3,..}^{\infty} n^4 W_{mn}^2\,] \qquad (2.24)$$

$$+ [\,\frac{A^*_{11}}{b^4}(2\sum_{q=2,4,..}^{\infty} q^4 b_{0q}^2 + \sum_{p=2,4,..}^{\infty}\sum_{q=2,4,..}^{\infty} q^4 b_{pq}^2) + \frac{k^2(2A^*_{12}+A^*_{66})}{a^2b^2}\sum_{p=2,4,..}^{\infty}\sum_{q=2,4,..}^{\infty} p^2q^2b_{pq}^2$$

$$+ \frac{k^4 A^*_{22}}{a^4}(2\sum_{p=2,4,..}^{\infty} p^4 b_{p0}^2 + \sum_{p=2,4,..}^{\infty}\sum_{q=2,4,..}^{\infty} p^4 b_{pq}^2)\,]\,\}$$

The above expression for the total potential energy does not include the bending-twisting coupling terms, D_{16} and D_{26}, although they are taken into account in the expression (2.22). These terms vanish during the integration due to the assumed form of the deflection (2.3). Due to the vanishing of the coupling terms, the present approach yields approximate solutions if the bending-twisting coupling terms exist, with the accuracy depending upon the magnitude of the coupling terms.

The total potential energy can also be expressed in terms of the applied end-shortenings and unknown parameters W_{mn}, if the load end-shortening relation (2.13) is introduced

$$\Pi = \Pi(\Delta_x, \Delta_y, W_{mn}) \qquad (2.25)$$

In the present study, the in-plane displacement, Δ_x, is applied along the sides of the plate as shown in Fig. (1).

2.5 Boundary Conditions along Y-normal Edges

So far, the boundary conditions on the y-normal edges of the plate have not been defined. In the present study, two boundary conditions of practical importance are considered for y-normal edges, namely, freely shifting straight and restrained edges. The former case resembles the skin section of a stiffened plate which is allowed to expand in a direction transverse to the applied load direction as shown in Fig. 2-(a). The presence of stiffeners provide enough in-plane stiffness such that the edges of the skin remain as straight lines, but allowed to move in the transverse direction. The latter case, on the other hand, resembles a panel in Fig. 2-(b) for which the longitudinal edges can not move in the plane of the plate, so that edges of the skin are also restrained against in-plane movement.

Case (a) Buckled plate with y-normal straight edges free to move in its plane

The average load, $\hat{N}_y$, is zero at these edges, i.e., $\hat{N}_y = 0$ along $y=0$ and $y=b$. The end-shortening in the y-direction can be expressed in terms of that in the x-direction, from the second of the Eqn. (2.14), as

$$\Delta_y = \frac{\pi^2 b}{8A_{22}} \sum_{m=1,3,..}^{\infty} \sum_{n=1,3,..}^{\infty} \left[\frac{m^2 k^2}{a^2} A^*_{12} + \frac{n^2}{b^2} A^*_{22} \right] W_{mn}^2 - \frac{bA_{12}}{aA_{22}} \Delta_x \qquad (2.26)$$

If the above expression is introduced into the expression (2.25), the total potential energy can be written as a function of the applied end-shortening in the x-direction and unknown parameters W_{mn} as

$$\Pi = \Pi(\Delta_x, W_{mn}) \qquad (2.27)$$

The average load can also be expressed as a function of Δ_x from Eqn. (2.13) as

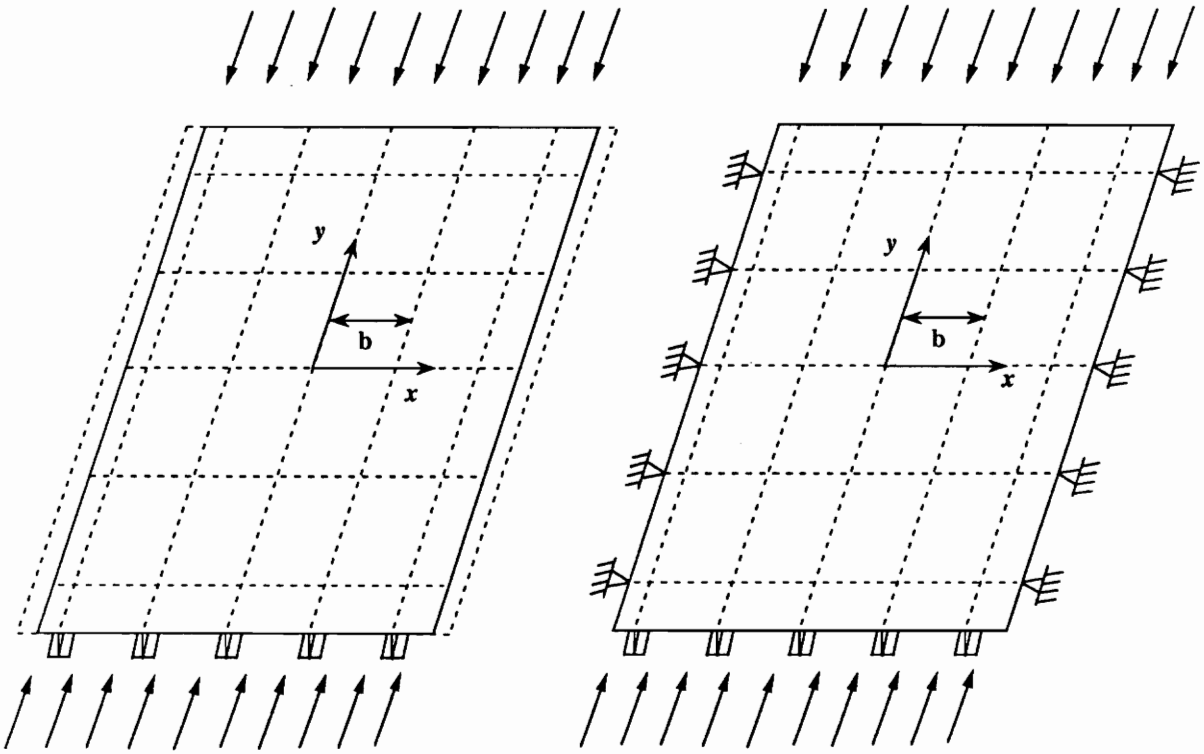

(a) Freely shifting sides
($\hat{N}y = 0$)

(b) Restrained sides
($\Delta y = 0$)

Fig. 2 Boundary conditions along y-normal edges

$$\hat{N}_x = \frac{\Delta_x}{aA^*_{11}} - \frac{k^2\pi^2}{8A^*_{11}a^2} \sum_{m=1,3,..}^{\infty} \sum_{n=1,3,..}^{\infty} m^2 W_{mn}^2 \tag{2.28}$$

Case (b) Buckled plate with y-normal edges restrained

In this case, the lateral expansion in the y-direction is prevented, i.e., $\Delta_y = 0$ along $y=0$ and $y=b$. From the Eqn. (2.13), the average loads in the x- and y-direction can be written as

$$\hat{N}_x = \frac{A_{11}}{a}\Delta_x - \frac{\pi^2}{8} \sum_{m=1,3,..}^{\infty} \sum_{n=1,3,..}^{\infty} [\frac{m^2k^2}{a^2} A^*_{11} + \frac{n^2}{b^2} A^*_{12}] W_{mn}^2 \tag{2.29}$$

$$\hat{N}_y = \frac{A_{12}}{a}\Delta_x - \frac{\pi^2}{8} \sum_{m=1,3,..}^{\infty} \sum_{n=1,3,..}^{\infty} [\frac{m^2k^2}{a^2} A^*_{12} + \frac{n^2}{b^2} A^*_{22}] W_{mn}^2$$

Substituting the above in-plane loads (2.29) into the expression (2.24), the total potential energy can be written as a function of the applied end-shortening in the x-direction and unknown parameters W_{mn} similar to the expression (2.27).

2.6 Nonlinear Algebraic Equations

For the two boundary conditions under consideration, the unknowns are reduced to the out-of-plane displacement parameters, W_{mn}, for an applied end-shortening, Δ_x. Finally, a system of nonlinear equations for the unknown parameters can be obtained from the principle of minimum potential energy as

$$\frac{\partial \Pi(\Delta_x, W_{mn})}{\partial W_{ij}} = 0 \tag{2.30}$$

The number of resulting nonlinear algebraic equations represented by Eqns. (2.30) is equal to the number of terms used for the out-of-plane displacement (2.3). The above equations (2.30) are solved by using the IMSL Subroutine DNEQNJ [67] which employs the Levenberg-Marquardt algorithm [68]. The subroutine DNEQNJ requires user-supplied first derivatives of Eqn. (2.30) with respect to the unknown parameters W_{ij} in addition to the Eqn. (2.30).

2.7 Buckling Load and Strain

Since the buckling mode is always represented as the first term of the assumed deflection (2.3), the linear critical load and end-shortening can be also determined by retaining only the linear terms in the first of the Eqn. (2.30),

$$\frac{\partial \Pi(\Delta_x, W_{mn})}{\partial W_{11}} = 0 \tag{2.31}$$

The linear critical load and end-shortening are found to be, for freely shifting y-normal edges,

$$\hat{N}_{xcr} = \pi^2 a^2 \left[k^2 \frac{D_{11}}{a^4} + \frac{2(D_{12} + 2D_{66})}{a^2 b^2} + \frac{1}{k^2} \frac{D_{22}}{b^4} \right] , \quad \Delta_{xcr} = a A^*_{11} \hat{N}_{xcr} \tag{2.32}$$

For the plate with restrained y-normal edges, the critical end-shortening and buckling load are obtained as

$$\Delta_{xcr} = \frac{a\pi^2}{\left(\frac{k^2 A_{11}}{a^2} + \frac{A_{12}}{b^2} \right)} \left[k^4 \frac{D_{11}}{a^4} + k^2 \frac{2(D_{12} + 2D_{66})}{a^2 b^2} + \frac{D_{22}}{b^4} \right] , \quad \hat{N}_{xcr} = \frac{A_{11}}{a} \Delta_{xcr} \tag{2.33}$$

2.8 Numerical Examples and Discussion

The present approach is applied to isotropic and generally orthotropic graphite-epoxy plates. The center deflections of unidirectional orthotropic and angle-ply laminates calculated by using different number of terms in deflection are compared with finite element solutions. Material properties of T300/5208 graphite-epoxy used in the present study are given in Table (1). The y-normal edges of the plates are free to move laterally unless otherwise stated.

2.8.1 Convergence study for orthotropic and angle-ply laminates

One of the most critical assumptions in the application of the Rayleigh-Ritz approach is the form of the displacements. For isotropic plates, it is well known that use of only the first few terms of the deflection function of Eqn. (2.3) can give a good approximate solution. In fact, by retaining only W_{11}, W_{31}, and W_{33} and further assuming $W_{33} = -1/2 W_{31}$ in the deflection, Marguerre [11] obtained an approximate solution for a square isotropic plate which was later proven to be in excellent agreement with Levy's exact solution [2] for which Levy retained six terms of deflection, W_{11}, W_{13}, W_{31}, W_{33}, W_{15}, and W_{51}. However, the effect of using different numbers of terms in the assumed sine form of deflection on the postbuckling response of orthotropic and anisotropic plates has not been well established. In order to examine convergence of the present series solution, an extensive numerical study using different numbers of terms in the assumed deflection was performed for isotropic, orthotropic, and angle-ply plates with different aspect ratios and stacking sequences. Those solutions with different number of terms are; one term (W_{11} survives), three terms (W_{11}, W_{31}, and W_{33} survive), four terms (W_{11}, W_{31}, W_{13}, and W_{33} survive), and six terms (

W_{11}, W_{31}, W_{13}, W_{33}, W_{51}, and W_{15} survive). For the case of a square isotropic plate, the present approach using six terms for the deflection resulted in the same center deflection as Levy's exact solution. The nonlinear algebraic equations when the out-of-plane displacement is assumed to be less than six terms of the Fourier sine series are given in Appendix B.

For orthotropic and angle-ply plates, the center deflections by the present method are compared with finite element solutions. The finite element program for the postbuckling analysis is coded based on the isoparametric, shear-deformable, nine noded, rectangular element [68] with five degrees of freedom (u, v, w, ϕ_x, and ϕ_y) per node. The finite element formulation using the nonlinear shear deformation plate equations is presented in Appendix C. To verify the finite element program, center deflections of various isotropic, orthotropic, and angle-ply plates are compared and proven to be in excellent agreement with the results obtained by commercially available computer code, ABAQUS [69]. Quarter plate models of 4*4 (81 nodes) and 2*4 (45 nodes) meshes are used, as shown in Figs. 3-(a) and 3-(b), for the finite element analysis of square and rectangular (a/b = 0.5) plates, respectively.

The normalized center deflections for angle-ply $[\pm 30]_{24s}$ laminates with aspect ratios (a/b) of 0.5 and 1.0 are shown as a function of the normalized applied end-shortening in Figs. 4-(a) and 4-(b), respectively. The y-normal edges of plates are restrained from lateral in-plane displacements. It can be seen from the figures that the center deflections by the present method using six terms of deflection and by the finite element solution agree well (differences are within 1%). The present solutions with more than three terms of deflection and the finite element solution for the square laminate are virtually the same, while only the six terms solution agrees well with the

finite element solution for the short (a/b = 0.5) angle-ply laminate. In Figs. 5-(a) and 5-(b), the center deflections of rectangular (a/b = 0.5) and square orthotropic laminates $[0]_{24}$, respectively, are compared with the finite element solutions. Like the angle-ply laminates, the center deflections by the present six terms approach and the finite element solution are in better agreement for the square orthotropic plate than for the short plate. However, the deviation in the center deflections between the present method using different numbers of terms and the finite element method is more pronounced for this orthotropic laminate than for the $[\pm 30]_{24s}$ angle-ply laminate.

The effect of plate orthotropy on postbuckling deformations can be observed from comparison of Figs. 4-(a) and 5-(a) or Figs. 4-(b) and 5-(b). It can be seen that for the same value of the normalized applied end-shortening the angle-ply laminates deflect more than the orthotropic ones with the same plate aspect ratio. For the short plates, the differences in the center deflection by the present six terms representation of deflection and by the finite element method are within 1.0 and 3.5% over the entire range of end-shortening considered for the angle-ply and orthotropic plates, respectively, while three or four term solutions are non-conservative and show 5.0 and 10.0% of differences from the finite element solutions, respectively. It can be concluded from these examples that both the aspect ratio and plate orthotropy mandate the use of different numbers of terms in the deflection. If a plate is very stiff in one direction relative to the other perpendicular direction or the aspect ratio of a plate is small, the assumed form of deflection in general requires more terms, and the use of a six term sine series results in good approximate solutions.

Table 1. Material properties of T300/5208 graphite-epoxy

$E_1 = 19.01$ msi
$E_2 = 1.89$ msi
$G_{12} = 0.93$ msi
$\nu_{12} = 0.38$
$\varepsilon_{11}^{tu} = 0.01$
$\varepsilon_{11}^{tl} = 0.01$
$\varepsilon_{22}^{tu} = 0.012$
$\varepsilon_{22}^{tl} = 0.006$
$\gamma_{12}^{u} = 0.015$

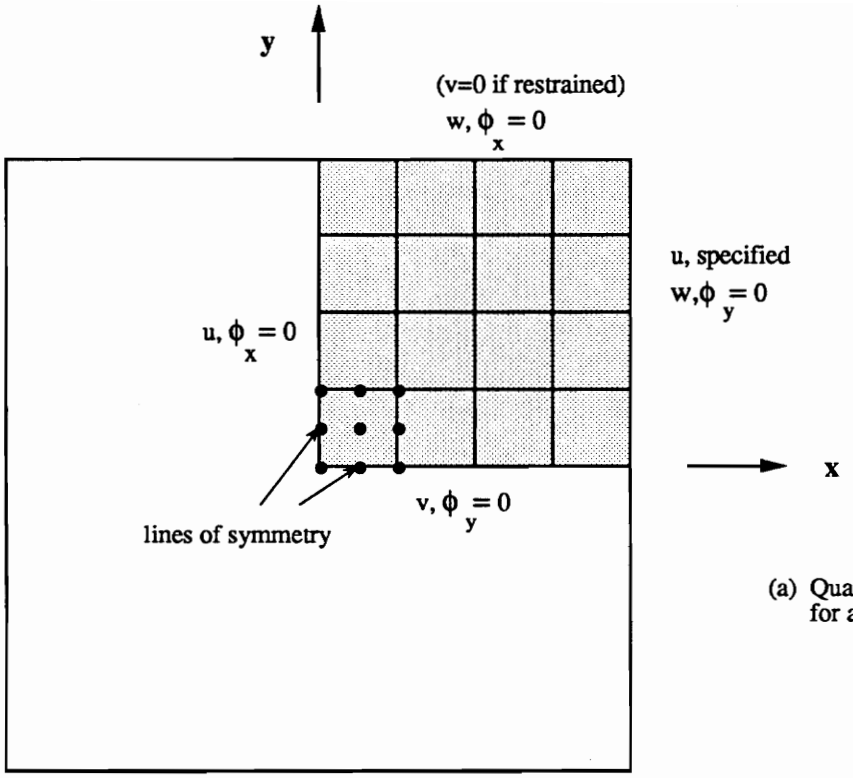

(a) Quarter plate model for a square plate

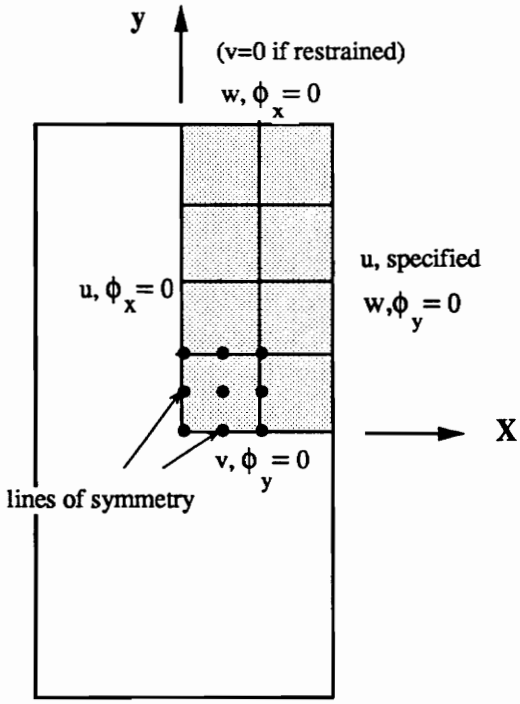

(b) Quarter plate model for a rectangular plate

Fig. 3 Finite element meshes

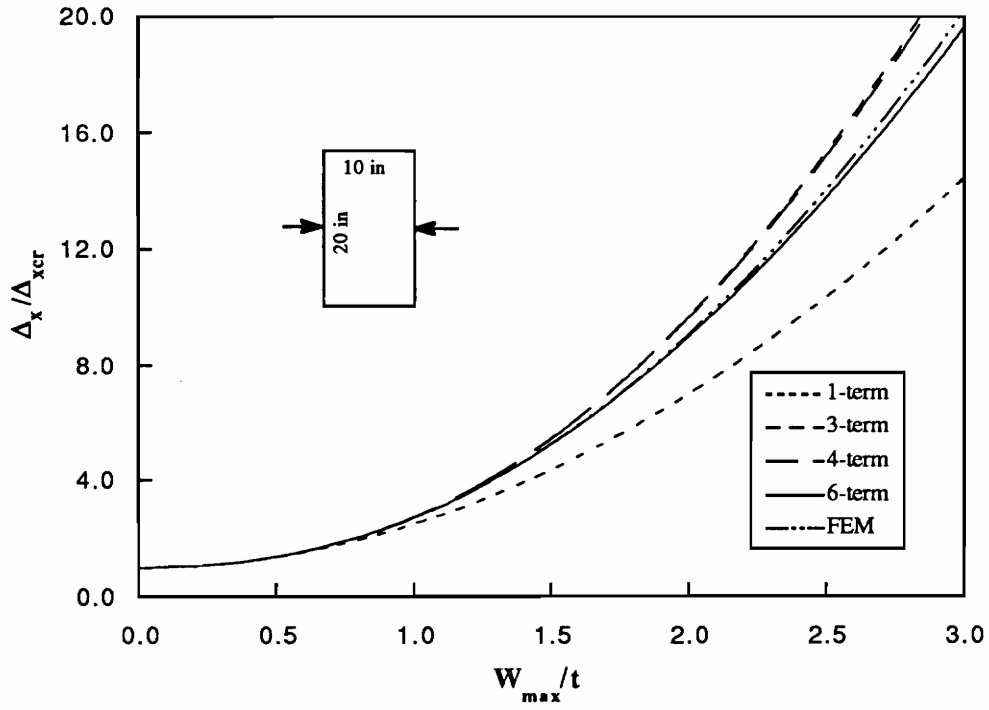

(a) Rectangular plate

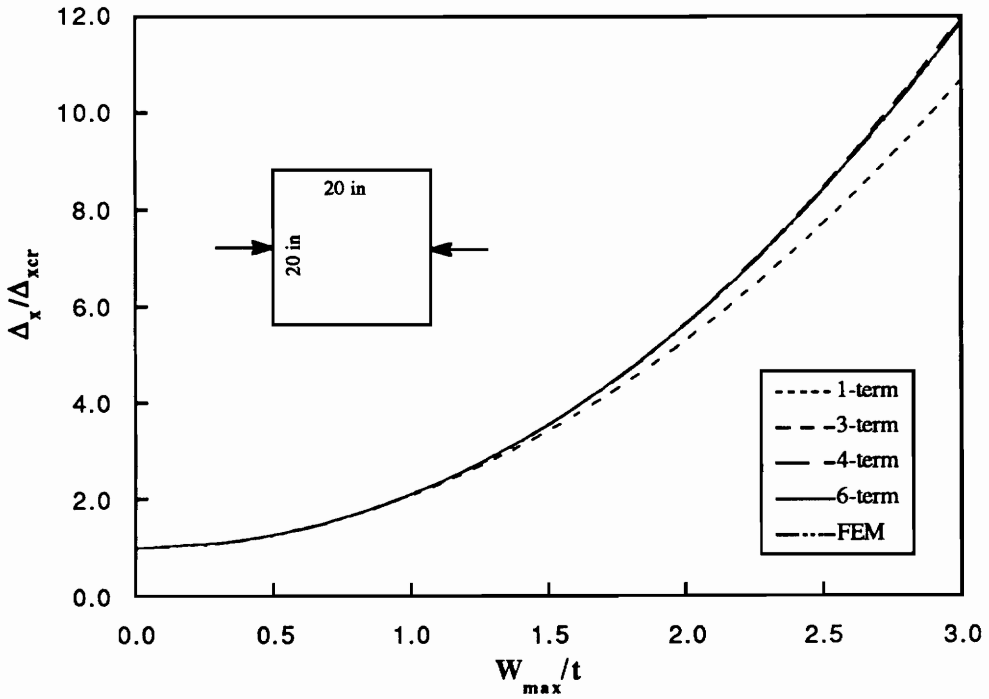

(b) Square plate

Fig. 4 Center deflection of $[\pm 30]_{24s}$ laminates with restrained y-normal edges (t=0.12 in)

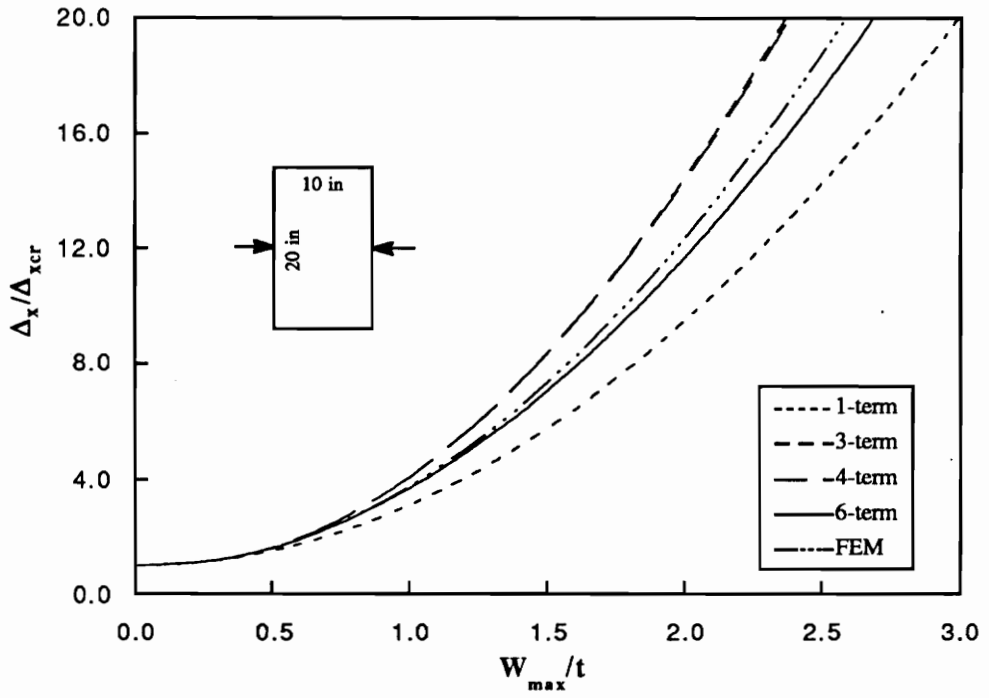

(a) Rectangular plate

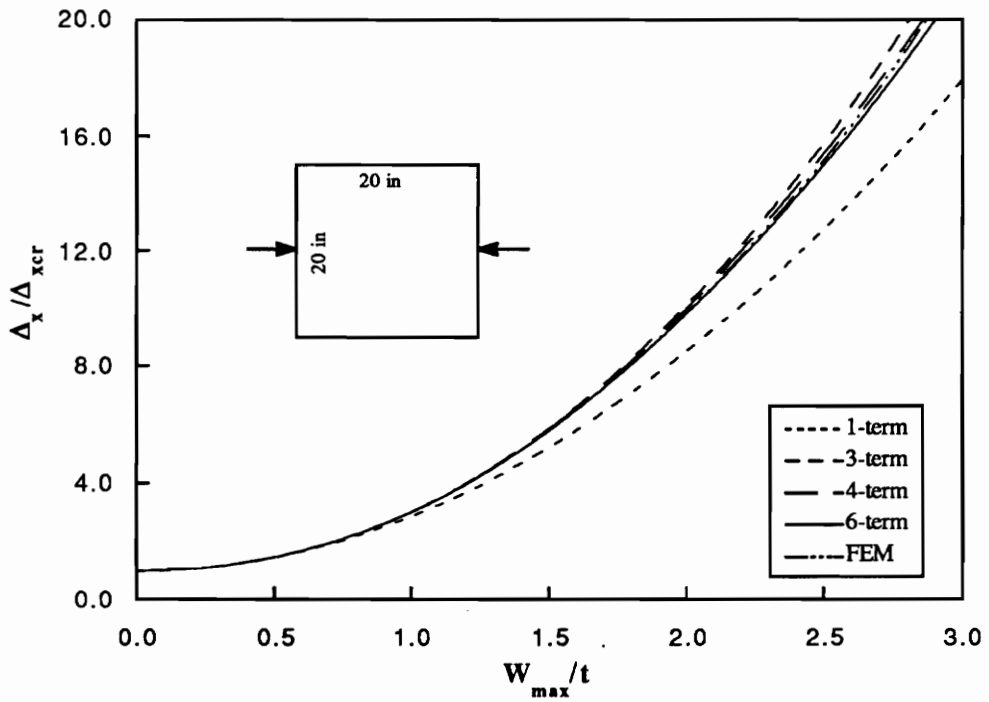

(b) Square plate

Fig. 5 Center deflection of unidirectional orthotropic $[0]_{24}$ laminates with restrained y-normal edges (t=0.12 in)

2.8.2 Effect of bending-twisting coupling terms

In the present approach, the bending-twisting coupling terms (D_{16} and D_{26}) disappeared in the derivation of the total potential energy due to the assumption of sine series deflection. The effect of ignoring these coupling terms on the buckling and postbuckling behavior of square angle-ply $[\pm 45]_{ns}$ laminates is examined next by varying the number of layers (n) while keeping the total plate thickness unchanged (t = 0.12 in). This is achieved by increasing the thicknesses of individual layers. As the number of layers increases, the magnitude of bending-twisting coupling terms D_{16} and D_{26} decreases. The finite element analysis we are using is capable of reflecting the effect of this change in the D_{16} and D_{26} terms on the postbuckling response. Center deflections, normalized by the panel thickness, of angle-ply laminates with freely shifting and restrained y-normal edges are presented in Figs. 6-(a) and 6-(b), respectively, as a function of end-shortening as they are calculated from the finite element program and from the present analysis. The applied end-shortening, Δ_x, for the finite element solutions is normalized by the critical end-shortening for each laminate calculated by including the coupling terms, while the normalization of the applied end-shortening for the present solution is performed with respect to the critical end-shortening obtained by ignoring the bending-twisting coupling terms (Eqns. (2.32) and (2.33)). The value of the critical end-shortening for each case is also printed next to the legends in the figure.

It can be seen that the coupling terms can significantly affect both buckling and postbuckling responses, depending upon the magnitudes of the coupling terms. For $[\pm 45]_{ns}$ laminates with $n \geq 6$, the end-shortening at buckling calculated by ignoring the coupling terms is within 5% of the critical shortening calculated by the finite

element method for the both boundary conditions. Also, the center deflections and the postbuckling end-shortening obtained by the present analysis agree well with finite element solutions if $n \geq 6$. The agreement is especially good for plates with restrained y-normal edges. This is, however, due to the inability of the finite element model used to exactly simulate freely shifting straight edges. While the in-plane displacements are assumed to be constant along the sides in the present approach, the finite element solutions show non-uniform in-plane displacement along the y-normal edges if these edges are unrestrained. As a result, the finite element method is expected to predict a softer response for the center deflection of a plate with freely shifting y-normal edges, Fig. 6-(a), than does the present approach. In the case of plates restrained from lateral in-plane displacement along the y-normal edges the boundary conditions along these edges are the same for the present and the finite element solution. Thus, it can be concluded that the present method can be applied to plates for which the magnitudes of bending-twisting coupling terms are not large. In the case of a laminate with large bending-twisting coupling, $n = 1$, the present solution can be in considerable error. For example, at the applied end-shortening $\Delta_x = 3\Delta_{xcr}$ the center deflections by the present analysis are observed to be about 25 and 18% in error compared to finite element solutions for freely shifting and restrained y-normal edges, respectively.

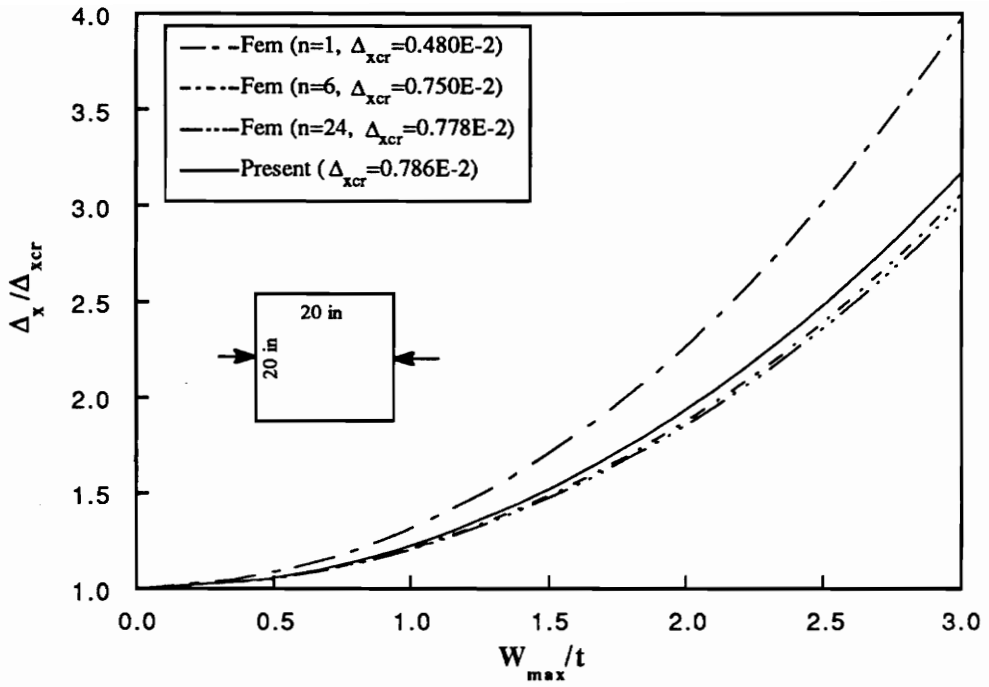

(a) Freely shifting y-normal edges

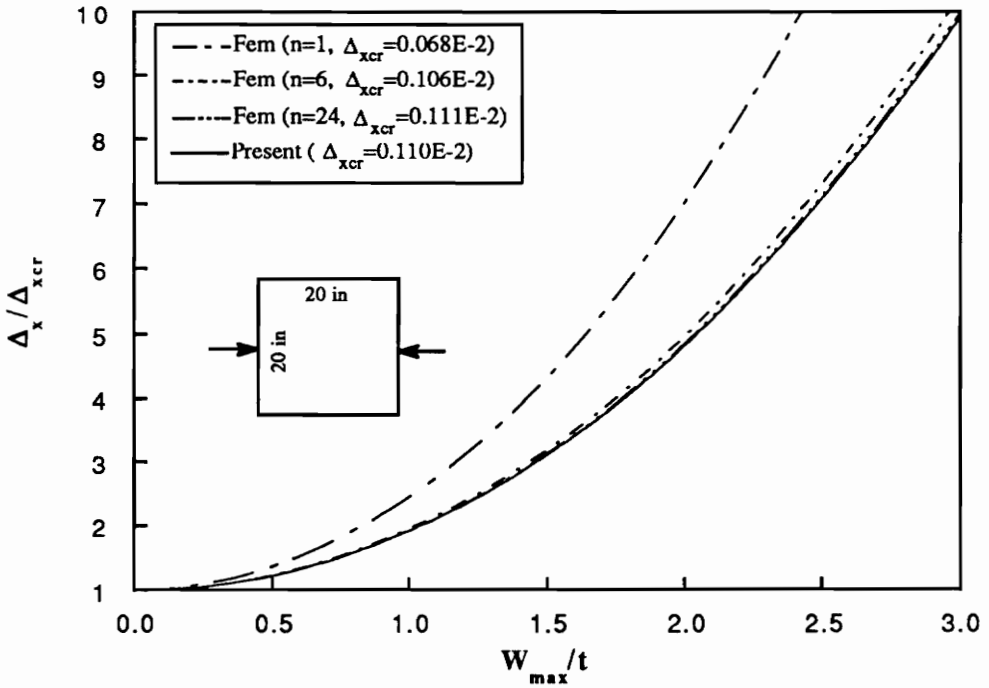

(b) Restrained y-normal edges

Fig. 6 Center deflection of square angle-ply $[\pm 45]_{ns}$ laminates (t=0.12 in)

2.8.3 Comparison of strain components

As will be discussed later in Chapter IV, the present study uses strain components in predicting laminate failure. To evaluate the accuracy of the present analysis in calculating strain components, the strains obtained by the present approach using six terms out-of-plane displacement function and by the finite element method are compared. The strain components for square angle-ply $[\pm 30]_{24s}$ and unidirectional orthotropic $[0]_{24}$ laminates are presented as a function of normalized applied end-shortening in Figs. (7) and (8), respectively. The laminates are restrained from lateral in-plane displacement along y-normal edges. All strain components are calculated at the corners of laminates, (x,y) = (0,0), (0,b), (a,0), (a,b), for the coordinate convention shown in Fig. (1). At these corners, the strains are calculated to have extremum values. The negative values indicate compressive strains and positive values tensile strains. The strain components in x- and y-direction are found to be the same through the thickness direction due to the absence of curvatures at the corner points of the plate. The shearing strains are calculated at the outer surfaces.

As can be seen from Figs. (7) and (8), the strain in x-direction is in excellent agreement between the two solutions throughout the range of the applied end-shortening. The strain in y-direction and the shearing strain also agrees well between the two solutions if the laminates are not in the deep postbuckling regime. The agreement between the two solutions for the strain in y-direction and the shearing strain in the deep postbuckling regime, however, becomes worse especially for the orthotropic plate although the magnitude of the strain in y-direction is small even in the deep postbuckling range compared with the value of the strain in x-direction.

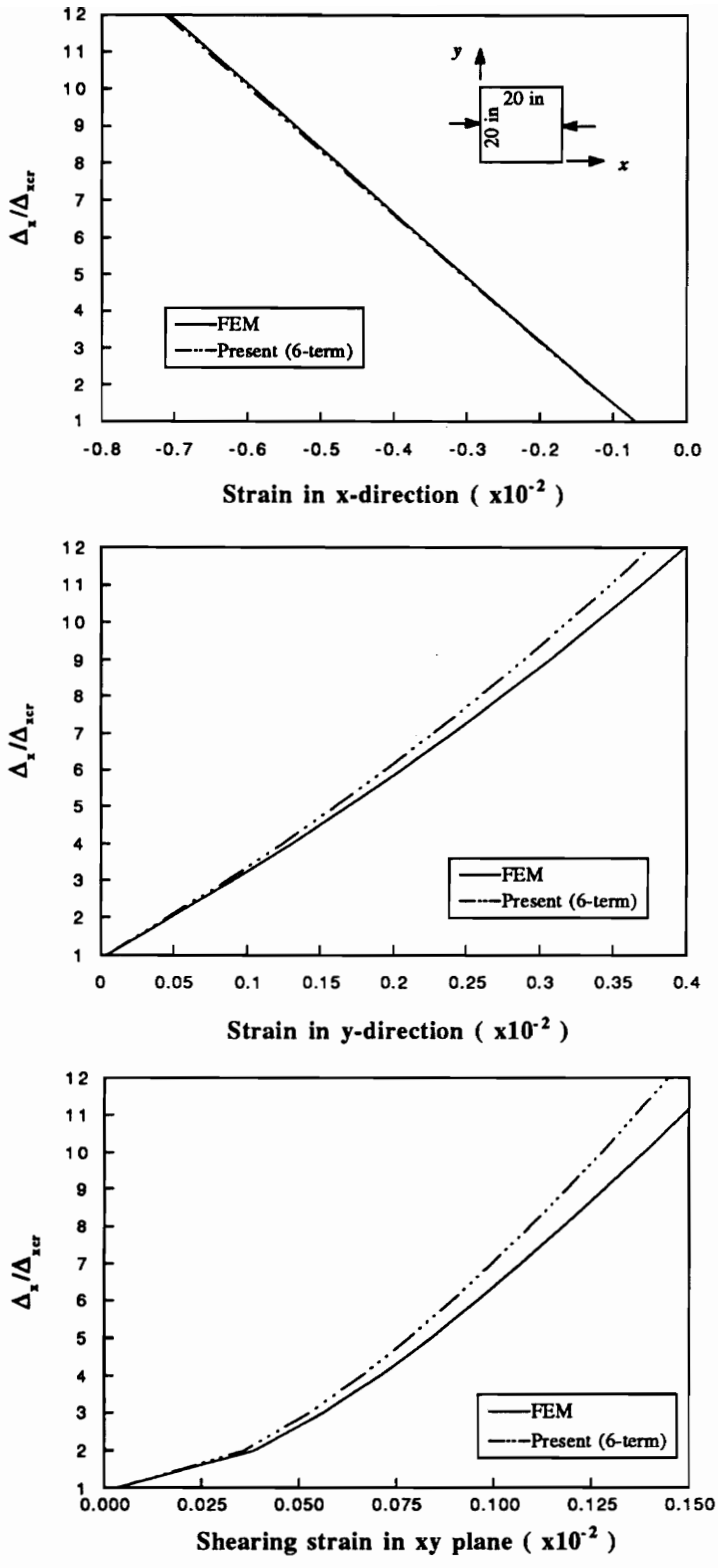

Fig. 7 Comparison of strain components for a square angle-ply $[\pm 30]_{24s}$ laminate at corner (a=b=20.0, t=0.12 in)

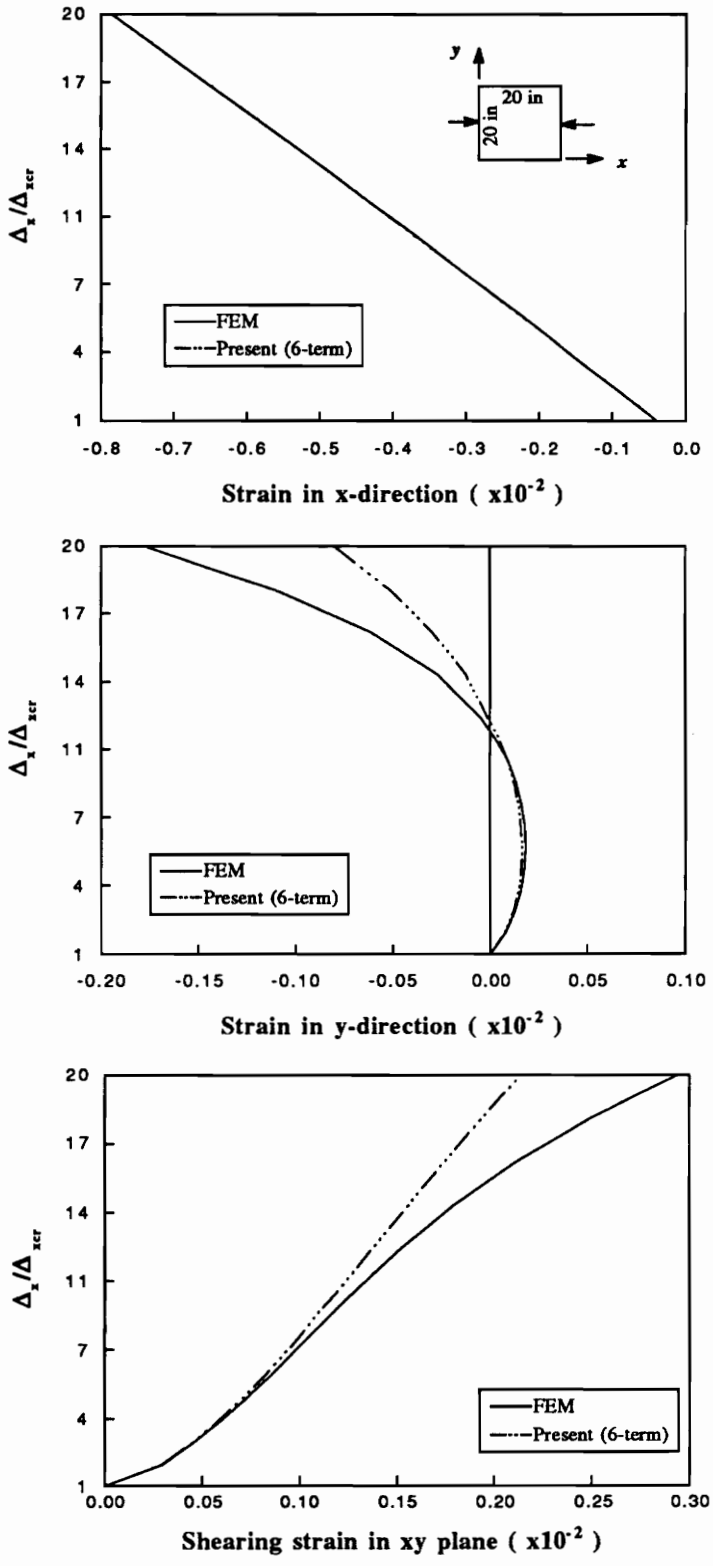

Fig. 8 Comparison of strain components for a square unidirectional orthotropic $[0]_{24}$ laminate at corner (a=b=20.0, t=0.12 in)

CHAPTER III

PHENOMENON OF BUCKLE PATTERN CHANGE

It is known that a plate in the postbuckling regime can undergo changes in the buckled form. Initially, the plate buckles into a mode which has the lowest strain energy among all of the possible kinematically admissible deformations. As the loading progresses, it is possible that the strain energy associated with the existing mode may become larger than the strain energy for an adjacent mode. If that is the case, the buckling mode may shift to the new, lower energy, mode. Such mode shifting may occur several times during the loading.

3.1 Assumption of Out-of-plane Displacement

In the following, for the sake of simplicity, the mode shifting phenomenon is discussed in detail for a plate which buckles initially into a single half wave and may change its buckled form as the applied end-shortening increases. The following simple form of the out-of-plane displacement is assumed

$$w = W_{11} \sin\frac{\pi x}{a} \sin\frac{\pi y}{b} + W_{21} \sin\frac{2\pi x}{a} \sin\frac{\pi y}{b} \tag{3.1}$$

Not only is the assumed deflection (3.1) easy to handle due to the simplicity of the expression, but it ensures that the plate can deform into a single half wave, double half waves, or a mode which is the superposition of the single and double half waves, depending upon the magnitudes of the unknown parameters, W_{11} and W_{21}. In this

sense, the assumption of the deflection (3.1) is useful to gain some insight into the phenomenon of buckle pattern change, although the resulting solutions are approximate.

3.2 Derivation of Nonlinear Algebraic Equations

Following the same procedure as before, the total potential energy, Π, can be expressed (refer Appendix D for an explicit form of the potential energy) as a function of an applied end-shortening and deflection parameters, W_{11} and W_{21} , as

$$\Pi = \Pi(\Delta_x, W_{11}, W_{21}) \tag{3.2}$$

and minimization of the total potential energy results in

$$\begin{aligned} (a_{11}W_{11}^2 + a_{12}W_{21}^2)\, W_{11} &= b_1\, W_{11} \\ (a_{21}W_{11}^2 + a_{22}W_{21}^2)\, W_{21} &= b_2\, W_{21} \end{aligned} \tag{3.3}$$

where

$$a_{11} = \frac{3}{16a^4A^*_{11}} + \frac{1}{16b^4A^*_{22}}$$

$$a_{12} = \frac{3}{4a^4A^*_{11}} + \frac{1}{4b^4A^*_{22}} + \frac{81r+s}{16a^2b^2} \quad , \quad a_{21} = a_{12}$$

$$a_{22} = \frac{3}{a^4A^*_{11}} + \frac{1}{16b^4A^*_{22}}$$

$$b_1 = \frac{\Delta_x}{\pi^2a^3A^*_{11}} - \left[\frac{D_{11}}{a^4} + \frac{2(D_{12}+2D_{66})}{a^2b^2} + \frac{D_{22}}{b^4}\right]$$

$$b_2 = \frac{4\Delta_x}{\pi^2a^3A^*_{11}} - \left[16\frac{D_{11}}{a^4} + 4\frac{2(D_{12}+2D_{66})}{a^2b^2} + \frac{D_{22}}{b^4}\right]$$

$$\frac{1}{r} = \frac{b^2}{a^2}A^*_{22} + 4(2A^*_{12} + A^*_{66}) + \frac{16a^2}{b^2}A^*_{11}$$

$$\frac{1}{s} = \frac{81b^2}{a^2}A^*_{22} + 36(2A^*_{12} + A^*_{66}) + \frac{16a^2}{b^2}A^*_{11}$$

The above equations are obtained for the freely shifting y-normal edges (the only case considered here). There exist three possible solutions for W_{11} and W_{21} in the cubic nonlinear Eqns. (3.3).

Case (a) Symmetric Mode

If $W_{11} \neq 0$ and $W_{21} = 0$, the plate deforms into a symmetric mode and the unknown parameters are

$$W_{11}^2 = \frac{b_1}{a_{11}} \quad , \quad W_{21} = 0 \tag{3.4}$$

Since W_{11} must be a real value, the following condition is implied

$$\Delta_x > \Delta_{xcr} \left(= \pi^2 a^3 A^*_{11} \left[\frac{D_{11}}{a^4} + \frac{2(D_{12} + 2D_{66})}{a^2 b^2} + \frac{D_{22}}{b^4} \right] \right) \tag{3.5}$$

Case (b) Anti-symmetric Mode

The plate buckles into an anti-symmetric mode if $W_{11} = 0$ and $W_{21} \neq 0$, and the solution is

$$W_{11} = 0 \quad , \quad W_{21}^2 = \frac{b_2}{a_{22}} \tag{3.6}$$

The requirement for W_{21} to be real yields the condition

$$\Delta_x > \frac{4\pi^2 a^3 A^*_{11}}{4} \left[16 \frac{D_{11}}{a^4} + 4 \frac{2(D_{12} + 2D_{66})}{a^2 b^2} + \frac{D_{22}}{b^4} \right] \tag{3.7}$$

Case (c) Interactive Mode

If $W_{11} \neq 0$ and $W_{21} \neq 0$, the plate deforms into a mode which is neither symmetric nor anti-symmetric but a superposition of both modes. The solution is

$$W_{11}^2 = \frac{a_{22}b_1 - a_{12}b_2}{a_{11}a_{22} - a_{12}^2} \quad , \quad W_{21}^2 = \frac{-a_{12}b_1 + a_{11}b_2}{a_{11}a_{22} - a_{12}^2} \tag{3.8}$$

For real solutions, the limitation imposed is

$$\Delta_x > \max \{ \Delta_1 , \Delta_2 \} \tag{3.9}$$

where Δ_1 and Δ_2 can be obtained from the real requirement of W_{11} and W_{21} , respectively.

3.3 Determination of Actual Deformed Shape

The three solutions with the limitations, (3.5), (3.7), and (3.9), represent equilibrium positions. To further ensure that these equilibrium configurations are stable, the second variation of the total potential energy should be positive definite in the arbitrary δW_{11} and δW_{21} for this configuration. The second variation of the potential energy, (3.2), is

$$\delta^2\Pi = \frac{\partial^2\Pi}{\partial W_{11}^2}(\delta W_{11})^2 + 2\frac{\partial^2\Pi}{\partial W_{11}\partial W_{21}}(\delta W_{11})(\delta W_{21}) + \frac{\partial^2\Pi}{\partial W_{21}^2}(\delta W_{21})^2 \tag{3.10}$$

For a stable equilibrium, following conditions must be fulfilled

$$\frac{\partial^2\Pi}{\partial W_{11}^2} > 0 \quad , \quad \frac{\partial^2\Pi}{\partial W_{21}^2} > 0 \quad , \quad \left(\frac{\partial^2\Pi}{\partial W_{11}^2}\right)\left(\frac{\partial^2\Pi}{\partial W_{21}^2}\right) - \left(\frac{\partial^2\Pi}{\partial W_{11}\partial W_{21}}\right)^2 > 0 \tag{3.11}$$

For a given equilibrium solution, the range of applied end shortening for stable configurations can be determined from the positive definite requirement of the second variation of the total potential energy (3.11) along with the limitations for a real solution. In an extensive numerical study, it was found that all three modes are always stable as long as the real solutions for the Eqns. (3.4), (3.6), and (3.8) exists. This means that any of the three modes can mathematically represent the deformed shape of a plate for a given end-shortening. To determine the actual deformed shape for a given loading, the magnitude of the total potential energy is calculated for each of the three modes. Since the problem was to minimize the total potential energy (3.2), the one with the least total potential energy among three modes is assumed to be the actual deformed shape of the plate for a given load.

The normalized magnitudes of the total potential energy for the three modes discussed above are plotted as a function of applied edge displacement in Fig. (9) for a square isotropic plate. It can be observed that the interactive mode, which is the superposition of a symmetric and anti-symmetric mode, has the largest value of total potential energy, and there exists a certain applied end-shortening (point A) where the values of total potential energy for symmetric and anti-symmetric modes intersect. Thus, for this example, the plate deforms into a symmetric mode for the applied end-shortening up to $5.5\Delta_{xcr}$ and changes its deformed shape to an anti-symmetric mode if Δ_x exceeds $5.5\Delta_{xcr}$. In the present study of buckle pattern change phenomenon for orthotropic and anisotropic plates, it was found that the interactive mode always has the largest amount of potential energy. This means the plates considered do not deform into the interactive mode in the entire postbuckling load range. Other available experimental results [19-24] also showed sudden mode change from symmetric to anti-symmetric mode without deforming into the interactive mode.

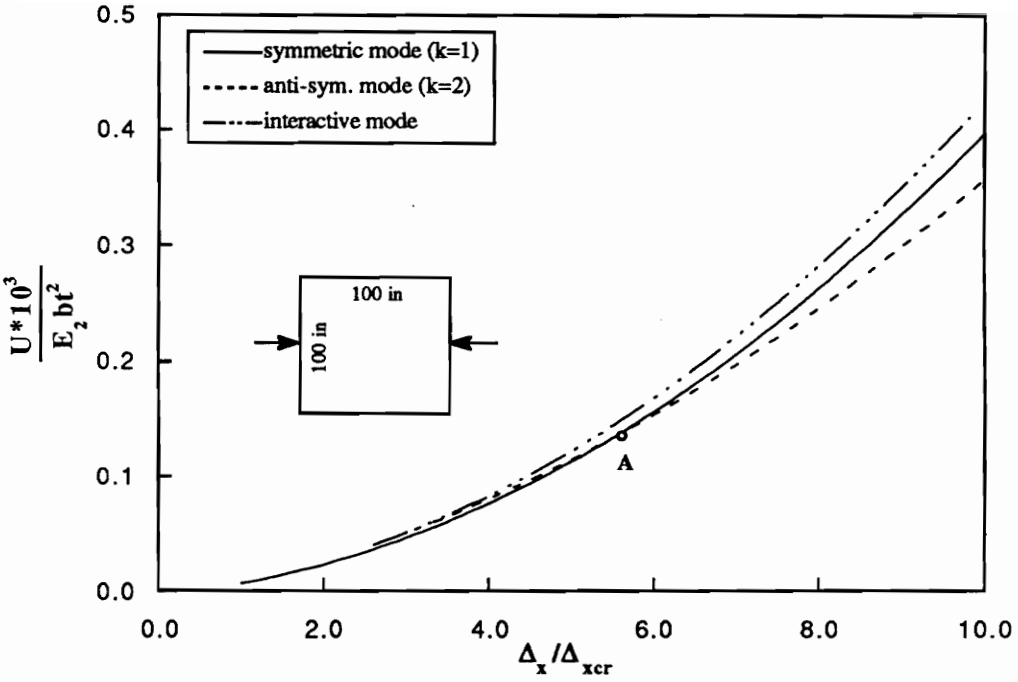

Fig. 9 Total potential energy of a square isotropic plate with freely shifting y-normal edges (t=1.0 in)

Although the assumed deflection (3.1) includes three possible modes of plate deformations, it has limitations in the sense that the solutions are approximate and cannot be used for a plate which initially buckles into more than a single half wave or for a plate which undergoes several mode changes. To overcome these shortcomings in using the deflection form (3.1), the Fourier series given in Eqn. (2.3) is employed in predicting the mode change. The value of the constant k in the assumed form of the deflection (2.3) is the number of half waves at initial buckling and can take an even or an odd value. Based on the assumed deflection (2.3), the actual deformed shape is determined by calculating the potential energy of the two successive modes with (k) and $(k+1)$ half waves in the loading direction for a given end-shortening. If the potential energy for the mode with $(k+1)$ half waves is smaller than the one with (k) half waves at a certain load step, the mode shape with $(k+1)$ half waves represents the deformed shape for that load level. In the next load step, the potential energy for $(k+1)$ and $(k+2)$ half waves is compared. Numerical examples on the phenomenon of buckle pattern change for isotropic, orthotropic, and anisotropic plates are given in the next section.

Even though the strain energy may be lower in a mode other than the existing mode at a given point in the loading, the source of instability which triggers the actual shifting is not understood. It is possible that the presence of imperfections plays a role in the initiation of mode shifting. In the current analysis, it is assumed that the instability which causes mode shifting is always present, and that the plate will always shift into the kinematically admissible mode which has the lowest strain energy for a given loading.

3.4 Numerical Examples and Discussion

In this section, mode change of a square isotropic plate predicted by the present approach is compared with an analytical result presented in Ref. [20]. Then, the load end-shortening curve of a long isotropic plate obtained by the present method is compared with an available experimental one in Refs. [20-21]. Also considered is the prediction of the applied end-shortening at mode change for rectangular isotropic, orthotropic, quasi-isotropic, and square angle-ply plates. The following examples are generated by using six terms of out-of-plane displacement function (2.3).

3.4.1 Load end-shortening curves for a square isotropic plate

The load end-shortening curves for an isotropic square plate by the present and Stein's analytical method [20] are compared in Fig. (10). Stein obtained his analytical solution by assuming the in-plane and out-of-plane displacements as a power series. In Fig. (10), Stein's solution (curve OACD) shows a smooth transition in the load end-shortening curve from a symmetric to anti-symmetric mode at the applied end-shortening $\Delta_x \cong 3.2\Delta_{xcr}$ while the present approach (curve OABCD) predicts an abrupt buckle pattern change at $\Delta_x \cong 5.4\Delta_{xcr}$. Stein's solution predicts earlier mode change than the present method does since he assumed the solution to be the one which yields the lowest bound in the load end-shortening curve for different half waves, without consideration of energy states of the deformed shapes. Except for the range ABC, it can be seen from Fig. (10) that the two results agree very well up to point A and beyond point C. Other researchers [22,26-27] who include the mode changing phenomenon on their postbuckling study used the same strategy proposed by Stein.

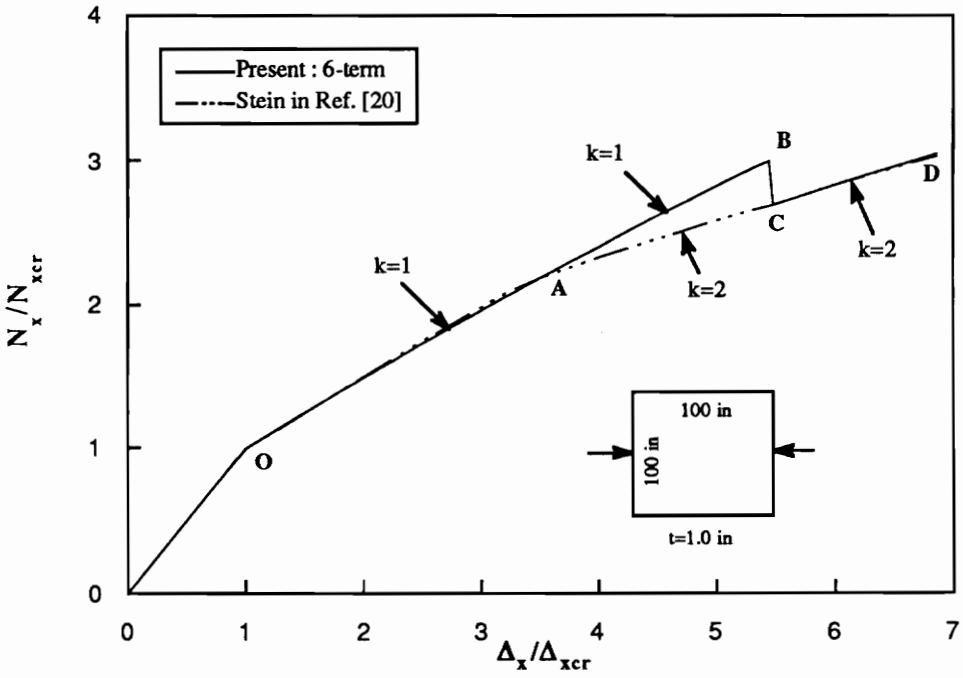

Fig. 10 Load end-shortening curves for a square isotropic plate

3.4.2 Comparison of load end-shortening curves with experimental results

Experimental load versus end-shortening curve for a 2024-T3 aluminum alloy plate is presented in Figs. 11-(a) and 11-(b) together with analytical curves generated by Stein and by the present approach. Stein, in Refs. [20-21], used this long panel to compare his analytical results with experimental results. It can be seen that the three curves in Fig. 11-(a) are in good agreement up to $\Delta_x \cong 4\Delta_{xcr}$ after which the difference in the load end-shortening curves between the analyses and test begins to increase. The discrepancy is suspected to be due to plastic behavior of the plate for applied shortening $\Delta_x > 5\Delta_{xcr}$ as reported in Ref. [20]. Plasticity is not included in either the present analysis or that of Ref. [20]. The load end-shortening curves by the present approach and by the test show a sudden drop at a mode change, while Stein's theoretical load end-shortening curve follows a smooth path. The experimental curve indicates that the plate buckles into five half waves in the initial postbuckling load range, then changes its mode to six buckles at $\Delta_x \cong 3.0\Delta_{xcr}$, to seven buckles at $\Delta_x \cong 5.4\Delta_{xcr}$, and then to eight buckles at $\Delta_x \cong 8.2\Delta_{xcr}$, while the present approach predicts the mode change from five to six at $\Delta_x \cong 1.1\Delta_{xcr}$, from six to seven at $\Delta_x \cong 3.0\Delta_{xcr}$, and from seven to eight buckles at $\Delta_x \cong 6.3\Delta_{xcr}$. The mode change by Stein's analysis occur at values of the applied end-shortening very close to those predicted by the present approach. However, both models predict mode change to be earlier in the postbuckling regime compared to the test. One of the strong possibilities for the discrepancy in the prediction of the applied end-shortenings at mode change between the test and analyses is that the test plate is not perfectly flat as is assumed in the analyses. In fact, Fig. 11-(a) shows a noticeable difference between the analytical and experimental load end-shortening curves in the prebuckling load range, which maybe a direct result of an initial imperfection. To obtain an idea of how the

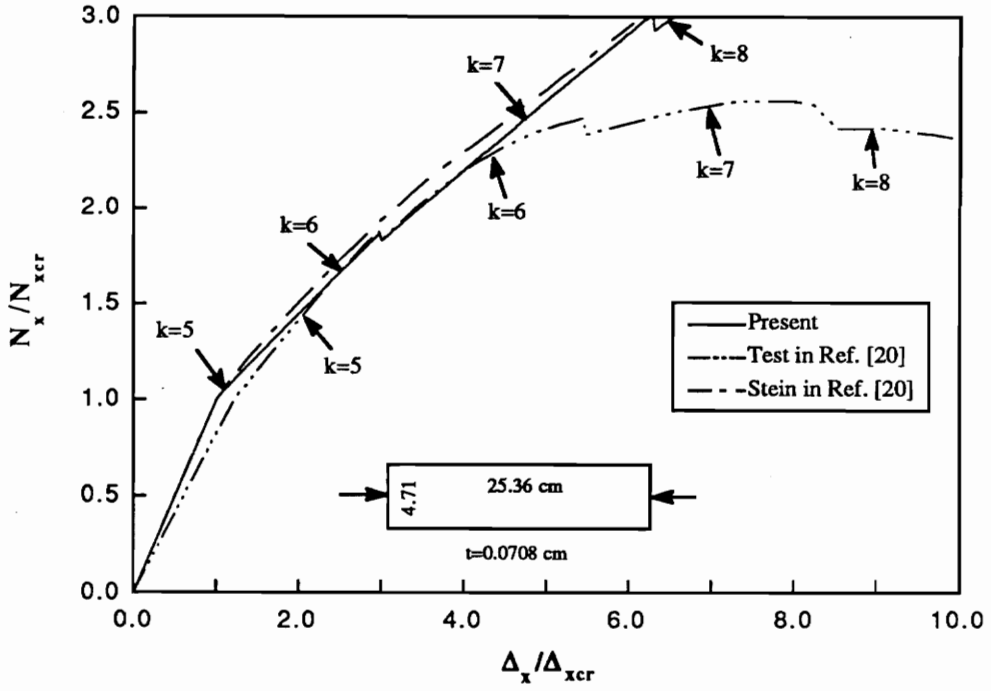

(a) Plate without initial curvature

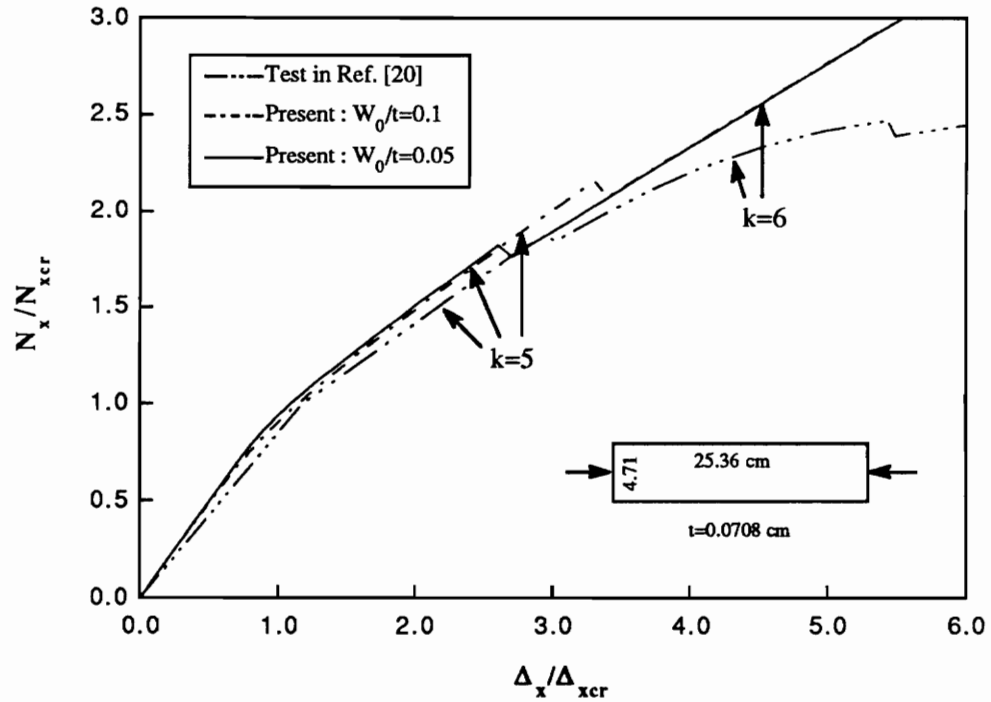

(b) Plate with initial curvature

Fig. 11 Load end-shortening curves for a long isotropic plate with freely shifting sides

initial imperfection affects buckle pattern change, another analysis is performed by introducing initial imperfection of the form

$$w_0 = W_0 \sin\frac{k\pi x}{a} \sin\frac{\pi y}{b} \tag{3.12}$$

to the assumed deflection (2.3). The stress function is obtained from the compatibility equation presented by Marguerre [71] for the plate with an initial deflection. Then, the procedure presented in Chapter II is applied to obtain the load end-shortening curves for the long aluminum alloy plate with some degree of initial curvature. The resulting curves with the amplitudes of initial curvature, 5 and 10 % of plate thickness are given in Fig. 11-(b). It can be seen that the introduction of the initial imperfection in the present analysis results in a better agreement with the test. As the initial imperfection magnitude increases, the plate has a tendency to change its buckled form at a larger value of the applied end-shortening.

3.4.3 Rectangular isotropic, orthotropic, and quasi-isotropic plates

In Fig. (12), the applied end-shortening at which plates change their buckled shape from a symmetric to an anti-symmetric mode are presented as a function of plate aspect ratio for rectangular isotropic, orthotropic $[0]_{24}$, and quasi-isotropic $[\pm 45/0/90]_{5s}$ plates with freely shifting and restrained y-normal edges. It can be seen from Fig. (12) that the quasi-isotropic and isotropic plates show a similar trend in mode change while the orthotropic laminates do not. For the same plate aspect ratio, the orthotropic plate undergoes mode change at a much higher value of the normalized applied end-shortening than its isotropic and quasi-isotropic counterparts. It can be also observed that high aspect ratio plates tend to change their buckled form

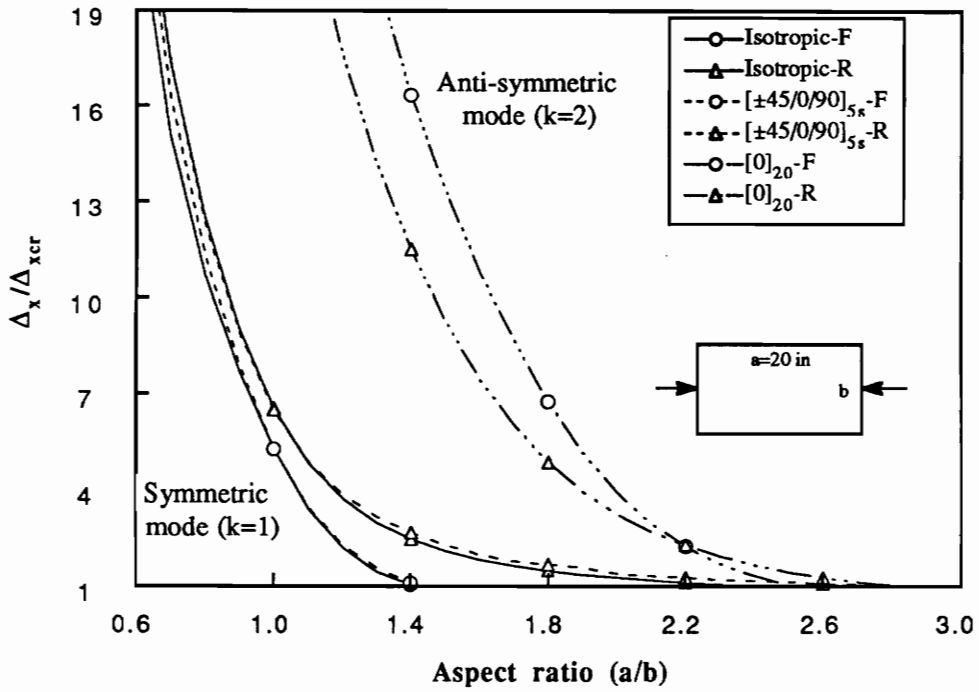

Fig. 12 Applied end-shortening at mode change for rectangular plates (t=0.2 in ; F- freely shifting, R- restrained y-normal edges)

at an earlier stage of postbuckling load while shorter plates change their buckled shape at a load level far beyond the critical end-shortening. If the y-normal edges are restrained from lateral displacement, there exists a wider range of aspect ratios, for isotropic and quasi-isotropic plates, in which the plates buckle initially into a symmetric mode but are likely to undergo mode change quickly as the applied end-shortening increases. For example, for an isotropic plate with a/b = 2.0 the plate will buckle into two half waves if the y-normal edges are free. If the y-normal edges are restrained, the same plate will initially buckle into a single half wave but will shift to two half waves as soon as Δ_x reaches $1.3\Delta_{xcr}$. An indication of tendency of a plate to change mode shape in the postbuckling regime is observed to be the spacing of its eigenvalues obtained from linear prebuckling analysis. For those plates which have an eigenvalue associated with their second mode of deformation very close in value to their lowest eigenvalue, the mode change from initial single half wave to two half waves is imminent. In fact, an isotropic plate of $a/b = \sqrt{2}$ with freely shifting y-normal edges has two modes, symmetric and anti-symmetric, that coalesce at the same buckling load. This is the aspect ratio beyond which the plate buckles into two half waves instead of a single half wave.

3.4.4 Square angle-ply laminates

The applied end-shortening at mode change for angle-ply, $[\pm\theta]_{6s}$, laminates is plotted as a function of fiber orientation in Fig. (13) to illustrate the effect of degree of orthotropy on the mode change. It is observed that the boundary conditions along the y-normal edges of laminates have a significant effect on the phenomenon of buckle pattern change. The angle-ply plates initially deform into a symmetric postbuckling mode if the fiber angle is smaller than 60^0 for freely shifting y-normal edges. The

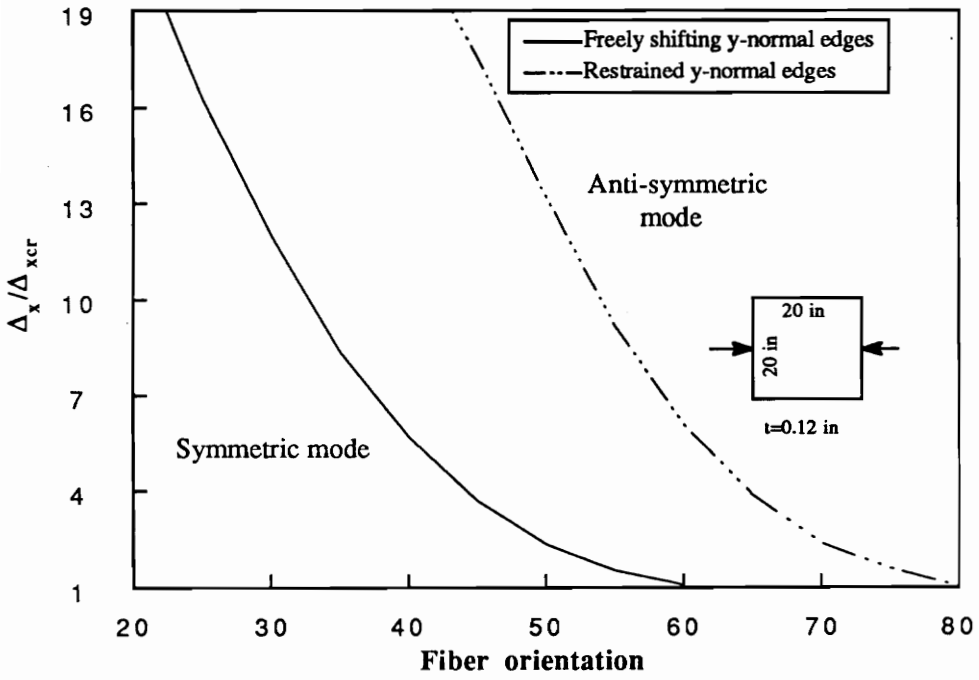

Fig. 13 Applied end-shortening at mode change for $[\pm\theta]_{6s}$ laminates

threshold for mode change at buckling is 80^0 for plates with restrained y-normal edges. At these fiber orientations the plates have repeated eigenvalues corresponding to the first and second modes of buckling. A $[\pm 45]_{6s}$ laminate, for instance, changes its buckled form from a symmetric to an anti-symmetric mode at about $3.5\Delta_{xcr}$ for freely shifting y-normal edges, whereas the same plate will not change mode until the end-shortening is more than 18 times Δ_{xcr} for the case of restrained y-normal edges. It is concluded that for angle-ply laminates the restrained boundary conditions along the y-normal edges force the laminates to change their buckling mode at a higher value of end-shortening than do the freely shifting sides.

The load versus end-shortening curves for square angle-ply laminates, $[\pm\theta]_{6s}$, with a wide range of fiber orientations are shown in Fig. (14). The applied end-shortening is normalized by the critical end-shortening of a corresponding angle-ply laminate. All the angle-ply laminates except the 0^0 orthotropic laminate undergo a mode change; from $k = 1$ to 2 for the $[\pm 30]_{6s}$ and $[\pm 45]_{6s}$ laminates, from $k = 1$ to 2 to 3 for the $[\pm 60]_{6s}$ laminate, and from $k = 2$ to 3 for the $[90]_{6s}$ orthotropic laminate. The 0^0 laminate never changes its buckled form since this plate is highly stiff in the loading direction. It can be observed that at mode change the load carried by a plate suddenly drops and slope of load end-shortening curves decreases, implying that the load carrying capability and postbuckling stiffness of the plate decrease after a mode change. It is also observed that the load drop at mode change is more drastical for those laminates which experience mode change deeper into the postbuckling range. It is likely that if a plate undergoes a violent change in the load end-shortening behavior as does the $[\pm 30]_{6s}$ laminate, the plate is likely to be vulnerable to failure at the instant of the mode change.

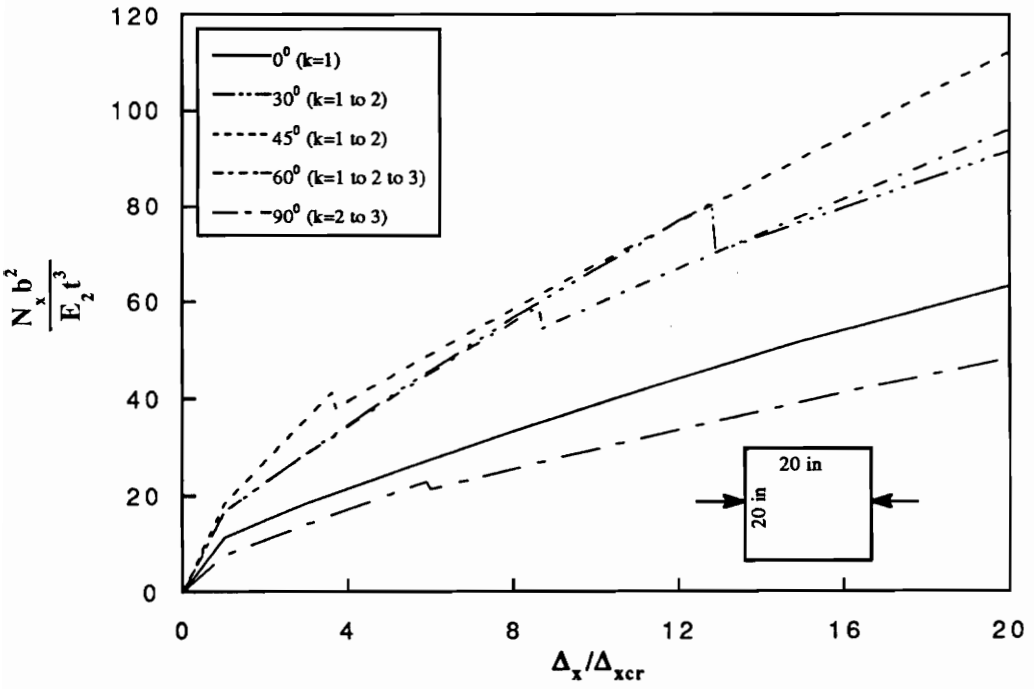

Fig. 14 Load end-shortening curves for angle-ply $[\pm\theta]_{6s}$ laminates (t=0.12 in)

3.4.5 Quasi-isotropic plates with various aspect ratios

The load end-shortening curves for quasi-isotropic plates, $[\pm 45/0/90]_{5s}$, with three different aspect ratios (a/b = 1, 4 and 8) are presented in Fig. (15). The loaded sides of plates are fixed to be 10 inches and total plate thickness is 0.2 inches. The y-normal edges of plates are free to move laterally. Fig. (15) shows that the square plate experiences the mode change once at $\Delta_x = 5.2\Delta_{xcr}$ while the long plates with aspect ratios a/b = 4 and 8 undergo the mode change two and four times, respectively, over the range of the applied end-shortening. The load end-shortening curve for the square plate shows an steep jump at mode change, which means that the load-carrying capability of the plate decreases considerably at the instant of mode change. The load end-shortening curves for the long plates, on the other hand, show no such an steep jump but only mild jumps at mode change, implying that the long plates loses its load-carrying capability only slightly at the instant of mode change. It can be also observed that after mode change the slope of load end-shortening curve for the square plate decreases more significantly than those for the long plates. The decrease of the slope in the load end-shortening curve after the mode change indicates the decrease of postbuckling stiffness. From this example, it can be concluded that shorter plates lose their load-carrying capability and postbuckling stiffness more significantly after they experience the mode change than do longer plates.

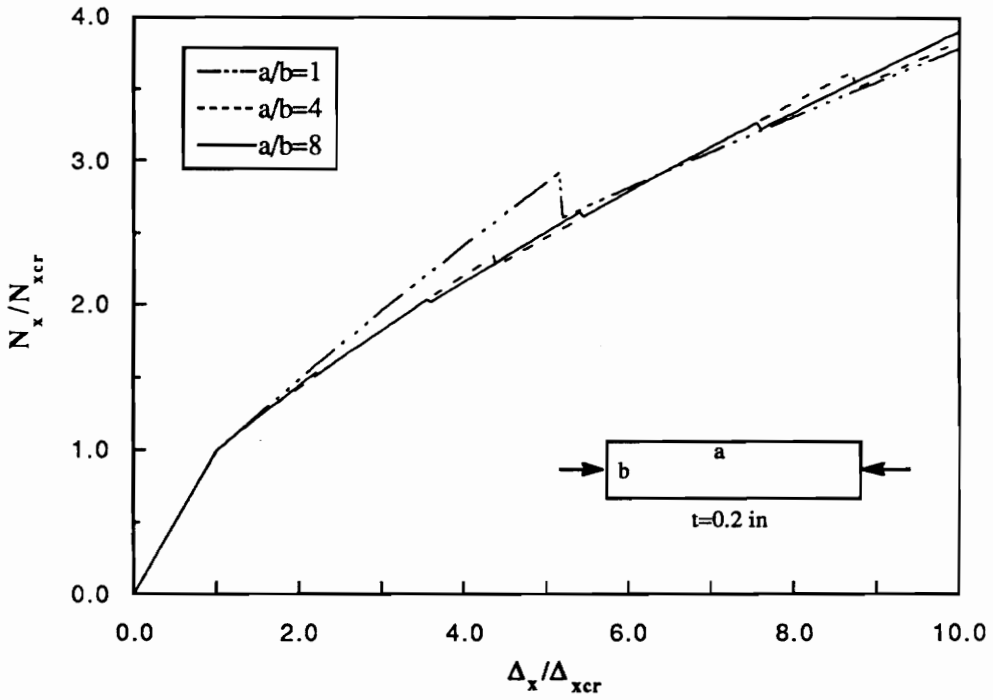

Fig. 15 Load end-shortening curves for rectangular quasi-isotropic $[\pm 45/0/90]_{5s}$ laminates (b=10.0 in)

CHAPTER IV

PREDICTION OF FAILURE LOAD OF LAMINATES IN THE POSTBUCKLING REGIME

One of the important issues that needs to be addressed for designing thin panels to operate in the postbuckling regime is the understanding of the failure characteristics of such panels. However, the mechanisms governing compression strength of laminated composite materials are very complicated and are not completely understood. Experimental reports in Refs. [54, 72-73] reveal that initiation of failure for laminates in the postbuckling load regime occurs at, or very close to, the nodal lines of the buckled panel close to the plate edges. Recently, Noor *et al.* [74] investigated structural response quantities at these locations and found that transverse shear strain energy density of panels reaches its maximum value at the location of initial failure. Although the transverse shear strain energy density may be a good candidate for characterizing the location or onset of local failure initiation, more investigations are needed to establish a failure criterion based on the observations in Ref. [74]. Identification of the exact failure mechanism for postbuckled plates is outside the scope of the present research. However, use of a simple criterion for the strain failure of laminates is investigated and prediction of such a model with the experimental results are presented.

4.1 Maximum Strain Failure Criterion

Micromechanical details are generally difficult to incorporate into the structural design and analysis. Consequently, macroscopic failure criteria are often used for failure prediction. In the present study, the maximum strain failure criterion is used in

prediction of the failure load of laminates under postbuckling compression. In fact, the work by Arnold *et al.* [53] indicates that the use of this criterion results in a reasonably good correlation between the experimental and analytically predicted failure loads. The failure surface for the maximum strain criterion is rectangular in strain space as shown in Fig. (16). In the maximum strain failure criterion, failure is assumed to occur if one of the following conditions is satisfied in any one of the plies within a laminate ;

$$\begin{aligned} \varepsilon_{11} > \varepsilon_{11}^{tu} \quad ; \quad \varepsilon_{11} < \varepsilon_{11}^{cu} \\ \varepsilon_{22} > \varepsilon_{22}^{tu} \quad ; \quad \varepsilon_{22} < \varepsilon_{22}^{cu} \\ |\gamma_{12}| > \gamma_{12}^{u} \end{aligned} \tag{4.1}$$

where ε_{11} and ε_{11} are ultimate tensile and compressive strains in the fiber direction, respectively, ε_{22} and ε_{22} are ultimate tensile and compressive strains in the direction perpendicular to fiber direction, respectively, and γ_{12} is the ultimate shearing strain.

The strain components in individual plies within a laminate can be calculated from the following equation,

$$\begin{Bmatrix} \varepsilon_x \\ \varepsilon_y \\ \gamma_{xy} \end{Bmatrix} = \begin{bmatrix} A^*_{11} A^*_{12} & 0 \\ A^*_{12} A^*_{22} & 0 \\ 0 \quad 0 & A^*_{66} \end{bmatrix} \begin{Bmatrix} \Phi_{,yy} \\ \Phi_{,xx} \\ -\Phi_{,xy} \end{Bmatrix} - z \begin{Bmatrix} w_{,xx} \\ w_{,yy} \\ 2w_{,xy} \end{Bmatrix} \tag{4.2}$$

where the definition of stresses (2.2), the inverse constitutive relation (2.8), and the Kirchhoff hypothesis (2.19) are used. The transformation of the above strain components in coordinate direction to the principal material direction is straight forward.

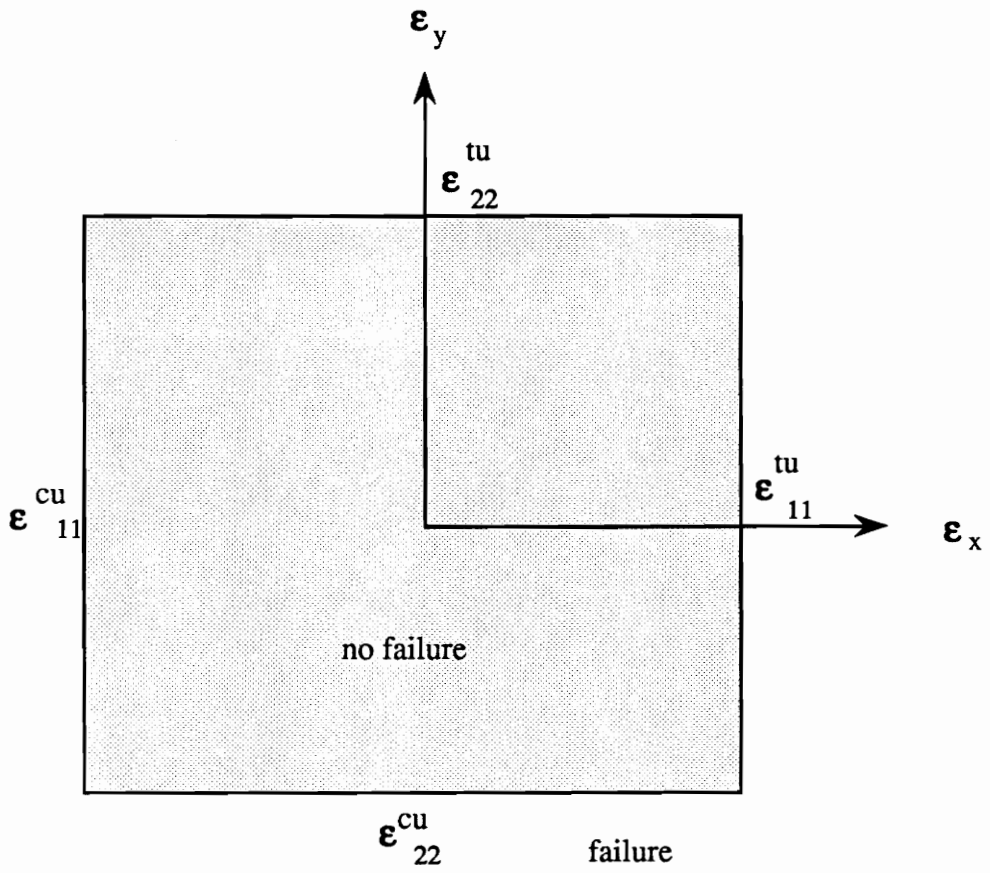

Fig. 16 Failure surface for maximum strain failure criterion

4.2 Correlation of Failure Load with Test

In this section, the failure loads of the specimens tested in Ref. [54] are compared with those predicted by the present postbuckling analysis in conjunction with the maximum strain failure criterion. The test specimens (T-300/5208 Gr/Ep) in Ref. [54] have three different stacking sequences; 24-ply orthotropic and quasi-isotropic laminates with $[\pm 45/0_2/\pm 45/0_2/\pm 45/0/90]_s$ and $[\pm 45/0/90]_{3s}$ sequences, respectively, and 16-ply quasi-isotropic laminates of $[\pm 45/0/90]_{2s}$. Material properties of the test specimens are given in Table (1). In test, the loaded sides of the specimen were clamped by fixtures and the y-normal edges were simply supported by knife-edge restraints to prevent the specimens from buckling as wide columns. Thus, the boundary conditions along the loaded sides between the test (clamped) and the present analysis (simply supported) are different. Nevertheless, if the aspect ratio is large, this difference in the boundary conditions along the loaded sides is believed to be negligible. In Ref. [54], the buckling loads of the test specimens were calculated using the STAGS computer code by applying boundary conditions similar to those of the test. The specimens were tested to failure by slowly applying a compressive load to simulate a static loading condition.

The failure loads of the specimens calculated by the present approach in conjunction with the maximum strain failure criterion and by the test are presented in Table (2). Also included in the table are the buckling loads of the specimens obtained by STAGS computer code in Ref. [54] and by the present orthotropic plate theory. The last three columns in Table (2) represent the number of half waves in the loading direction at failure. It can be observed from Table (2) that the buckling load calculated by the present analysis (Eqn. (2.32)) and by STAGS is in good agreement, especially for high

aspect ratio plates. The buckling loads calculated by the present orthotropic plate theory normalized by the STAGS results range from 0.81 to 1.00. The larger difference for short aspect ratio plates may be attributed to the difference in the boundary conditions along the loaded edges. As mentioned earlier, the use of simply supported condition for loaded edges in the present analysis may result in lower values of the buckling load for short panels compared to the STAGS results. The failure load of the specimens by the present method is calculated in two ways, i.e., by including the mode change and by ignoring it. To monitor failure of the specimens, the strain components at the top and bottom fiber of every layer are calculated in the principal material direction at potentially critical six points in the portion of a plate which includes one complete half-wave as shown in Fig. (17). For plates under postbuckling load, the maximum longitudinal membrane strain (ε_{11}) occurs along the unloaded sides parallel to x-axis in Fig. (17). This strain increases with increasing load. The longitudinal membrane strain in the center portion of the plate (along the line ABC), on the other hand, remains essentially constant and equals to its value at initial buckling. Large bending strains exist in this region of the plate and, as a result, the total compressive strain in the center portion of the plate may exceed the strain along the edges parallel to x-axis. The cross sections A-D and C-F represent the loaded side and buckling-mode nodal line, respectively. Along the cross section B-E, the out-of-plane displacements have maximum values. It can be seen from test result that the relatively short thin laminate (C20) fails at a load level five times of its buckling load. Table (2) shows that the failure load predicted by the present approach is also in good agreement with test results. The normalized failure load by maximum strain failure criterion with respect to test data is in the range of 0.81-1.01. If the mode change option is included in the analysis, the present approach predicts that specimens (C2, C3, C4, C13, and C16) fail after undergoing a mode change. The failure load of

these specimens, if the mode change is allowed in the analysis, is slightly smaller than that obtained by excluding this change. This is due to the sudden decrease of load-carrying capability and postbuckling stiffness after experiencing the mode change as was shown in Figs. (12)-(15). The present prediction of the failure load indicates that failure of all specimens occurs at the top layer of point F due to the excessive compressive strain in the fiber direction (ε_{11}). The difference in boundary conditions along the loaded sides between the test (clamped) and present analysis (simply supported) can be one of the reasons why both the buckling and failure loads of the specimens predicted by the present approach are smaller than the STAGS and test results. From this comparison, it seems that the maximum strain failure criterion can be used in predicting the failure load for graphite-epoxy plates under in-plane load beyond buckling although more tests covering a wide range of laminate stacking sequences and plate configurations are needed to use the criterion with more confidence.

Table 2. Comparison of buckling and failure load †

Specimen ID	b	a/b	b/t	Buckling load (lb/in)			Failure load (lb/in)					No. of half waves		
				N_{cr}^{ST}	N_{cr}^{Pr}	$\frac{N_{cr}^{Pr}}{N_{cr}^{ST}}$	Nf^{s}	Nf^{P1}	$\frac{Nf^{P1}}{Nf^{s}}$	Nf^{P2}	$\frac{Nf^{P2}}{Nf^{s}}$	m_T	m_{P1}	m_{P2}
(a) 24-ply orthotropic laminates, $[\pm 45/0_2/\pm 45/0_2/\pm 45/0/90]_s$ (a = 20.0, t = 0.126 in)														
C1	3.0	6.7	23.75	6292	6286	1.00	8314	6916	0.83	6956	0.84	6	6	5
C2	4.0	5.0	31.88	3652	3472	0.95	5506	4503	0.82	4723	0.86	4	5	4
C3	5.5	3.6	43.75	2002	1844	0.92	3759	3216	0.86	3469	0.93	3	4	3
C4	7.0	2.8	55.63	1284	1160	0.90	3146	2770	0.88	2956	0.94	2	3	2
C5	9.5	2.1	75.31	781	636	0.81	2556	2411	0.94	2411	0.94	1	2	2
(b) 24-ply quasi-isotropic laminates, $[\pm 45/0/90]_{3s}$ (a = 20.0, t = 0.122, C9; a = 19.76, C8,C10,C15; t = 0.134, C14; t = 0.126 in)														
C6	3.0	6.7	24.52	6609	6154	0.93	7285	6594	0.91	6594	0.91	7	7	7
C7	4.0	5.0	32.90	3749	3403	0.91	4756	4242	0.89	4242	0.89	6	5	5
C8	4.0	5.0	30.00	4421	4268	0.97	5596	5007	0.89	5007	0.89	6	5	5
C9	5.5	3.6	45.16	2038	1836	0.90	3302	3032	0.92	3032	0.92	4	4	4
C10	5.5	3.6	41.18	2487	2296	0.92	3629	3525	0.97	3525	0.97	4	4	4
C11	6.5	3.1	53.23	1522	1300	0.85	2767	2762	1.00	2762	1.00	3	3	3
C12	7.5	2.7	61.61	1166	989	0.85	2511	2418	0.96	2418	0.96	3	3	3
C13	8.5	2.4	69.68	925	771	0.83	2220	2194	0.99	2275	1.02	2	3	2
C14	9.0	2.2	71.56	823	719	0.87	2269	2261	1.00	2261	1.00	2	2	2
C15	9.0	2.2	67.95	972	850	0.87	2542	2570	1.01	2570	1.01	2	2	2
(c) 16-ply quasi-isotropic laminates, $[\pm 45/0/90]_{2s}$ (a = 20.0, t = 0.079 in)														
C16	4.0	5.0	51.00	1011	919	0.91	2134	1731	0.81	1821	0.85	6	6	5
C17	5.5	3.6	70.00	531	495	0.93	1756	1473	0.84	1473	0.84	5	4	4
C18	5.5	3.6	70.00	531	495	0.93	1716	1473	0.86	1473	0.86	4	4	4
C19	9.0	2.2	114.50	225	183	0.81	1125	1062	0.94	1062	0.94	2	2	2
C20	9.0	2.2	114.50	225	183	0.81	1125	1062	0.94	1062	0.94	2	2	2

† Test and STAGS results taken from Ref. [54]
N_{cr}^{ST}, N_{cr}^{Pr} ; buckling load by STAGS and Eqn. (2.33), respectively
Nf^{s}, Nf^{P1}, Nf^{P2} ; failure load by test, present method with and without mode change, respectively
m_T, m_{P1}, m_{P2} ; No. of half waves before failure by test, present method with and without mode change, respectively

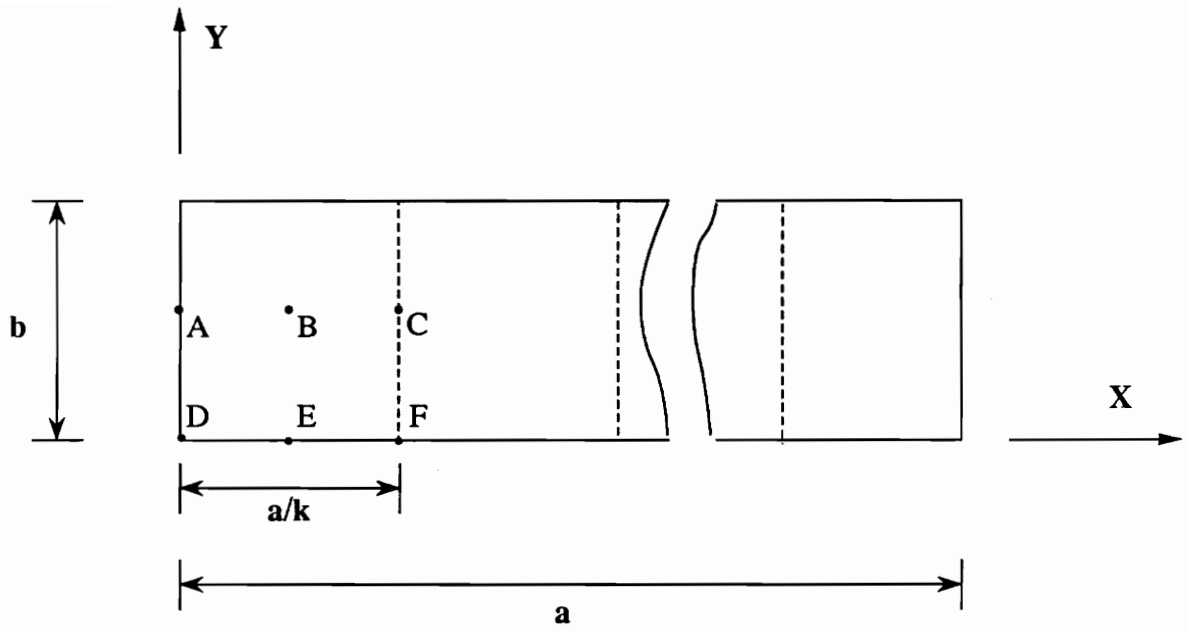

Fig. 17 Location where strains are calculated for the plate buckled into k half waves

CHAPTER V

OPTIMIZATION WITH DISCRETE DESIGN VARIABLES

In the optimum design of fiber reinforced composite materials, some or even all of the design variables such as fiber orientations and layer thicknesses are discrete-valued. In the present study, a penalty approach for the solution of nonlinear discrete optimization problems [75] is proposed. In addition to the standard penalty terms for constraint violation, the proposed approach introduces penalty terms to reflect the requirement that the design variables take discrete values. A variable-magnitude penalty term in the form of a sine function is introduced to force the design variables to take prescribed discrete values. Presently, the proposed approach is implemented with the extended interior penalty method of the optimization package NEWSUMT-A to solve nonlinear integer programming (NIP) problems. The extension of this technique to the nonlinear mixed-integer programming (NMIP) problems is expected to be achieved without difficulty. In the following sections, for the sake of clarity, a brief description of the SUMT is first presented. The form of the penalty function for the discrete-valued design variables and strategy used for the implementation of the procedure are discussed next. Finally, several design examples are considered to demonstrate the procedure, and results are compared with the those available in the literature.

5.1 Sequential Unconstrained Minimization Technique (SUMT)

The SUMT algorithm transforms the constrained optimization problem into a sequence of unconstrained problems. The classical approach to using SUMT is to

create a pseudo-objective function by combining the original objective function and the constraint equations. The constraints are added to the objective function in a way to penalize it if the constraint relations are not satisfied. That is, the constrained minimization problem,

$$\begin{aligned} &\text{Minimize} \quad : \quad F(X) \\ &\text{Such that} \quad : \quad g_j(X) \geq 0, \qquad j = 1,2,\ldots,n_g \\ &\text{where} \qquad\quad X = \{x_1, x_2, \ldots, x_n\}^T \end{aligned} \tag{5.1}$$

n : total number of design variables

n_g : number of constraints

is replaced by the following unconstrained problem,

$$\text{Minimize} \quad : \quad \Phi(X,r) = F(X) + r\sum_{j=1}^{n_g} y(g_j) \tag{5.2}$$

where $y(g_j)$ takes different forms depending on the method of penalty introduction [47]. The positive multiplier, r, in Eqn. (5.2) controls the contribution of the constraint penalty terms. For a given value of the penalty multiplier, r, Eqn. (5.2) describes the bounds of the feasible design space, often referred to as the response surface. As the penalty multiplier is decreased, the contours of the response surface conform with the original objective function and the constraints more closely. Therefore, minimization of the unconstrained problem is performed repeatedly as the value of r is decreased until the minimum value of the pseudo-objective function coincides with the value of the original objective function. Several response surfaces generated by using the extended interior penalty technique [47] for a problem with one design variable and a single constraint are shown in Fig. (18).

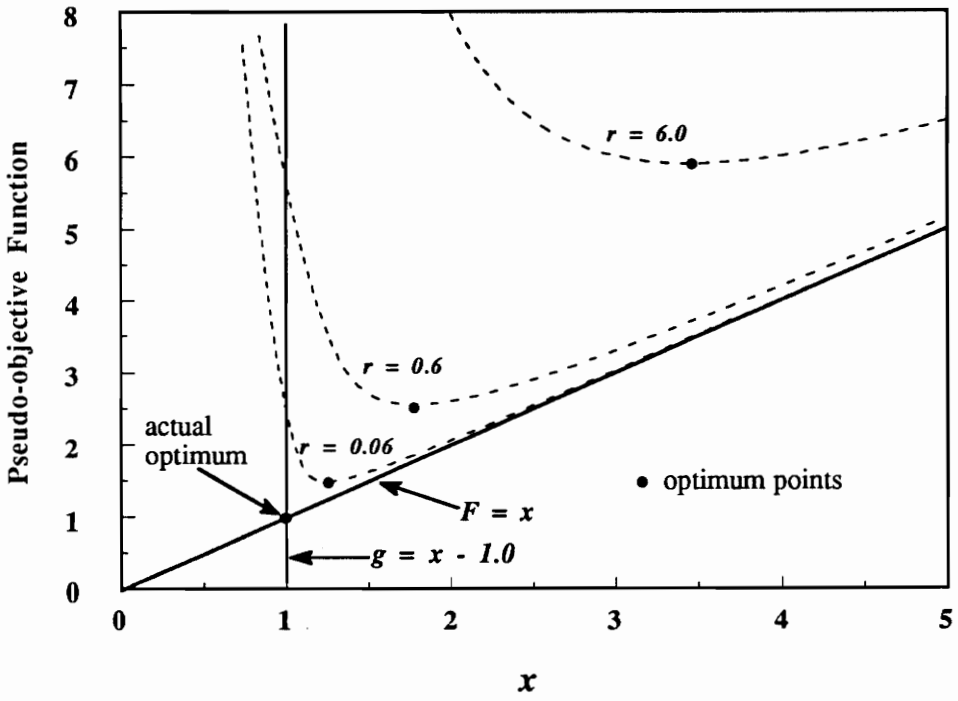

Fig. 18 Response surfaces for extended interior penalty function (Minimize f=x subject to g=x-1.0>0)

5.2 SUMT with Discrete-Valued Design Variables

The basic idea behind the proposed method is to include additional penalty terms in the pseudo-objective function to reflect the requirement that the design variables take discrete values. The general formulation for a problem having discrete variables is presented below.

$$\begin{aligned} &\text{Minimize} \quad : \quad F(X) \\ &\text{Subject to} \quad : \quad g_j(X) \geq 0 \quad , \quad j = 1,2,...,n_g \\ &\text{where} \qquad\quad x_i = \{d_{i1}, d_{i2}, ..., d_{iq}\}^T, \; i = 1,2,...,n_d \end{aligned} \tag{5.3}$$

n_d : number of discrete design variables

d_{ik} : k-th discrete value of the i-th design variable

q : number of discrete values for each design variable

In general, the number of available discrete values for each design variable may be different, or even in some cases continuous variation of some of the design variables may be allowed. The modified pseudo-objective function Ψ which includes the penalty terms due to constraints and the non-discrete values of the design variables is defined as

$$\Psi(X, r, s) = F(X) + r\sum_{j=1}^{n_g} p^*(g_j) + s\sum_{i=1}^{n_d} \Phi_d^i(X) \tag{5.4}$$

where r is the penalty multiplier for constraints, $p^*(g_j)$ can be chosen as $[\max\{-g_j(x), 0\}]^2$ for exterior penalty, $\frac{1}{g_j(x)}$ for interior penalty, and a linear or quadratic extension function [76] for extended interior penalty technique, s is the penalty multiplier for non-discrete values of the design variables, and $\Phi_d^i(X)$ denotes the penalty term for non-discrete values of the i th design variable. Different forms

for the discrete penalty function are possible. In the present study, the penalty terms $\Phi_d^i(X)$ are assumed to take the following sine-function form,

$$\Phi_d^i(X) = \frac{1}{2}\left(\sin\frac{2\pi\left[x_i - \frac{1}{4}(d_{ij+1} + 3d_{ij})\right]}{d_{ij+1} - d_{ij}} + 1\right) \tag{5.5}$$

where $d_{ij} < x_i < d_{ij+1}$. The proposed functions $\Phi_d^i(X)$ penalize only non-discrete design variables and assure the continuity of the first derivatives of the modified pseudo-function at the discrete values of the design variables. The discrete penalty functions of sine and elliptical forms were investigated. The elliptical function was found to be numerically unstable due to the discontinuity of its first derivative at the discrete values, although it can reflect the original response surface better than the sine function because of the wide flat range between discrete values of the elliptical function. The sine and elliptical functions are shown in Fig. (19).

The proposed method can be implemented with either exterior, interior, or extended interior penalty function approaches. In fact, the exterior and interior penalty techniques have limitations since the exterior penalty function is defined only in the infeasible domain, whereas the interior penalty method requires the initial design be feasible. These disadvantages can be overcome by using the extended interior penalty method which combines the interior penalty function in most of the feasible domain with an exterior continuation. The additional penalty terms for non-discrete design variables are incorporated into the optimization package NEWSUMT-A which employs the extended interior penalty approach; hence, the following discussion is confined to the extended interior penalty technique. In Eqn. (5.4), the response surfaces are determined according to the values of the penalty multipliers r and s, since they control the amount of penalty for the constraints and for the non-discrete values,

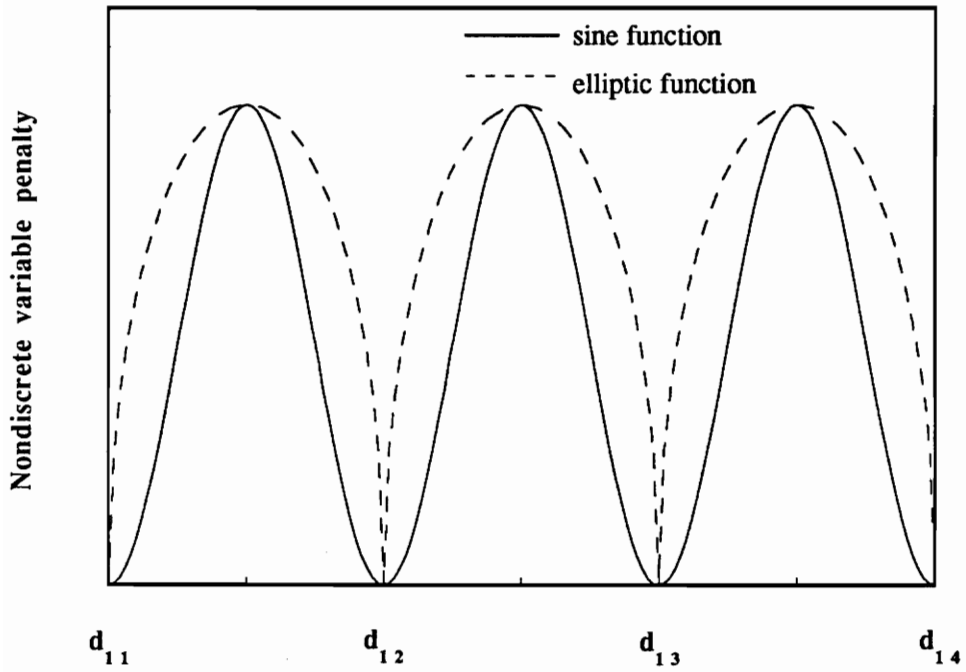

Fig. 19 Penalty functions for discrete design variables

respectively. As opposed to the multiplier r, the value of the multiplier s is initially zero and is increased slowly from one response surface to another. One of the important factors in the application of the proposed method is to determine when to activate s, and how fast to increase it to obtain a discrete optimum design. Clearly, if s is introduced too early in the design process, the design variables will be trapped by a local minimum, resulting in a sub-optimal solution. To avoid this problem, the multiplier s must be activated after several response surfaces which include only constraint penalty terms. In fact, since the optimum design with discrete values is often in the neighborhood of the continuous optimum, it may be desirable not to activate the penalty for the non-discrete design variables until a reasonable convergence to the continuous solution is achieved. This is especially true for problems with a large number of design variables and/or if the intervals between discrete values are very close. The modified pseudo-objective function Ψ defined in Eqn. (5.4) is shown in Fig. (20) for a problem with one design variable and one constraint.

5.3 Discussion of Implementation and Convergence Criterion

In using the SUMT, convergence is usually examined by comparing the total objective function with the corresponding value of the original objective function. A similar scheme is used to determine how close the design approaches to the continuous optimum before activating the discrete penalty. A criterion,

$$\varepsilon_c = \frac{\text{amount of constraint penalty}}{\text{objective function}} \tag{5.6}$$

is used, where ε_c denotes the tolerance to activate the discrete optimization process.

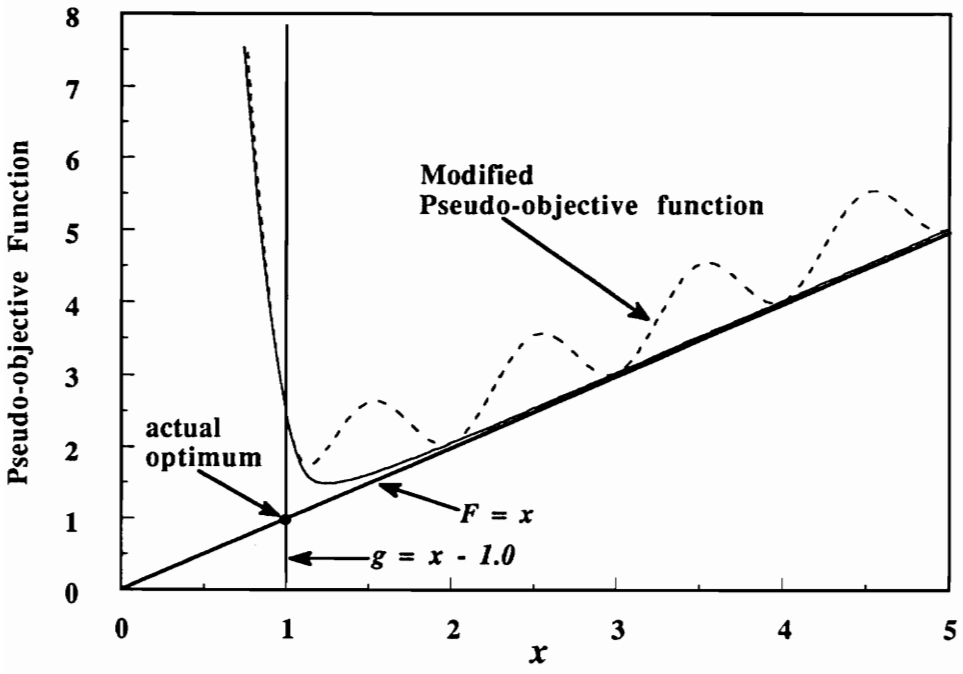

Fig. 20 Modified pseudo-objective function
(Minimize F=x subject to g=x-1>0 and x=1,2,3 ...)

One of the important aspects of the present procedure is to determine how big a penalty term to apply at the first discrete response surface. If a large s is applied in the first few discrete iterations, the design can be trapped at a local minimum. To prevent the design from stalling, s must be applied slowly. The magnitude of the non-discrete penalty multiplier, s, at the first discrete iteration, is calculated such that the amount of penalty associated with the non-discrete design variables is 10 percent of the constraint penalty. As the iteration for discrete optimization proceeds, the non-discrete penalty multiplier for the new iteration, $s^{(i+1)}$, is calculated by multiplying the $s^{(i)}$ by 3. Increasing $s^{(i)}$ implies that the discrete values for design variables are becoming more important than the constraint violation as the discrete optimization process continues.

Another important aspect of the proposed procedure is how to control the other penalty multiplier for the constraints, r, during the discrete optimization process. If r is decreased for each discrete optimization iteration as for the continuous optimization process, the design can be stalled due to excessively strict penalty on constraint violation. On the other hand, if r is increased, the design may move away from the optimum, resulting in a sub-optimal solution. Thus, it is logical to freeze the penalty multiplier r at the end of the continuous optimization process. However, the nearest discrete solution at this response surface may not be a feasible design, in which case the design is forced to move away from the continuous optimum by moving back to the previous response surface. This was achieved by increasing the penalty multiplier, r, by a factor of 10.

The solution process for the discrete optimization is terminated if the design variables are sufficiently close to the prescribed discrete values. The convergence criterion for discrete optimization used in this effort is

$$\varepsilon_d = \max\{ \min\{ \frac{|x_i - d_{ij}|}{d_{ij+1} - d_{ij}} , \frac{|x_i - d_{ij+1}|}{d_{ij+1} - d_{ij}} \}\}, i = 1,2,...,n_d \tag{5.7}$$

where ε_d is the convergence tolerance.

During the discrete iteration process, it was experienced that some of the design variables were sometimes trapped at the middle of two discrete values, especially for a large value of the penalty multiplier s. This is due to the vanishing nature of the first derivative of the sine function (5.5) at the mid-point. If it is detected that any one of the design variables is at the mid-point where the values of the first and second derivative of the sine function (5.5) approach 0 and -1, respectively, the trapping was avoided by removing the penalty terms for non-discrete values. This means only the original objective function and constraint penalty terms take part in the minimization process. The move direction is determined from the original response surface excluding the penalty terms due to non-discrete values. The flow chart for the proposed method combined with the extended interior approach is shown in Fig. (21).

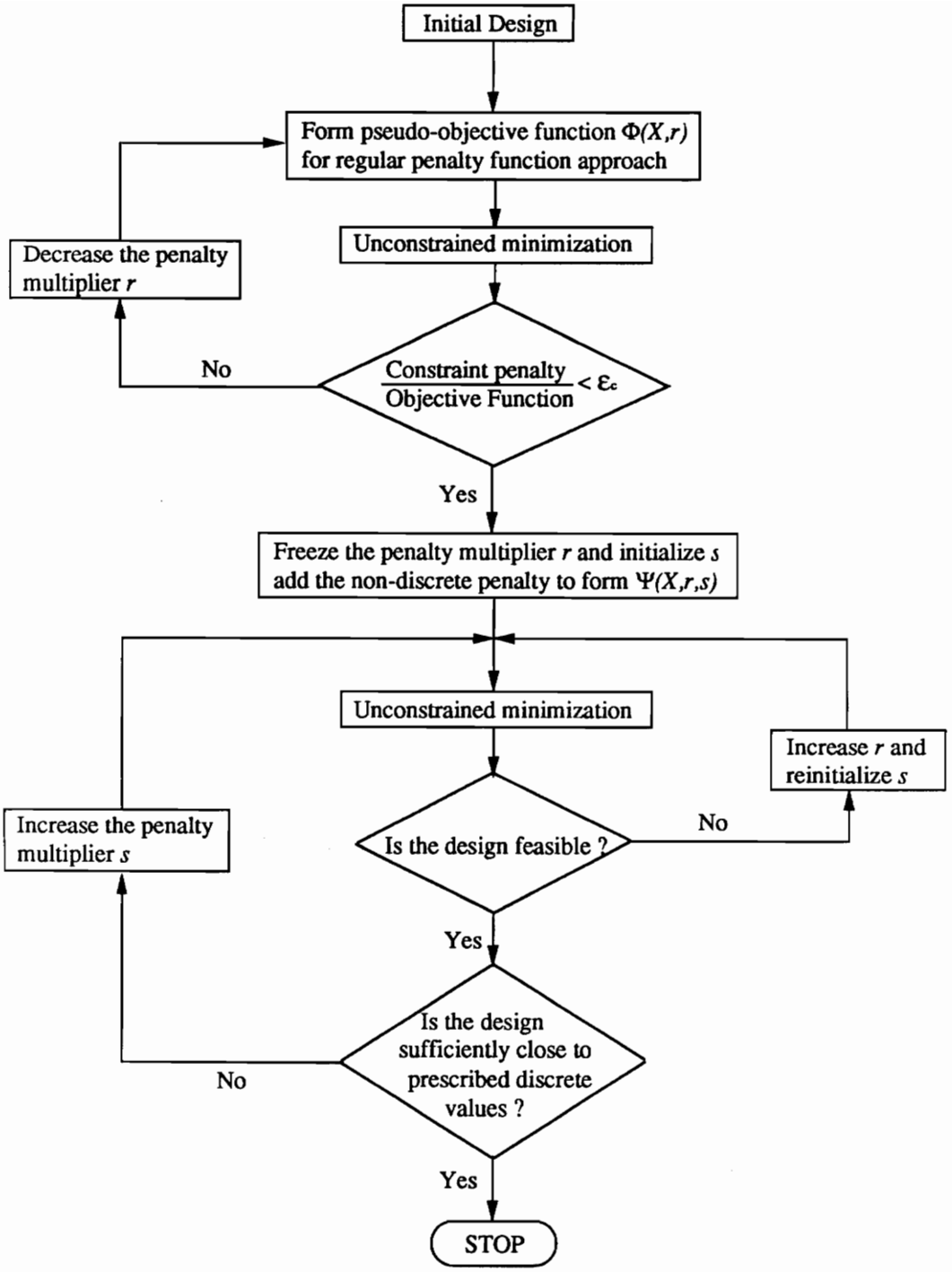

Fig. 21 Flow chart for continuous and discrete optimization process

5.4 Numerical Examples and Discussion

5.4.1 One Design Variable Problem

For pictorial demonstration, the following simple problem with one design variable and one constraint is presented.

$$\begin{aligned} &\text{Minimize} \quad : \quad F = x \\ &\text{Subject to} \quad : \quad g = x - 1.0 \geq 0 \\ &\text{where} \qquad\quad\; x = \{1.0, 2.0, ...\} \end{aligned}$$

The process of the discrete optimization is shown in Figs. 22-(a) and 22-(b) for two different values of ε_c. For each discrete iteration, the amount of penalty on the non-discrete values is increased, and the design converges to one of the discrete values. Fig. 22-(a) shows that the final design is trapped at the local minimum, $x = 2$, if the discrete design process begins too early ($\varepsilon_c = 0.5$). For this example, correct discrete optimum was obtained if $\varepsilon_c < 0.5$.

5.4.2 Ten-Bar Truss Problem

The classical 10 bar truss is shown in Fig. (23). The design variables are the cross-sectional areas of the 10 bars. The structural weight, W, is minimized subject to a maximum stress limit of 25,000 psi and maximum displacement limit of 2.0 in. All design variables are assumed to take the discrete values, x_i = { 0.1, 0.5, 1.0, 1.5, 2.0, 2.5,.... }. The discrete optimum solution obtained by proposed method is compared in Table (3) with other solutions by different techniques obtained from Ref. [62]. The solution by the proposed method is different from all other solutions. The

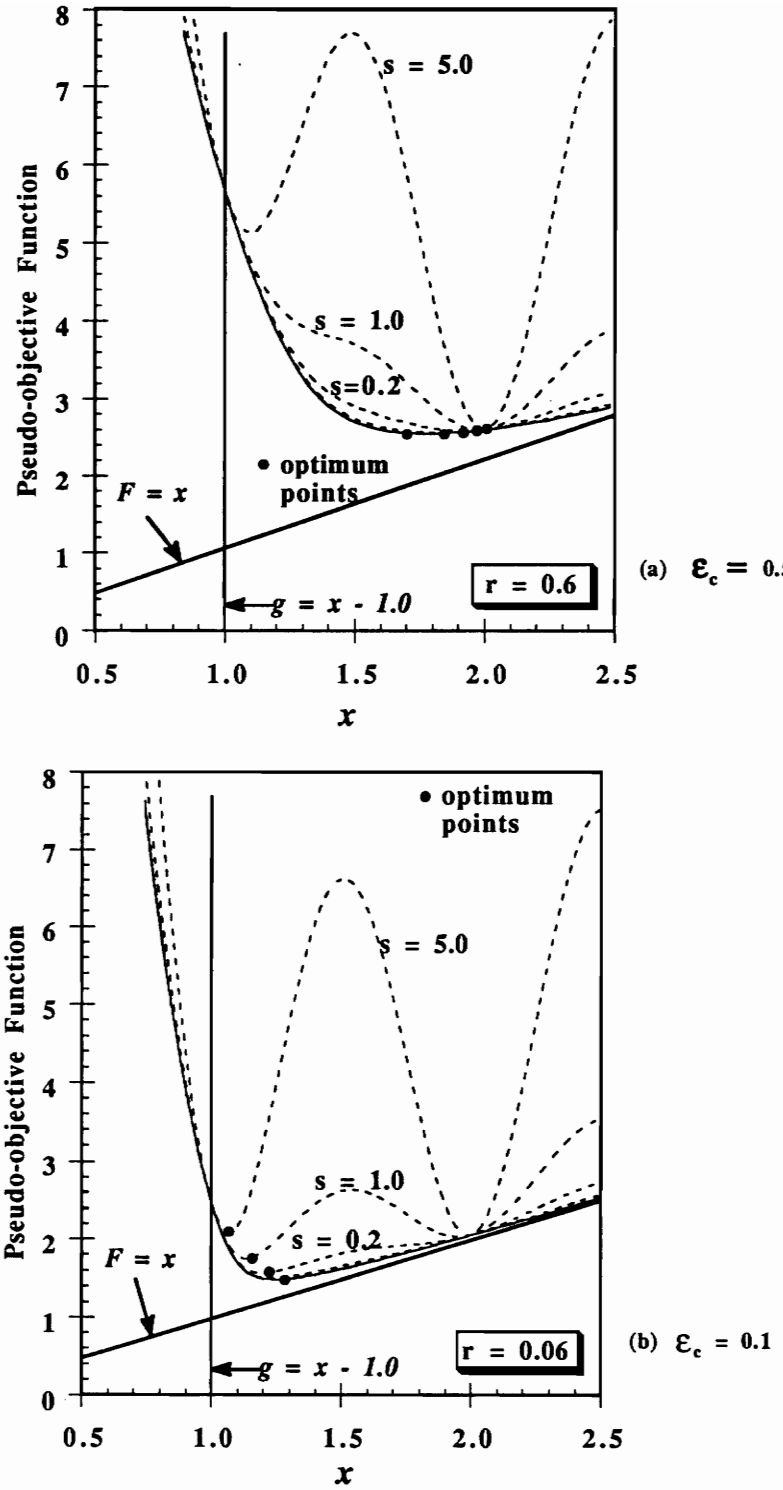

Fig. 22 Discrete optimization for different starting points

results by Branch & Bound, Lagrangian relaxation, and the proposed method are slightly infeasible though negligible in an engineering sense. It can be seen from Table (3) that a different starting point for discrete optimization, ε_c, can result in different discrete solutions. The continuous solution was obtained in 8 response surfaces, and discrete solutions were found in 12 and 16 response surfaces for $\varepsilon_c = 0.01$ and 0.005, respectively. With a relatively large number of design variables as in this case, the continuous solution process must be terminated in the close neighborhood of the continuous optimum.

5.4.3 Twenty-five Bar Truss Problem

The classical 25 bar truss is shown in Fig. (24). The material data, the constraints on displacements and stresses, and two loading conditions are summarized in Tables (4), (5), and (6), respectively. Due to the geometrical symmetry of the space truss, only eight different member sizes are allowed, as shown in Table (7). All design variables are allowed to take following discrete values; x_i = { 0.1, 0.4, 0.7, 1.1, 1.5, 1.8, 2.0, 2.5, 3.0, 3.5, 4.0, 4.5 }. The continuous and discrete optimum solutions are summarized in Table (7). The discrete solution by the proposed technique is feasible whereas the solution presented in Ref. [60] violates the displacement constraints. The continuous optimum was found in 6 response surfaces and discrete solutions in 9, 10, and 14 response surfaces for $\varepsilon_c = 0.1$, 0.01, and 0.001, respectively. For the above three different values of ε_c, the same discrete optimum solutions were found.

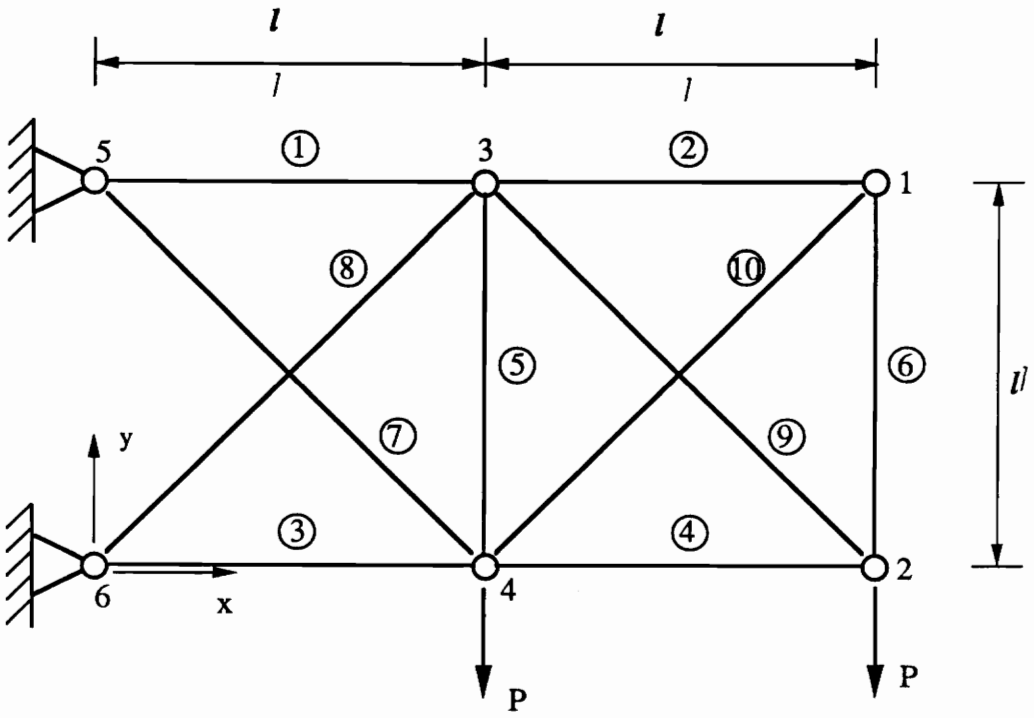

E = 10 msi

P = 100 kips

$l/$ = 360 in

$\rho = 0.1$ lbm/in^3

Fig. 23 Ten bar truss

Table 3. Discrete solutions for 10 bar truss ($\varepsilon_d = 0.001$)

	Branch & Bound	Generalized Lagrangian	Dynamic Round-off	Schmit & Fluery	Proposed Method(1)	Proposed Method(2)
Feasible	no	yes	yes	no	no	yes
W(lbs)	5059.9	5067.3	5077.9	5059.9	5059.9	5077.9
$x_1(in^2)$	30.5	30.0	30.0	30.5	30.5	30.5
x_2	0.1	0.1	0.1	0.1	0.1	0.1
x_3	23.0	23.5	23.5	23.0	23.5	24.0
x_4	15.5	15.0	15.5	15.5	15.0	15.0
x_5	0.1	0.1	0.1	0.1	0.1	0.1
x_6	0.5	0.5	1.0	0.5	0.5	0.5
x_7	7.5	7.5	7.5	7.5	7.5	7.5
x_8	21.0	21.0	21.0	21.0	21.0	21.0
x_9	21.5	22.0	21.5	21.5	21.5	21.5
x_{10}	0.1	0.1	0.1	0.1	0.1	0.1

(1) $\varepsilon_c = 0.005$, (2) $\varepsilon_c = 0.01$

Table 4. Material data for 25 bar truss

Material	:	Aluminum
Young's modulus	:	10^7 psi
Specific mass	:	0.1 lbm/in
Minimum area	:	0.01 in^2

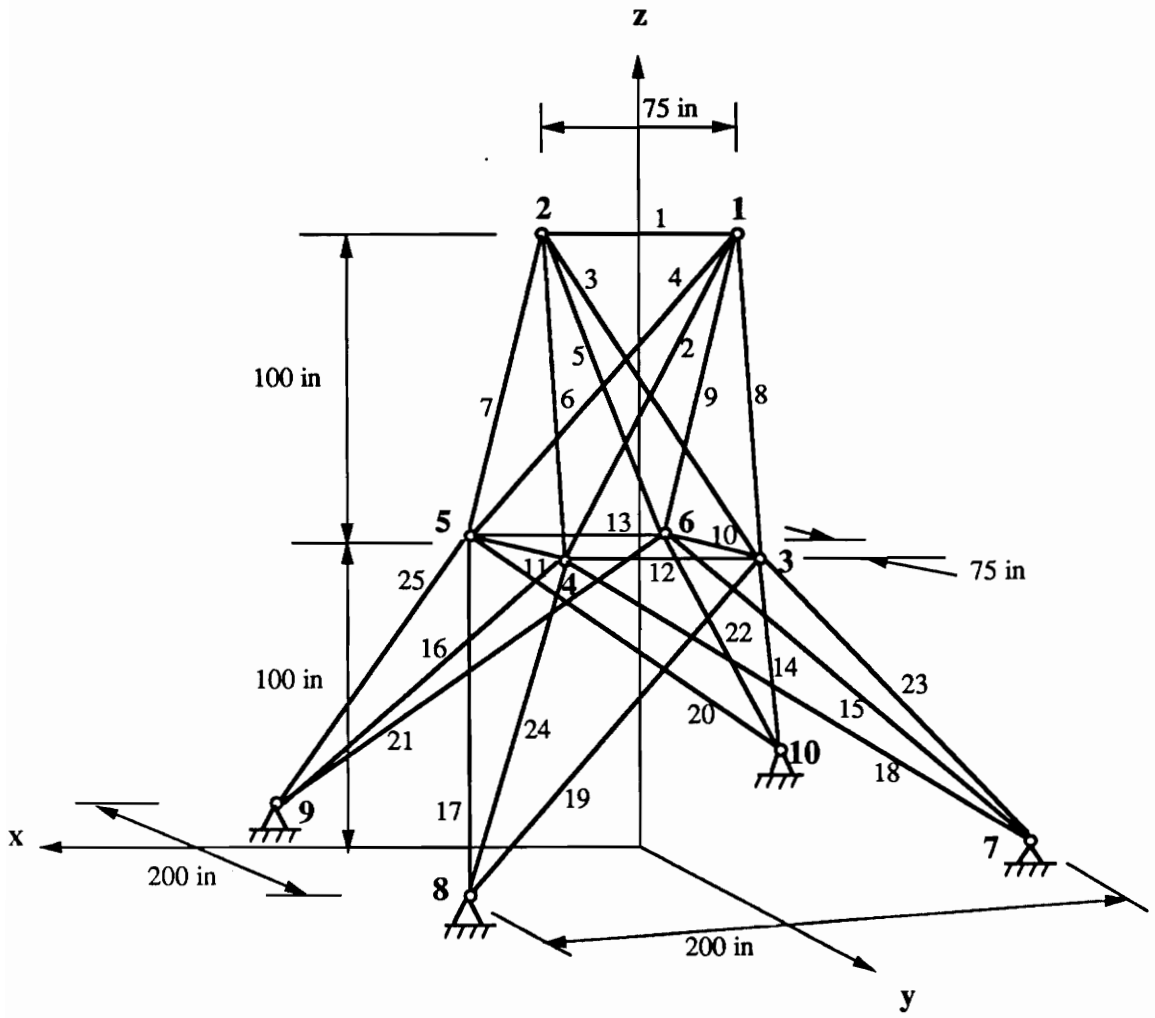

Fig. 24 Twenty-five bar truss

Table 5. Displacement and stress limits for 25 bar truss

	Displacement limits (in)		
Node	X	Y	Z
1	± 0.35	± 0.35	± 0.35
2	± 0.35	± 0.35	± 0.35

	Stress limits (psi)	
Members	Tension	Compression
1,10-13	40,000	-35,092
2-5	40,000	-11,590
6-9	40,000	-17,305
14-17	40,000	-6,759
18-21	40,000	-6,959
22-25	40,000	-11,082

Table 6. Loading conditions for 25 bar truss

Load case	Node	X	Y	Z
1	1	1,000 †	10,000	-5,000
	2	0	10,000	-5,000
	3	500	0	0
	6	500	0	0
2	5	0	20,000	-5,000
	6	0	-20,000	-5,000

† lb

Table 7. Continuous and discrete solutions for 25 bar truss

Design variables (members)	Continuous optimum solution	Rounded upward solution	Discrete solution (Ref. 55)	Proposed method
1 (1)	0.03	0.10	0.10	0.10
2 (2-5)	0.08	0.10	0.10	0.10
3 (6-9)	3.27	3.50	3.50	3.50
4 (10,11)	1.29	1.50	1.50	1.50
5 (12,13)	1.90	2.00	1.50	1.80
6 (14-17)	2.00	2.00	2.00	2.00
7 (18-21)	0.03	0.10	0.10	0.10
8 (22-25)	3.65	4.00	3.50	3.50
W(lbs)	535.1	573.7	539.5	544.0
Feasible	yes	yes	no	yes

CHAPTER VI

MINIMUM-WEIGHT DESIGN OF LAMINATED PLATES FOR POSTBUCKLING STRENGTH

In this chapter, the optimum design of laminated composite plates for postbuckling strength is considered. During the optimization process, the Marguerre-type energy method developed in Chapter II is used for the postbuckling analysis with the out-of-plane displacement assumed in the form of a six terms Fourier sine series. Using six terms series was shown to predict the postbuckling responses accurately for a wide range of generally orthotropic plates. In addition, plates are allowed to change their buckled shape in the postbuckling regime to observe the effect of mode change on the optimum designs. The mode change during the postbuckling load step is predicted based on the energy consideration described in Chapter III. The design variables are assumed to take discrete values, and the discrete optimization is carried out by the modified penalty approach presented in Chapter V.

6.1 Description of Minimum-Weight Design Problems

One of the purposes of the present study is to compare the weight of a plate designed to serve in the postbuckling load regime with that of the one designed for buckling strength. To investigate the resulting weight savings, two types of minimum-weight design problems for a simply-supported, rectangular, symmetrically laminated plate under in-plane compression are considered. One of the design problems is to minimize the weight of a plate such that the buckling and failure loads of the plate are greater

than a prescribed design load, N_D. The linear buckling load of the plate is calculated from Eqns. (2.32) and (2.33) for freely shifting and restrained y-normal edges, respectively, based on the orthotropic plate theory. In the second case the weight of a plate is minimized such that the laminate does not fail due to the constraint in the postbuckling regime when the same in-plane design load N_D is applied. The maximum strain failure criterion is used in predicting the failure load of laminates. Only the thicknesses of each layer with a specified fiber orientation are treated as design variables, and are assumed to take discrete values which are the integer multiples of the thickness of a single layer. In addition to the thickness design variables being forced to assume only discrete values, a side constraint that forces each layer with the same fiber direction not to have more than four repeating plies is imposed to avoid excessive interlaminar stresses. For an $N-$layered laminate with length a and width b, the minimum-weight design problem with constraints on the buckling and failure load is posed as

$$
\begin{aligned}
\text{Minimize} \quad &: \quad F = \frac{W}{\rho} = ab\sum_{i=1}^{N} t_i \\
\text{Subject to} \quad &: \quad g_1 = \frac{\hat{N}_{xcr}}{N_D} - 1.0 \geq 0 \\
&\qquad\quad g_2 = \frac{\hat{N}_f}{N_D} - 1.0 \geq 0 \\
&\qquad\quad 0.0 \leq t_i \leq 0.02 \text{ in} \quad , \quad i = 1,2,...,n \\
&\qquad\quad t_i = \{\ 0.0,\ 0.005,\ 0.010,\ 0.015,\ 0.020\ \} \text{ in}
\end{aligned}
\tag{6.1}
$$

where g_1 and g_2 are the constraints on the buckling and postbuckling strength, respectively, N_f is the failure load, n is the number of design variables, and t_i 's are the layer thicknesses design variables.

If the panel is to be designed for postbuckling performance, the optimization problem is stated as

$$\begin{aligned} \text{Minimize} \quad &: \quad F = \frac{W}{\rho} = ab\sum_{i=1}^{N} t_i \\ \text{Subject to} \quad &: \quad g = \frac{N_f}{N_D} - 1.0 \geq 0 \\ & \quad 0.0 \leq t_i \leq 0.02 \text{ in} \quad , \quad i = 1,2,...,n \\ & \quad t_i = \{\ 0.0,\ 0.005,\ 0.010,\ 0.015,\ 0.020\ \} \text{ in} \end{aligned} \tag{6.2}$$

6.2 Implementation and Efficiency Measures

Calculation of the failure load in Eqn. (6.2) requires the nonlinear postbuckling analysis, since failure of a thin plate occurs far beyond its buckling load. In the present optimization process, the postbuckling procedure discussed in Chapters II and III is applied. Although thin plates are known to change their buckled form before failure in the postbuckling regime, an option to include or exclude mode change is provided in the analysis module to evaluate the effects of this phenomenon on minimum-weight designs. If a plate is allowed to change its buckled form before reaching the failure load, the postbuckling analyses for two successive mode shapes are required. The postbuckling analysis procedure for the optimization is schematically illustrated in Fig. (25) where $k^{(i)}$ denotes the number of buckle half waves at the i th postbuckling load step, $\Delta^{(i)}$, $\Pi(k)$ is the total potential energy of the plate which buckles into k half waves, and Δ_{inc} is the increment of applied end-shortening. If the mode change is not taken into account during the optimization, the analysis for the next deformed shape with $k+1$ half waves is not necessary. The values of buckling and failure load calculated from the buckling and postbuckling analysis are used by NEWSUMT-A optimizer in calculating the buckling and postbuckling

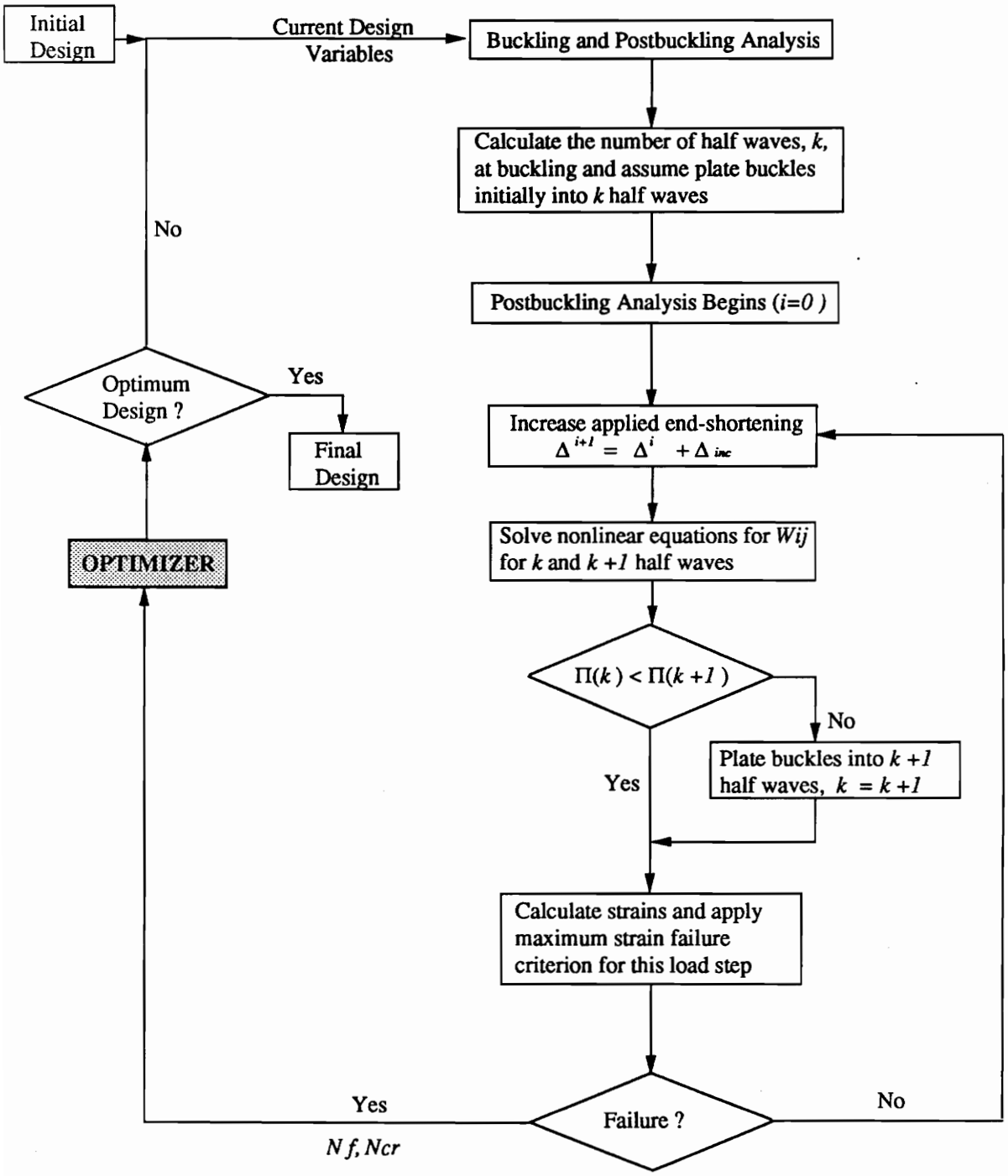

Fig. 25 Flow chart for postbuckling analysis during optimization

constraints. The derivatives of buckling and failure load are calculated by the finite difference method with a step size 0.01.

Some measures to save computing time can be introduced in the nonlinear analysis module. As can be seen from Fig. (25), the only information that the optimizer uses from the analysis program is the failure load of the plate for a given set of design variables, which is calculated based on a step-by-step load increment. If the number of load increment steps can be reduced by half, for instance, the total computing time for the optimization can also be reduced roughly by the same amount. However, the convergence in solving the nonlinear equations can be jeopardized if a step size which is too large is used. Several different analyses prior to the optimization can help selecting a proper step size. Another measure to reduce the computing time is the use of unequal step sizes. For a thin plate, failure usually occurs not at an initial load step, but at a deep postbuckling load step. Thus, the initial step size can be much larger than the step size near failure. The appropriate size of a certain load step can be determined by monitoring the strain state of a laminate for a previous load step, since the maximum strain failure criterion is used to calculate the failure load. If in the current load step failure is judged to be near, a smaller step size needs to be used in the next load increment. By starting the nonlinear analysis not from the initial postbuckling load range but from several times the buckling load for very thin plates, the computing time involved in the optimization can also be reduced. These efficiency measures are implemented in the computer program.

6.3 Numerical Examples and Discussion

The plate design problems expressed in Eqns. (6.1) and (6.2) are applied to square and rectangular graphite-epoxy plates with 0, ± 45, and 90 degree plies. Since the bending-twisting coupling terms, D_{16} and D_{26}, are assumed to be small compared to the D_{66} term in the present buckling and postbuckling analyses, care is taken in the selection of fiber orientations and stacking sequences of a laminate to reflect this restriction. Initially, a quasi-isotropic laminate is generated internally in the computer program to represent the stacking sequence of $[+45/-45/0/90]_{5s}$, for which D_{16} and D_{26} are expected to be less than 10% of D_{66}. The design variables are thicknesses of individual $\pm 45^0$, 0^0, and 90^0 layers such that the design problems have three design variables. The $+45^0$ and -45^0 layers are controlled by a single design variable so that the laminate is maintained to be a balanced one throughout the optimization process. The ply orientations of $\pm 45^0$, 0^0 and 90^0 are widely used in practical applications. Furthermore, the maximum strain failure criterion has been successfully used in Chapter IV in predicting the failure load of laminates with similar stacking sequences. When a constraint on the failure load is imposed, the mode change option is included. The design variables are forced to take prescribed discrete values by the approach presented in the previous chapter.

6.3.1 Square quasi-isotropic plates

Continuous optimum solutions covering a wide range of design loads are summarized in Tables (8) and (9) for square laminates with freely shifting and restrained y-normal edges, respectively. For each design load level, three optimum solutions for different behavioral constraints are presented. The first row represents optimum solutions for

the problem with constraints on buckling and failure load, and the second and third rows are the optimum solutions for design problems with a constraint on failure load by excluding and including a mode change option, respectively. Final values of the design variables are given in the third, fourth and fifth column. Total laminate thickness and plate slenderness ratio (b/t) are given in the sixth and seventh column, respectively. In the last two columns, normalized values of the applied end-shortening with respect to critical end-shortening at failure (Δ_x^f) and at mode change (Δ_x^{mc}) are presented. The values in parenthesis in the last column are obtained by postbuckling analysis with the mode change included after obtaining optimum solutions without consideration of mode change. The initial thickness of all layers are chosen as 0.01 in (2 plies). When the values of initial design variables are changed, optimal individual layer thicknesses showed slight variations, but almost the same values of the objective function (weight) were obtained regardless of the initial values of the design variables. The converged solutions in Tables (8) and (9) are obtained in 7 to 9 response surfaces.

For a buckling resistant design problem (6.1), $\pm 45^0$ layers tend to be thicker than 0° and 90° layers, whereas the 0° and 90° layers have the same thickness for the square laminate with freely shifting y-normal edges. In fact, sensitivities of the objective function and the buckling load are shown to be always the same with respect to the thicknesses of the 0° and 90° layers as long as the square plate buckles into a single half wave (see Appendix E for proof). Accordingly, the 0° and 90° layers can be treated as one design variable for this buckling design problem similar to the θ and -θ layers. When the laminates with restrained y-normal edges are designed to be buckling resistant, $\pm 45^0$ and 0° layers are more evenly distributed and thicker than the 90° layers. For the postbuckling strength design problems, however, relative

thicknesses of individual layers show a wide scatter for different values of the design load.

For some postbuckling strength design problems (6.2) with small values of design load (N_D = 1-2 and 1-3 kips/in for freely shifting and restrained y-normal edges, respectively), no optimum solutions can be obtained if the mode changes are not allowed in the analysis. These plates tend to be very thin (b/t > 100) for such small values of design load, and failure of the plates occurs at a load level into the deep postbuckling regime. At the large values of the applied end-shortening the solution of the nonlinear equations (2.30) experiences convergence difficulties if the mode changes are not taken into account. For very thin plates, the mode change is likely to occur at some load level along the load range before the failure load. For instance, the failure of plates designed for $N_D = 1$ kips/in with mode change option occurs at load levels 100 Δ_{xcr} and 156 Δ_{xcr} for freely shifting and restrained y-normal edges, respectively. The postbuckling analysis shows that these plates, which have slenderness ratios (b/t) of 223 and 229, undergo mode change twice before the failure load is reached. For relatively larger values of design load ($N_D \geq 6$ and $N_D = 10$ kips/in for freely shifting and restrained y-normal edges, respectively), on the other hand, optimum postbuckling strength designs show no mode change before failure. The postbuckling analysis of the optimum design for $N_D = 10$ kips/in shows that the plate with freely shifting y-normal edges, for instance, fails at a load level 2.5 Δ_{xcr} while changing its buckled shape from a symmetric to anti-symmetric mode at 5 Δ_{xcr}. For intermediate values of design load ($3 \leq N_D \leq 6$ and $4 \leq N_D \leq 10$ kips/in for freely shifting and restrained y-normal edges, respectively), two different optimum solutions can be obtained, depending upon the mode change option. Among two optimum solutions, the design for which a plate is allowed to change its buckled shape is 5.7 to

15.0% heavier than the design without consideration of mode change. If a plate fails shortly after experiencing a mode change (e. g. $N_D = 5$ and $N_D = 6 - 8$ kips/in for freely shifting and restrained y-normal edges, respectively), the difference in the final weight between the two designs is in the range of 5.7 to 10.0%. If a plate fails far beyond the load level at mode change (e. g. $N_D = 3$ and 4 kips/in for freely shifting and restrained y-normal edges, respectively), the difference in the final plate weight between two designs is more significant and is in the range of 9.1 to 15.0%.

Total laminate thickness of the optimal designs listed in Tables (8) and (9) is plotted as a function of the design load in Fig. (26). It can be seen that for buckling resistant designs plates with freely shifting y-normal edges have an advantage over the plates with restrained y-normal edges from the stand point of weight. On the contrary, plates restrained from the lateral in-plane movement along the y-normal edges are lighter than plates with freely shifting y-normal edges if they are designed for postbuckling performance. It can also be seen from Fig. (26) that the laminates designed for postbuckling strength require more material if the mode change allowed, compared to designs without mode change. This is because of the decrease of load-carrying capability and postbuckling stiffness after a mode change. In fact, a similar trend was observed when the failure load of laminates with and without mode change are compared with Starnes' test results [54] in Chapter IV. To quantify the weight savings when plates are designed for postbuckling strength, the weight of laminates normalized by the weight of their buckling resistant counterparts is plotted in Fig. (27) as a function of the design load. It can be seen that the weight savings, if designed for the postbuckling strength, are substantial, especially for lightly loaded thin plates and for plates with restrained y-normal edges. The weights of plates designed to buckle are 16 to 62% and 34 to 67% lighter than those of plates designed not to buckle for freely

shifting and restrained y-normal edges, respectively, over the range of design service load considered. It can be also observed that as the value of design load decreases, the slope of the curves in Fig. (27) reduces rapidly, which indicates that the achievement in weight savings becomes much more significant as the decrease of design load. In addition, the mode change affects the postbuckling strength design and results in more conservative design for lightly loaded plates while it has no effect on the optimum solutions for heavily loaded plates.

In Tables 10a and 10b, the discrete solutions obtained by the approach in the previous chapter along with some other neighboring discrete solutions are presented for the buckling and postbuckling strength designs, respectively. The laminates have the same stacking sequence and boundary conditions along the y-normal edges as the ones shown in Table (9). The discrete optimization processes are activated at $\varepsilon_c = 0.02$, and the present approach yielded feasible discrete solutions for every case considered. Some other neighborhood discrete solutions obtained manually are also presented in the Tables, but better designs without violating the constraint were not possible. The numerical values inside parenthesis in Tables (8) and (9) indicate that designs are not in the feasible domain.

All the manually obtained discrete solutions that were lighter than the optimally obtained discrete design had their buckling failure or strength failure loads to be lower than the design loads given in the first column. However, it was possible, for both the buckling and postbuckling designs, that some manual discrete designs which had the same weight as the optimal designs were capable of carrying loads larger than the design requirement load. Such designs would provide a wider strength margin than the optimal ones and, therefore, are better than the optimal designs. While the continuous

optimum solutions are obtained in 7 to 9 response surfaces, the number of response surfaces for discrete optimum solutions varies rather widely from 8 to 15. It was seen that the optimizer experiences difficulty in convergence when the discrete solutions are forced to infeasible regions. If this happens, the optimizer moves to other response surfaces and as a result requires many response surfaces.

Table 8. Continuous optimum solutions for $[\pm 45/0/90]_{s}$, laminates with freely shifting y-normal edges (a = b = 20 in)

N_D (lb/in)	Behavior constraint[1]	$t^{45°}, t^{-45°}$ (in)	$t^{0°}$ (in)	$t^{90°}$ (in)	$\sum t_i$ (in)	b/t	Δ_x^f ($\times \Delta_{xcr}$)	Δ_x^{mc} ($\times \Delta_{xcr}$)
1000	Buckling	0.007144	0.004631	0.004631	0.23550	84.9	---	---
	FLR1 †	---	---	---	---	---	---	---
	FLR2	0.002770	0.002900	0.000529	0.08969	223	100.0	8.0, 49.0[2]
2000	Buckling	0.008914	0.005938	0.005938	0.29704	67.3	---	---
	FLR1 †	---	---	---	---	---	---	---
	FLR2	0.004096	0.006131	0.001525	0.15848	126.2	25.0	8.8
3000	Buckling	0.011704	0.005089	0.005089	0.33586	59.6	---	---
	FLR1	0.005838	0.006468	0.000790	0.18934	105.6	13.4	(8.2) *
	FLR2	0.005868	0.006758	0.002338	0.20832	96.0	12.4	7.4
4000	Buckling	0.011998	0.006603	0.006603	0.37202	53.8	---	---
	FLR1	0.006678	0.006443	0.003984	0.23783	84.1	8.0	(6.1)
	FLR2	0.007013	0.006623	0.005168	0.25817	77.5	7.2	5.8
5000	Buckling	0.016426	0.003178	0.003178	0.39208	51.0	---	---
	FLR1	0.007564	0.007880	0.003968	0.26976	74.1	6.6	(6.6)
	FLR2	0.007532	0.006951	0.006852	0.28867	69.3	6.0	5.5
6000	Buckling	0.017056	0.003813	0.003813	0.41738	47.9	---	---
	FLR1	0.009459	0.007208	0.004550	0.30676	65.2	4.7	(5.6)
	FLR2 ‡	---	---	---	---	---	---	---
8000	Buckling	0.016593	0.006649	0.006649	0.46484	43.0	---	---
	FLR1	0.010849	0.008176	0.006541	0.36415	54.9	3.4	(5.3)
	FLR2 ‡	---	---	---	---	---	---	---
10000	Buckling	0.017105	0.008033	0.008033	0.50276	39.8	---	---
	FLR1	0.014217	0.008169	0.005516	0.42119	47.5	2.5	(5.0)
	FLR2 ‡	---	---	---	---	---	---	---

Δ_x^f, Δ_x^{mc} : Applied end-shortening at failure and at mode change, respectively
(1) FLR1 and FLR2 : failure constraint without and with mode change, respectively
(2) Mode changes from 1 to 2 buckle waves at $8\Delta_{xcr}$ and 2 to 3 waves at $49\Delta_{xcr}$
† Unstable solutions in postbuckling analysis
‡ No mode change up to failure
* Values in parenthesis are obtained by analysis after optimization

Table 9. Continuous optimum solutions for $[\pm 45/0/90]_s$, laminates with restrained y-normal edges (a = b = 20 in)

N_D (lb/in)	Behavior constraint[1]	$t^{45°}$, $t^{-45°}$ (in)	$t^{0°}$ (in)	$t^{90°}$ (in)	$\sum t_i$ (in)	b/t	Δ_x^f ($\times \Delta_{xcr}$)	Δ_x^{mc} ($\times \Delta_{xcr}$)
1000	Buckling	0.008262	0.006278	0.003209	0.26011	76.9	---	---
	FLR1 †	---	---	---	---	---	---	---
	FLR2	0.001954	0.002597	0.002228	0.08733	229.0	156.0	7.0, 45.0[2]
2000	Buckling	0.011194	0.008019	0.002230	0.32637	61.3	---	---
	FLR1 †	---	---	---	---	---	---	---
	FLR2	0.003249	0.004288	0.003895	0.14681	132.2	43.5	6.5, 43.5[2]
3000	Buckling	0.012089	0.009516	0.003691	0.37385	53.5	---	---
	FLR1 †	---	---	---	---	---	---	---
	FLR2	0.004692	0.007598	0.003071	0.20053	100.0	21.5	9.0
4000	Buckling	0.012383	0.010307	0.006244	0.41317	48.4	---	---
	FLR1	0.001851	0.011910	0.004848	0.20460	97.8	19.2	(9.2) *
	FLR2	0.004436	0.010860	0.004352	0.24084	83.0	13.8	8.8
5000	Buckling	0.013441	0.011067	0.006553	0.44502	44.9	---	---
	FLR1	0.006920	0.007751	0.002585	0.24176	82.7	14.0	(9.6)
	FLR2	0.009432	0.008086	0.000477	0.27427	74.9	12.2	8.4
6000	Buckling	0.014248	0.011757	0.007044	0.47297	42.3	---	---
	FLR1	0.007908	0.005554	0.006799	0.28169	71.0	9.2	(6.6)
	FLR2	0.007439	0.009697	0.006825	0.31220	64.1	7.4	7.0
8000	Buckling	0.015589	0.013128	0.007730	0.52036	38.4	---	---
	FLR1	0.007929	0.009153	0.007051	0.32062	62.4	7.8	(7.2)
	FLR2	0.009204	0.007693	0.007887	0.33988	58.8	6.6	6.5
10000	Buckling	0.016277	0.014154	0.009423	0.56131	35.6	---	---
	FLR1	0.005694	0.013346	0.010168	0.34902	57.3	6.8	6.9
	FLR2 ‡	---	---	---	---	---	---	---

Δ_x^f, Δ_x^{mc} : Applied end-shortening at failure and at mode change, respectively
(1) FLR1 and FLR2 : failure load constraint without and with mode change, respectively
(2) Plates undergo two mode changes
† Unstable solutions in postbuckling analysis
‡ No mode change up to failure
* Values in parenthesis are obtained by analysis after optimization

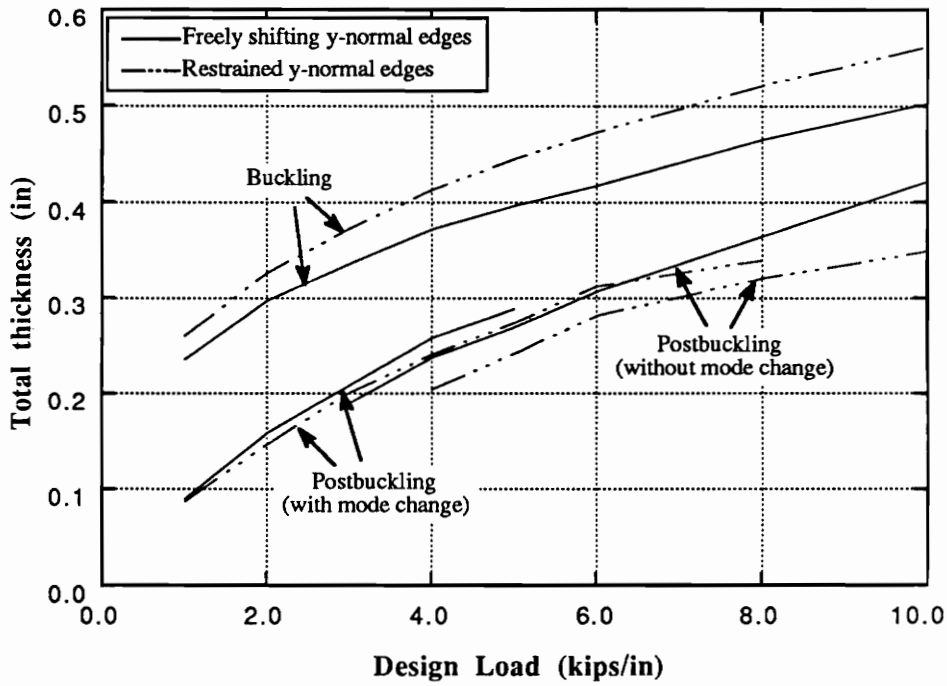

Fig. 26 Total thicknesses of square $[\pm 45/0/90]_{5s}$ laminates designed for buckling and postbuckling strength (a=b=20 in)

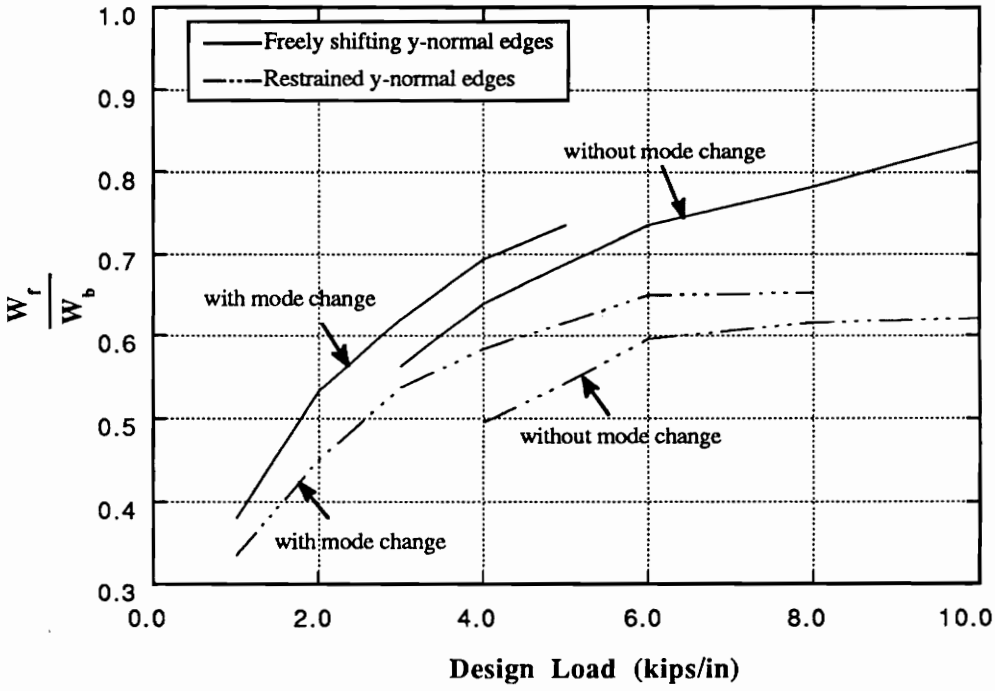

Fig. 27 Weight comparison of square $[\pm 45/0/90]_{5s}$ laminates with different in-plane boundary conditions along y-normal edges (a=b=20 in)

Table 10a. Discrete optimum solutions for $[\pm 45/0/90]_{5s}$ laminates with restrained y-normal edges and designed for buckling strength (a = b = 20.0 in)

N_D (lb/in)	Discrete solutions	$t^{45°}, t^{-45°}$ (in)	$t^{0°}$ (in)	$t^{90°}$ (in)	W/ρ (weight)	$\hat{N}_{cr}$ (lb/in)	Response surfaces
4000	Present	0.015	0.010	0.005	180.0	5166	15
	Other discrete solutions	0.010	0.015	0.005	160.0	(3737)	---
		0.010	0.010	0.010	160.0	(3555)	---
		0.010	0.020	0.000	160.0	(3868)	---
		0.010	0.015	0.010	180.0	5175	---
		0.015	0.015	0.000	180.0	5434	---
10000	Present	0.015	0.015	0.015	240.0	11999	8
	Other discrete solutions	0.015	0.015	0.010	220.0	(9435)	---
		0.015	0.020	0.005	220.0	(9779)	---
		0.020	0.015	0.000	220.0	(9785)	---
		0.015	0.020	0.010	240.0	12430	---
		0.020	0.015	0.005	240.0	12423	---

( ) infeasible

Table 10b. Discrete optimum solutions for $[\pm 45/0/90]_s$, laminate with restrained y-normal edges and designed for postbuckling strength (a = b = 20.0 in)

N_D (lb/in)	Discrete solutions	$t^{45°}$, $t^{-45°}$ (in)	$t^{0°}$ (in)	$t^{90°}$ (in)	W/ρ (weight)	N_f (lb/in)	Response surfaces
4000	Present(1)	0.005	0.010	0.005	100.0	5483	14
	Other(1) discrete solutions	0.000	0.010	0.010	80.0	(3586)	-
		0.000	0.015	0.005	80.0	(3997)	-
		0.000	0.020	0.000	80.0	(3677)	-
		0.005	0.005	0.005	80.0	(3040)	-
		0.005	0.015	0.000	100.0	5753	-
	Present(2)	0.005	0.010	0.005	100.0	4133	13
	Other(2) discrete solutions	0.000	0.020	0.000	80.0	(3029)	-
		0.005	0.005	0.010	100.0	(3680)	-
		0.000	0.020	0.005	100.0	4576	-
		0.005	0.015	0.000	100.0	4600	-
10000	Present(1)	0.010	0.010	0.010	160.0	10293	11
	Other(1) discrete solutions	0.005	0.020	0.005	140.0	(9878)	-
		0.010	0.010	0.005	140.0	(8642)	-
		0.010	0.015	0.000	140.0	(8392)	-
		0.010	0.020	0.000	160.0	(9667)	-
		0.010	0.015	0.005	160.0	10531	-

(1) Designed without consideration of mode change
(2) Designed with consideration of mode change
( ) infeasible

6.3.2 Long quasi-isotropic plates

The plate design problems of Eqns. (6.1) and (6.2) are considered in this section for large aspect ratio $[\pm 45/0/90]_{5s}$ plates, 80 inches long and 20 inches wide, with freely shifting y-normal edges. The continuous optimum solutions obtained in 7 to 9 response surfaces are presented in Table 11a for various design loads. For some postbuckling strength designs with very small values of design load, such as $N_D = 1$ and 2 kips/in, no optimum solutions are obtained if the mode changes are not allowed because of the numerical difficulty explained in the previous example. Unlike the previous example, however, two different solutions can be obtained even for large values of design loads up to $N_D = 10$ kips/in, by including and excluding the mode change option. For these long plates, several lowest eigenvalues associated with buckling analysis are very closely spaced. As a result, mode change occurs at the earlier stage of postbuckling load and plates undergo mode change several times before the failure load is achieved especially for the lightly loaded panels. When two different solutions are obtained according to the mode change option, the difference in final weight is not as significant (2.1 to 6.3%) as the previous square plate design problem. This is due to the fact that for long plates the slopes in the load end-shortening curve between adjacent two half waves are not much different and a deep jump does not occur at mode change as seen in Fig. (15).

Comparison of the total thicknesses of the long plates designed for buckling and postbuckling strength with those of the square plates considered in the previous example are presented in Fig. (28). It can be seen that the total thicknesses of square and long plates are almost the same for the same design load. Fig. (29) shows the weight of square and long rectangular plates designed for the postbuckling strength

normalized by that for the buckling strength. Again, it can be seen that similar degrees of weight savings are achieved for two different plate aspect ratios. From this comparison, it can be concluded that the weight savings are independent of the plate aspect ratio.

The discrete solutions for the long aspect ratio plate obtained by the present approach are presented in Tables 11b and 11c, along with some other possible discrete solutions for buckling and ultimate strength designs, respectively. The $\varepsilon_c = 0.02$ is used and all feasible discrete solutions are obtained by the present method. Although several other neighboring discrete solutions were considered, better designs without violating the constraint were not possible. The continuous optimum solutions are obtained in 7 to 9 response surfaces and discrete optimum solutions in 8 to 15 response surfaces.

Table 11a. Continuous optimum solutions for $[\pm 45/0/90]_{5s}$ laminates with freely shifting y-normal edges (a = 80,b = 20 in)

N_D (lb/in)	Behavior constraint[1]	$t^{45°}$, $t^{-45°}$ (in)	$t^{0°}$ (in)	$t^{90°}$ (in)	$\sum t_i$ (in)	Δ_x^f ($\times \Delta_{xcr}$)	Δ_x^{mc} ($\times \Delta_{xcr}$)
1000	Buckling	0.007171	0.004587	0.004622	0.23551	---	---
	FLR1 †	---	---	---	---	---	3.0,6.5,12.0,19.0,
	FLR2	0.002668	0.002825	0.000805	0.08966	99.0	28.5,41.5,59.0 ,84.5[2]
2000	Buckling	0.009712	0.005028	0.005028	0.29480	---	---
	FLR1 †	---	---	---	---	---	---
	FLR2	0.003715	0.005800	0.002617	0.15847	25.0	3.0,7.0,12.5 ,20.5[2]
3000	Buckling	0.012102	0.004636	0.004636	0.33476	---	---
	FLR1	0.005288	0.007153	0.001568	0.19297	13.5	(3.5,7.5)*
	FLR2	0.004682	0.008953	0.001996	0.20313	15.5	4.0,9.0[2]
4000	Buckling	0.013060	0.005403	0.005403	0.36926	---	---
	FLR1	0.005901	0.009004	0.002367	0.23173	9.6	(2.0,5.6)[2]
	FLR2	0.006925	0.007440	0.003441	0.24731	8.6	2.2,5.8[2]
5000	Buckling	0.016177	0.003449	0.003449	0.39252	---	---
	FLR1	0.007206	0.009802	0.002300	0.26514	7.4	(3.2)
	FLR2	0.008809	0.009560	0.000398	0.27576	7.0	3.4
6000	Buckling	0.017028	0.003854	0.003854	0.41964	---	---
	FLR1	0.008897	0.008753	0.003560	0.30107	5.4	(2.4)
	FLR2	0.009273	0.008803	0.004215	0.31564	5.0	2.4
8000	Buckling	0.017157	0.006006	0.006006	0.46326	---	---
	FLR1	0.011149	0.007995	0.006185	0.36478	3.4	(1.8)
	FLR2	0.012527	0.010320	0.002233	0.37607	3.4	2.6
10000	Buckling	0.017670	0.007387	0.007387	0.50114	---	---
	FLR1	0.014172	0.007067	0.006164	0.41575	2.6	(2.2)
	FLR2	0.014892	0.009415	0.003264	0.42463	2.6	2.2

Δ_x^f, Δ_x^{mc} : Applied end-shortening at failure and at mode change, respectively
(1) FLR1 and FLR2 : failure load constraint without and with mode change, respectively
(2) Plates undergo more than one mode change
† Unstable solutions in postbuckling analysis
* Values in parenthesis are obtained by analysis after optimization

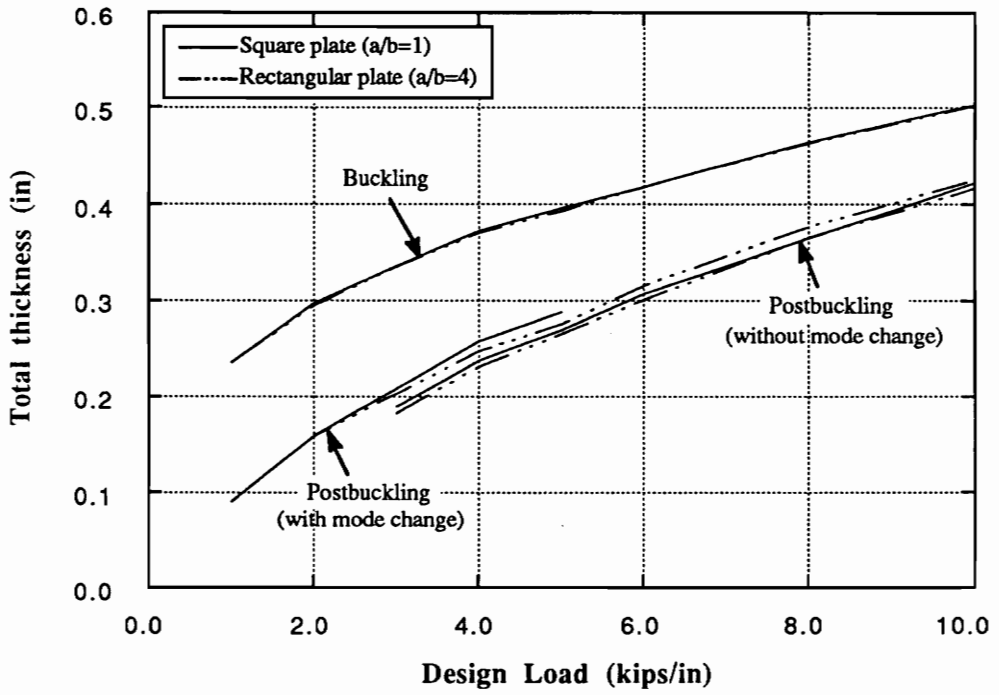

Fig. 28 Total thickness of square and rectangular $[\pm 45/0/90]_{5s}$ laminates with freely shifting y-normal edges and designed for buckling and postbuckling strength (b=20 in)

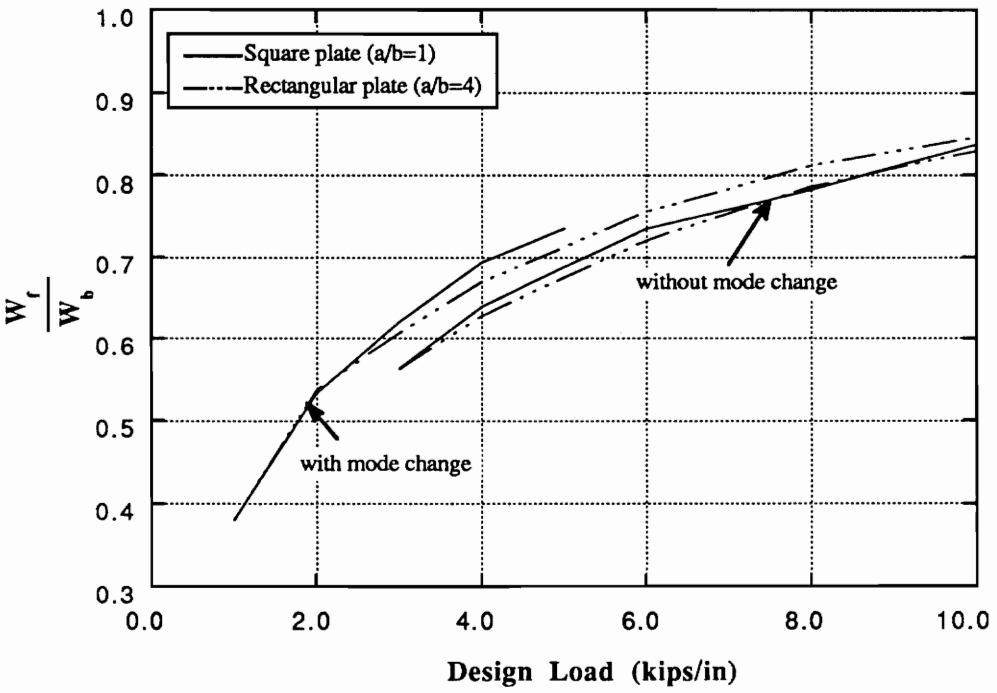

Fig. 29 Weight comparison of square and rectangular $[\pm 45/0/90]_{5s}$ laminates with freely shifting y-normal edges (b=20 in)

Table 11b. Discrete optimum solutions for long $[\pm 45/0/90]_{s,r}$ laminates with freely shifting y-normal edges and designed for buckling strength (a = 80, b = 20 in)

N_D (lb/in)	Discrete solutions	$t^{45°}$, $t^{-45°}$ (in)	$t^{0°}$ (in)	$t^{90°}$ (in)	W/ρ (weight)	$\hat{N}_{cr}$ (lb/in)	Response surfaces
4000	Present	0.015	0.005	0.005	640.0	5168	14
	Other discrete solutions	0.015	0.005	0.000	560.0	(3586)	-
		0.015	0.010	0.000	640.0	5168	-
		0.015	0.000	0.010	640.0	5168	-
		0.020	0.000	0.000	640.0	5581	-
10000	Present	0.020	0.005	0.005	800.0	10266	12
	Other discrete solutions	0.020	0.005	0.000	720.0	(7697)	-
		0.020	0.010	0.000	800.0	10266	-
		0.015	0.020	0.000	800.0	(9345)	-

( ) infeasible

Table 11c. Discrete optimum solutions for long $[\pm 45/0/90]_s$ laminates with freely shifting y-normal edges and designed for postbuckling strength (a = 80, b = 20 in)

N_D (lb/in)	Discrete solutions	$t^{45°}$, $t^{-45°}$ (in)	$t^{0°}$ (in)	$t^{90°}$ (in)	W/ρ (weight)	N_f (lb/in)	Response surfaces
4000	Present(1)	0.005	0.010	0.005	400.0	4382	10
	Other(1) discrete solutions	0.005	0.010	0.000	320.0	(3134)	-
		0.005	0.015	0.000	400.0	4534	-
		0.010	0.005	0.000	400.0	4398	-
		0.010	0.000	0.005	400.0	(3650)	-
	Present(2)	0.005	0.010	0.005	400.0	4066	8
	Other(2) discrete solutions	0.005	0.010	0.000	320.0	(3004)	-
		0.005	0.005	0.005	320.0	(2684)	-
		0.010	0.005	0.000	400.0	(3829)	-
		0.010	0.000	0.005	400.0	(3133)	-
10000	Present(1)	0.015	0.010	0.005	720.0	11736	13
	Other(1) discrete solutions	0.015	0.005	0.005	640.0	(9173)	-
		0.015	0.010	0.000	640.0	(9116)	-
		0.015	0.015	0.000	720.0	13046	-
		0.010	0.015	0.005	640.0	(9493)	-
		0.010	0.015	0.010	720.0	11305	-
	Present(2)	0.015	0.010	0.005	720.0	10724	10
	Other(2) discrete solutions	0.015	0.005	0.005	640.0	(8197)	-
		0.015	0.010	0.000	640.0	(8431)	-
		0.015	0.015	0.000	720.0	11214	-
		0.010	0.015	0.005	640.0	(9052)	-
		0.010	0.015	0.010	720.0	10835	-

(1) Designed without consideration of mode change
(2) Designed with consideration of mode change
( ) infeasible

6.3.3 Square angle-ply plates

The minimum-weight design of square angle-ply $[\pm\theta]_{5s}$ laminates for buckling and postbuckling strength is considered. The fiber angle is varied from 0 to 90 degrees to evaluate the effect of fiber orientation on the buckling and postbuckling strength design. The thickness of θ degree layer is the design variable which is assumed to be continuous-valued. The plates are 10 inches long and wide and have freely shifting y-normal edges. The design load, N_D, is chosen to be 5.0 kips/in. The mode change option is not included in this example since the laminates are relatively heavily loaded so that the possibility of mode change is small. The material properties of T300/5208 graphite-epoxy listed in Table (1) are used.

Continuous optimum solutions are presented in Table (12) for various fiber orientations. For each fiber orientation, three optimum solutions are included. The first row is the final design for buckling strength, and the second row (FLR-A) is the optimum solution for postbuckling strength design by applying the maximum strain failure criterion in Eqn. (4.1). In the last column, the ultimate strain which causes the strain failure is presented. It can be seen from the second rows for each fiber orientation in Table (12) that the failure of the angle-ply laminates is due to an excessive tensile or compressive strain in the matrix direction if the standard maximum strain failure criterion, Eqn. (4.1), is used. However, it is known that the matrix failure is only a localized failure by matrix cracking and the laminate may still has its load-carrying capability because of unbroken fibers even after the laminate reaches the ultimate strain in the matrix direction. The final design for postbuckling strength presented in the third row (FLR-B) for each fiber angel is obtained by assuming that

the laminates can fail only when the strain in the fiber direction exceeds the ultimate strain in that direction.

The weight of angle-ply laminates normalized by mass density is plotted as a function of fiber orientation in Fig. (30). It can be seen that the ± 45 degree laminate is the best buckling-resistant design. For the postbuckling strength design, the cushioning (shaded) area exists because of two different failure characteristics (matrix and fiber failure). It can be seen that the designs with matrix failure mode are heavier and therefore more conservative than the designs with fiber breakage. The differences in the final weight of the two designs (matrix failure and fiber breakage) are more pronounced as the fiber orientation approaches to 90 degrees while the differences are minimal for fiber directions near 45 degrees. Fig. (30) also shows that the laminates with fiber orientation near 0 degree have the greatest postbuckling strength while the laminates with fiber angle approaching 90 degrees have almost no postbuckling strength when all the ultimate strain components are included. If the matrix failure is excluded and only fiber breakage is accounted for as failure, the weight of the laminates with fiber direction near 0 degree are the lightest, and continuously increases as the fiber orientation increases up to 70 degrees, and then gradually decreases as the fiber angle increases further up to 90 degrees. However, it is believed that although the laminates with fiber orientation running from 0 to 70 degrees can sustain more load even after the matrix failure, the laminates with fiber orientations higher than near 70 degrees may fail not by fiber breakage but by matrix failure which will eventually cause total collapse of laminates. This is especially true for these $\pm \theta$ laminates where there are no other plies that loads can be transferred to. It can be concluded from this angle-ply example that the 45 and 0 degree laminates have the best buckling and postbuckling strength, respectively.

Table 12. Optimum solutions for square angle-ply $[\pm\theta]_{s_r}$ laminates with freely shifting y-normal edges (a = b = 10 in, N_D = 5 kips/in)

θ (degree)	Behavior Constraint	t^θ (in)	W/ρ (in^3)	Δ_x^* ($\times \Delta_{xcr}$)	Cause of Failure
0	Buckling	0.01424	28.47	---	---
	FLR-A†	0.00905	18.11	11.82	ε_{22}^{ult}
	FLR-B‡	0.00607	12.14	55.55	ε_{11}^{ult}
10	Buckling	0.01391	27.83	---	---
	FLR-A	0.00948	18.96	8.60	ε_{22}^{ult}
	FLR-B	0.00875	17.50	12.05	ε_{11}^{ult}
20	Buckling	0.01321	26.43	---	---
	FLR-A	0.01150	22.99	2.51	ε_{22}^{ult}
	FLR-B	0.01015	20.30	4.75	ε_{11}^{ult}
30	Buckling	0.01256	25.13	---	---
	FLR-A	0.01203	24.06	1.37	ε_{22}^{ult}
	FLR-B	0.01089	21.78	2.43	ε_{11}^{ult}
40	Buckling	0.01220	24.40	---	---
	FLR-A	0.01170	23.40	1.30	ε_{22}^{ult}
	FLR-B	0.01113	22.26	1.71	ε_{11}^{ult}
45	Buckling	0.01215	24.31	---	---
	FLR-A	0.01141	22.83	1.42	ε_{22}^{ult}
	FLR-B	0.01113	22.26	1.61	ε_{11}^{ult}
50	Buckling	0.01220	24.40	---	---
	FLR-A	0.01115	22.29	1.56	ε_{22}^{ult}
	FLR-B	0.01110	22.20	1.59	ε_{11}^{ult}
60	Buckling	0.01256	25.13	---	---
	FLR-A	0.01197	23.93	1.23	ε_{22}^{ult}
	FLR-B	0.01121	22.42	1.63	ε_{11}^{ult}
70	Buckling	0.01392	27.85	---	---
	FLR-A	0.01379	27.59	1.07	ε_{22}^{ult}
	FLR-B	0.01258	25.16	1.87	ε_{11}^{ult}
80	Buckling	0.01549	30.99	---	---
	FLR-A	0.01536	30.72	1.06	ε_{22}^{ult}
	FLR-B	0.01143	22.86	4.53	ε_{11}^{ult}
90	Buckling	0.01627	32.54	---	---
	FLR-A	0.01615	32.30	1.05	ε_{22}^{ult}
	FLR-B	0.00813	16.26	23.05	ε_{11}^{ult}

Δ_x^* : applied end-shortening at failure

† FLR-A : Postbuckling strength design including all the ultimate strain components

‡ FLR-B : Postbuckling strength design including only the ultimate strain in fiber direction

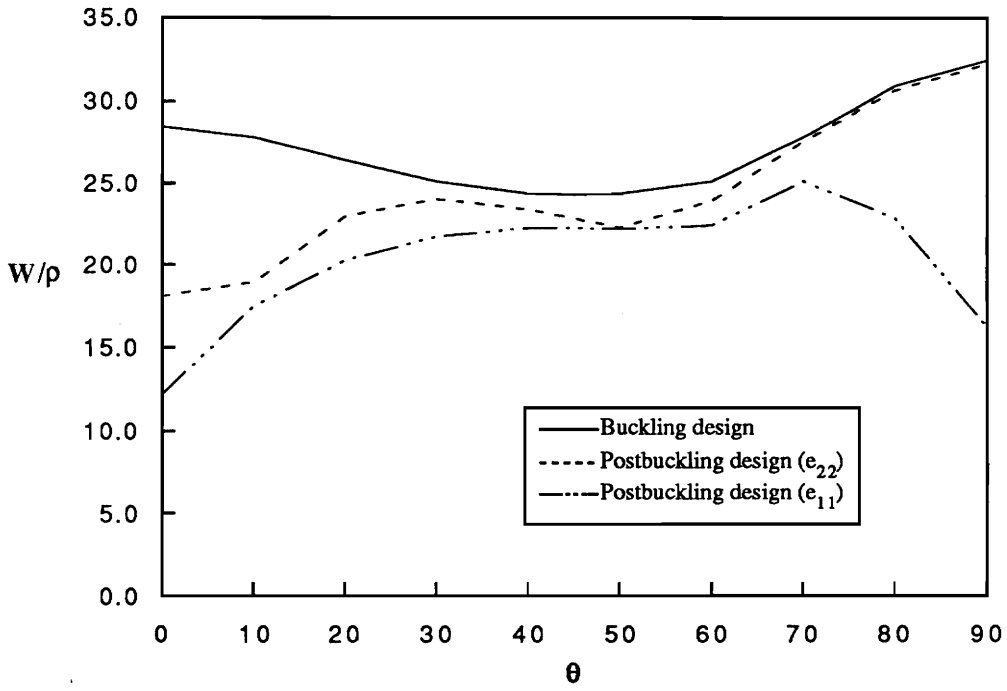

Fig. 30 Weight of angle-ply $[\pm\theta]_{5s}$ laminates designed for buckling and postbuckling strength (N_D=5 kips/in)

CHAPTER VII

CONCLUDING REMARKS

The postbuckling behavior of simply supported isotropic, orthotropic, and anisotropic plates under uniaxial compression is investigated by a Marguerre-type energy method. The phenomenon of buckle pattern change is included, and a systematic approach to predict plate mode change is proposed. By using the proposed energy approach for postbuckling analysis with consideration of the mode change phenomenon, minimum-weight design of laminated composite plates for buckling and postbuckling strength is performed. The design variables are assumed to take prescribed discrete values and a simple approach for the nonlinear optimization with discrete design variables is proposed by introducing an additional sine function for the discrete constraint into the regular pseudo-objective function of the extended-interior penalty method. Based on numerical examples considered in the present study, it is concluded that

1) If a plate is very stiff in one direction relative to the other perpendicular direction or the aspect ratio of a plate is small, in general, the assumed form of deflection requires more terms. The present approach by the six terms representation of the assumed deflection results in good approximate solutions for various orthotropic and anisotropic laminates.

2) The bending-twisting coupling terms can significantly affect the buckling and postbuckling behavior of laminated plates. Ignoring the coupling terms underestimates plate deformations and results in non-conservative solutions for both

buckling and postbuckling analysis. If the values of these coupling terms are small enough (D_{16} and D_{26} is less than 10 percent of D_{66}), however, the present approach can be applied to obtain good approximate solutions.

3) A plate can change its buckled form abruptly during compressive loading depending upon the aspect ratio, total thickness, boundary conditions along the unloaded sides, and stacking sequence of the plate. In general, thin or long plates are more vulnerable to mode change than thick or short plates are. If the first and second lowest eigenvalues of a plate associated with linear prebuckling analysis are very close, the plate changes its buckled form in the initial postbuckling load range.

4) As a result of a mode change, the load-carrying capability and postbuckling stiffness of a plate decrease. Consequently, the postbuckling solutions obtained without consideration of the mode change can be non-conservative. Furthermore, if a plate undergoes its first mode change in the deep postbuckling load range, a deep jump in load-shortening occurs, implying severe decrease of load-carrying capability.

5) The maximum strain failure criterion can be applied in predicting approximate values of the failure load of graphite-epoxy laminates under postbuckling load although more tests covering a wide range of laminate stacking sequences and plate configurations are needed in order to use the criterion with more confidence.

6) From minimum-weight design problems of laminated plates, it was found that the weight savings are substantial if plates are designed for ultimate postbuckling strength, depending upon plate thickness or design service load. For lightly loaded thin plates, it is more advantageous to design such plates to buckle. The weight savings are almost independent of plate aspect ratio.

7) The mode change in general affects the postbuckling strength design and results in more conservative final design. For lightly loaded thin plates, the optimum solutions by the present procedure can be obtained only if the mode change of such plates is allowed during postbuckling analysis. For heavily loaded short and thick plates, however, the mode change does not occur before failure and does not affect optimum designs.

8) According to the in-plane boundary conditions along the unloaded sides, the buckling and postbuckling strength designs show different trends. A plate with freely shifting unloaded sides designed for buckling strength has an advantage over a plate with restrained unloaded sides, while the latter is more failure resistant in the postbuckling regime than the former.

9) Without resorting to an expensive integer programming software, a penalty approach for nonlinear discrete optimization is used successfully in solving several discrete optimum problems. During the discrete optimization, the non-discrete penalty multiplier has to be increased step-by-step to reflect original response surfaces as much as possible. The continuous penalty multiplier, which is frozen after obtaining an approximate continuous optimum solution, needs to be relaxed if the regular constraints are violated in the discrete optimization.

10) In general, the discrete optimization process can be activated several response surfaces away from the final response surface at which the converged continuous optimum exists. If the problem has a large number of design variables and/or the prescribed discrete values are closely spaced, however, the penalty terms for non-discrete values need to be activated in the close neighborhood of the continuous optimum.

REFERENCES

1. Von Karman, Th., "Festigkeitsprobleme im Maschinenbau", *Vol. 5, pt. 4 of Encyk. der Math. Wiss.*, 1910.

2. Levy, S., "Bending of Rectangular Plates with Large Deflections," *Tech. Rept., No. 737, NACA*, 1942.

3. Yusuff, S., "Large Deflection Theory for Orthotropic Rectangular Plates Subjected to Edge Compression", *J. Appl. Mech., Vol. 19, Trans. ASME*, 1952, pp. 446-450.

4. Prabhakara, M. K. and Chia, C. Y., "Postbuckling Behavior of Rectangular Orthotropic Plates", *J. Mech. Eng. Sci., Vol. 15*, 1973, pp. 25-33.

5. Chia, C. Y. and Prabhakara, M. K., "Postbuckling Behavior of Unsymmetrically Layered Anisotropic Rectangular Plates", *J. Appl. Mech., Vol. 41*, 1974, pp. 155-162.

6. Chia, C. Y. and Prabhakara, M. K., "Nonlinear Analysis of Orthotropic Plates", *J. Mech. Eng. Sci., Vol. 17*, 1975, pp. 155-162.

7. Chandra, R., "Postbuckling Analysis of Cross-ply Laminated Plates", *AIAA J., Vol. 13*, 1975, pp. 1388-1389.

8. Harris, G. Z., "The Buckling and Post-buckling Behavior of Composite Plates under Biaxial Loading", *Int. J. Mech. Sci., Vol. 17*, 1975, pp. 187-202.

9. Zhang, Y. and Matthews, F. L., "Postbuckling Behavior of Anisotropic Laminated Plates Under Pure Shear and Shear Combined with Compressive Loading", *AIAA J., Vol. 22*, 1984, pp. 281-286.

10. Zhang, Y. and Matthews, F. L., "Large Deflection Behavior of Simply Supported Laminated Panels Under In-Plane Loading", *J. App. Mech., Vol. 52*, 1985, pp. 553-558.

11. Marguerre, K., "The Apparent Width of the Plates in Compression," *Tech. Memo., No. 833, NACA*, 1937.

12. Timoshenko, S., *Theory of Elastic Stability*, McGraw-Hill Book Co., 1959.

13. Banks, W. M., "The Post Buckling Behavior of Composite Panels", *Proceedings of 1975 International Conference on Composite Materials, Geneva, Switzerland, ICCM Vol. 2*, 1976, pp. 272-295.

14. Dickson. J. N., Cole, R. T., and Wang, J. T. S., "Design of Stiffened Composite Panel in the Postbuckling Range", *Fibrous Composites in Structural Design* , edited by Lenoe *et al.* , Plenum Press, New York, 1980, pp. 313-327.

15. Koiter, W. T., "Het Schuifplooiveld by Grote Overschrydingen van de Knikspanning", *National Luchtvaart Laboratorium, Report S295,* November 1946, in Dutch.

16. Feng, M., "An Energy Theory for Postbuckling of Composite Plates under Combined Loading", *Computers & Structures, Vol. 16,* 1983, pp. 423-431.

17. Stein, M., "Postbuckling of Orthotropic Composite Plates Loaded in Compression", *AIAA J., Vol. 21,* 1983, pp. 1729-1735.

18. Stein, M., "Postbuckling of Long Orthotropic Composite Plates in Combined Shear and Compression", *AIAA J., Vol. 23,* 1985, pp. 788-794.

19. Jensen, D. W. and Legace, P. A., "Influence of Mechanical Couplings on the Buckling and Postbuckling of Anisotropic Plates", *AIAA J., Vol. 26,* 1988, pp. 1269-1277.

20. Stein, M., "Postbuckling of Eccentric Open-Section Stiffened Composite Panels", *AIAA Paper 88-2215,* 1988, pp. 57-61.

21. Stein, M., "Loads and Deformations of Buckled Rectangular Plates", *NASA TR R-40,* 1959.

22. Arnold, R. R., "A Correlative Analysis of Northrop Metal Compression Panels MC1-MC4, IC1", *Anamet Laboratories, Inc., Report No. 84.033,* August, 1984.

23. Dinardo, M. T., "Buckling and Postbuckling Behavior of Laminated Composite Plates with Ply Dropoffs", *TELAC Rept. 86-13,* MIT, 1986.

24. Minguet, P. J., Dugundji, J., and Lagace, P., " Postbuckling Behavior of Laminated Plates Using a Direct Energy-Minimization Technique", *AIAA J., Vol. 27,* 1989, pp. 1785-1792.

25. Stein, M., "The Phenomenon of Change in Buckle Pattern in Elastic Structures", *NASA TR R-39,* 1959.

26. Chandra, R. and Raju, B. B., "Postbuckling Analysis of Rectangular Orthotropic Plates", *Int. J. Mech. Sci., Vol. 15,* 1973, pp. 81-97.

27. Rushton, K.R., "Post-Buckling of Rectangular Plates with Various Boundary Conditions", *Aero. Quart., Vol. 21,* 1970, pp. 163-181.

28. Almroth, B. O. and Brogan, F. A., "The STAGS Computer Code", *NASA CR-2950,* 1978.

29. Thurston, G. A., "Postbuckling Analysis Using General-Purpose Code", *AIAA J., Vol. 24,* 1986, pp. 1013-1020.

30. Schmit, L. and Farshi, B., "Optimum Laminate Design for Strength and Stiffness," *Int. J. Num. Meth. Eng., Vol. 7,* 1973, pp. 519-536.

31. Schmit, L. and Farshi, B., "Optimum Design of Laminated Fibre Composite Plates," *Int. J. Num. Meth. Eng., Vol. 11,* 1977, pp. 623-640.

32. Knot, N. S., Venkayya, V. B., Johnson, C. D., and Tischler, V. A., "Optimization of Fiber Reinforced Composite Structures", *Int. J. Solids Structures, Vol. 9,* 1973, pp. 1225-1236.

33. Starnes, J. H. Jr. and Haftka, R. T., "Preliminary Design of Composite Wigns for Buckling, Strength, and Displacement Constraints", *J. Aircraft, Vol. 16,* 1979, pp. 564-570.

34. Rao, S. S. and Singh, K., "Optimum Design of Laminates with Natural Frequency Constraints," *J. Sounds Vibration, Vol. 67,* 1979, pp. 101-112.

35. Stroud, W. J., and Anderson, M. S., "PASCO : Structural Panel Analysis and Sizing Code, Capability abd Analytical Foundations," *NASA TM 80181,* 1981.

36. Swnason, G. D., Gürdal, Z., and Starnes, J. H., Jr., "Structural Efficiency Study of Graphite-Epoxy Aircraft Rib Structures", *Journal of Aircraft,* accepted for publication.

37. Phillips, J. L., and Gürdal, Z., "Analysis and Optimum Design of Geodesically Stiffened Composite Panels", *Composite Materials Design and Analysis,* Eds. W. P de Wilde, and W. R. Blain, 1990, pp. 509-528.

38. Young, R. D., and Gürdal, Z., "Importance of Anisotropy on Buckling of Compression Loaded Composite Corrugated Panels", *Journal of Aircraft, Vol. 27, No. 4,* 1990, pp. 378-380.

39. Gürdal, Z., and Haftka, R. T., "Automated Design of Composite Plates for Improved Damage Tolerance," *Composite Materials: Testing and Design,* Ed., J. D. Whitcomb, ASTM-STP 972, 1988, PP. 5-22.

40. Vanderplaats, G. N., "CONMIN - a Fortran Program for Constrained Function Minimization, User's Manual," *NASA TM X-62, 282,* 1973.

41. Hirano, Y., "Optimum Design of Laminated Plates under Axial Compression," *AIAA J., Vol. 17,* 1979, pp. 1017-1019.

42. Hirano, Y., "Optimum Design of Laminated Plates under Shear," *J. Composite Materials, Vol. 13,* 1979, pp. 329-334.

43. Bert, C. W., "Optimal Design of a Composite-material Plate to Maximize its Fundamental Frequency," *J. Sounds Vibration, Vol. 50,* 1977, pp. 229-237.

44. Bert, C. W., "Design of Clamped Composite-material Plates to Maximize Fundamental Frequency," *J. Mechanical Design, Vol. 100,* 1978, pp. 274-278.

45. Shin, Y. S., Haftka, R. T., Watson, L. T., and Plaut, R. A., "Design of Laminated Plates for Maximum Buckling Load," *J. Composite Materials, Vol. 23,* 1989, pp. 348-369.

46. Mesquita, L. and Kamat, M. P., "Optimization of Stiffened Laminated Composite Plates with Frequency Constraints", *Engineering Optimization, Vol. 11,* 1987, pp. 119-145.

47. Haftka, R. T., Gürdal, Z., and Kamat, M. P., *Elements of Structural Optimization,* 2nd Ed., Kluwer Academic Publishers, the Netherlands, 1990.

48. Shin, Y. S., Haftka, R. T., Watson, L. T., and Plaut, R. A., "Tracing Structural Optima as a Function of Available Resources by a Homotopy Method," to be published in *Computer Methods in Applied Mechanics and Engineering.*

49. Chao, C. C., Koh, S. L., and Sun, C. T., "Optimization of Buckling and Yield Strengths of Laminated Composites," *AIAA J., Vol. 13,* 1975, pp. 1131-1132.

50. Tauchert, T. R. and Adibhatla, S., "Design of Laminated Plates for Maximum Stiffness," *J. Composite Materials, Vol. 18,* 1984, pp. 58-69.

51. Tauchert, T. R. and Adibhatla, S., "Design of Laminated Plates for Maximum Bending Strength," *Engineering Optimization, Vol. 8,* 1985, pp. 253-263.

52. Dickson. J. N. and Biggers, S. B., "POSTOP : Postbuckled Open-Stiffener Optimum Panels - Theory and Capability", *NASA CR-172259,* January 1984.

53. Arnold, R. R. and Mayers, J., "Buckling, Postbuckling, and Crippling of Materially Nonlinear Laminated Composite Plates", *Int. J. Solids Structures, Vol. 20,* 1984, pp. 863-880.

54. Starnes, J. H., Jr. and Rouse, M., "Postbuckling and Failure Characteristics of Selected Flat Rectangular Graphite-Epoxy Panels Loaded in Compression", *Proceedings of the AIAA/ASME/ASCE/AHS 22nd Structures, Structural Dynamics and Materials Conference,* Atlanta, GA, Technical Papers, Part 1, AIAA, April 1981, pp. 423-434.

55. Land, A. H. and Doig, A.G., "An Automatic Method for Solving Discrete Programming Problems", *Econometrica, Vol. 28,* 1960, pp. 497-520.

56. Reinschmidt, K., "Discrete Structural Optimization," *ASCE, J. Struct. Div., Vol. 97,* 1971, pp. 133-156.

57. Garfinkel, R. and Nemhauser, G., *Integer Programming,* John Wiley, New York, 1972.

58. John, K. V., Ramakrishnan, C. V. and Sharma, K. G., "Optimum Design of Trusses from Available Sections - Use of Sequential Linear Programming

with Branch and Bound Algorithm," *Engineering Optimization, Vol. 13,* pp. 119-145, 1988.

59. Darkin, R. J., "A Tree Search Algorithm for Mixed Integer Programming Problems", *Computer J., Vol. 8,* 1965, pp. 250-255.

60. Olson, G. R. and Vanderplaats, G. N., "Method for Nonlinear Optimization with Discrete Design Variables," *AIAA J., Vol. 27,* 1989, pp. 1584-1589.

61. Schmit, L. and Fleury, C., "Discrete-Continuous Variable Structural Synthesis Using Dual Methods," *AIAA J., Vol. 18,* 1980, pp. 1515-1524.

62. Ringertz, U. T., "On Methods for Discrete Structural Optimization", *Engineering Optimization, Vol. 13,* 1988, pp. 47-64.

63. Fiacco, A. V. and McCormick, G. P., *Nonlinear Programming : Sequential Unconstrained Minimization Techniques,* John Wiley, New York, 1968.

64. Grandhi, R. V., Thareja, R. and Haftka, R. T., "NEWSUMT-A : A General Purpose Program for Constrained Optimization Using Constraint Approximation," *ASME Journal of Mechanisms, Transmissions and Automation in Design, Vol. 107,* pp. 94-99, March 1985.

65. Lekhnitskii, S. G., *Anisotropic Plates,* Gordon & Breach, 1968.

66. Jones, R. M., *Mechanics of Composite Materials,* McGraw-Hill, 1975.

67. *IMSL User's Manual, Math/Library,* Vol. 2, Version 1.0, April 1987, pp. 780-783.

68. Moré, J., Garbow, B. and Hillstrom, K., "User Guide for MINIPACK-1", *Argonne National Labs. Report ALN-80-74,* Argonne, Illinois, 1980.

69. Reddy, J. N., "Geometrically Nonlinear Transient Analysis of Laminated Composite Plates", *AIAA J., Vol. 21,* 1983, pp. 621-629.

70. *ABAQUS, User's Manual,* Version 4.8, Hibbit, Karlsson & Sorensen, Inc., 1989.

71. Marguerre, K., "Zur Theorie der gekrümmten Platte grosser Formänderung", *Proceedings of the Fifth International Congress for Applied Mechanics,* Cambridge, 1938, pp. 93-101.

72. Starnes, J. H. Jr., Knight, N. F., Jr., and Rouse, M., "Postbuckling Behavior of Selected Flat Stiffened Graphite-Epoxy Panels Loaded in Compression", *AIAA J., Vol. 23,* 1985, pp. 1236-1246.

73. Jeffrey, G. L., "Postbuckling of Laminated Anisotropic Panels", *NASA TM-100509,* 1987.

74. Noor, A. K., Starnes, J. H., Jr. and Waters, W. A., Jr., "Numerical and Experimental Simulations of the Postbuckling Response of Laminated Anisotropic Panels", *Proceedings of the AIAA/ASME/ASCE/AHS 31st Structures, Structural Dynamics and Materials Conference,* Long Beach, CA, April 1990, pp. 848-861.

75. Shin, D. K., Gürdal, Z., and Griffin, O. H., Jr., "A Penalty Approach for Nonlinear Optimization with Discrete Design Variables", *Engineering Optimization, Vol. 16,* 1990, pp. 29-42.

76. Haftka, R. T. and Starnes, J. H., Jr., "Applications of a Quadratic Extended Penalty Function to Structural Optimization," *AIAA J., Vol. 14,* 1976, pp. 718-724.

77. Bathe, K. J., *Finite Element Procedures in Engineering Analysis,* Prentice-Hall, Inc., 1982, pp. 489-491.

APPENDIX - A

The coefficients, B_n, in the expression (2.6) are found to be

$$B_1 = \sum_{k=1}^{p-1}\sum_{t=1}^{q-1}[kt(p-k)(q-t) - k^2(q-t)^2]W_{k,t}W_{(p-k),}(q-t)\,, \quad \text{if } q \neq 0 \text{ and } p \neq 0$$

$$B_1 = 0\,, \quad \text{if } q = 0 \text{ or } p = 0$$

$$B_2 = \sum_{k=1}^{\infty}\sum_{t=1}^{q-1}[kt(k+p)(q-t) + k^2(q-t)^2]W_{k,t}W_{(k+p),}(q-t)\,, \quad \text{if } q \neq 0$$

$$B_2 = 0\,, \quad \text{if } q = 0$$

$$B_3 = \sum_{k=1}^{\infty}\sum_{t=1}^{q-1}[kt(k+p)(q-t) + (k+p)^2(q-t)^2]W_{(k+p),t}W_{k,}(q-t)\,, \quad \text{if } q \neq 0 \text{ and } p \neq 0$$

$$B_3 = 0\,, \quad \text{if } q = 0 \text{ or } p = 0$$

$$B_4 = \sum_{k=1}^{p-1}\sum_{t=1}^{\infty}[kt(p-k)(t+q) + k^2(t+q)^2]W_{k,t}W_{(p-k),}(t+q)\,, \quad \text{if } p \neq 0$$

$$B_4 = 0\,, \quad \text{if } p = 0$$

$$B_5 = \sum_{k=1}^{p-1}\sum_{t=1}^{\infty}[k(t+q)(p-k)t + k^2t^2]W_{k,}(t+q)W_{(p-k),t}\,, \quad \text{if } q \neq 0 \text{ and } p \neq 0$$

$$B_5 = 0\,, \quad \text{if } q = 0 \text{ or } p = 0$$

$$B_6 = \sum_{k=1}^{\infty}\sum_{t=1}^{\infty}[kt(k+p)(t+q) - k^2(t+q)^2]W_{k,t}W_{(k+p),}(t+q)\,, \quad \text{if } q \neq 0$$

$$B_6 = 0\,, \quad \text{if } q = 0$$

$$B_7 = \sum_{k=1}^{\infty}\sum_{t=1}^{\infty}[k(t+q)(k+p)t - k^2t^2]W_{k,}(t+q)W_{(k+p),t}\,, \quad \text{if } q \neq 0 \text{ or } p \neq 0$$

$$B_7 = 0\,, \quad \text{if } q = 0 \text{ and } p = 0$$

$$B_8 = \sum_{k=1}^{\infty}\sum_{t=1}^{\infty}[(k+p)tk(t+q) - (k+p)^2(t+q)^2]W_{(k+p),t}W_{k,}(t+q)\,, \quad \text{if } q \neq 0 \text{ and } p \neq 0$$

$$B_8 = 0\,, \quad \text{if } q = 0 \text{ or } p = 0$$

$$B_9 = \sum_{k=1}^{\infty}\sum_{t=1}^{\infty}[(k+p)(t+q)kt - (k+p)^2t^2]W_{(k+p),}(t+q)W_{k,t}\,, \quad \text{if } p \neq 0$$

$$B_9 = 0\,, \quad \text{if } p = 0$$

APPENDIX - B

The nonlinear algebraic equations when the out-of-plane displacement is assumed to be six terms of the Fourier series can be obtained as

$$0 = \frac{4}{\pi^4}\left[A^*_{11}\hat{N}_x\frac{\partial\hat{N}_x}{\partial W_{ij}} + A^*_{12}\left(\hat{N}_x\frac{\partial\hat{N}_y}{\partial W_{ij}} + \hat{N}_y\frac{\partial\hat{N}_x}{\partial W_{ij}}\right) + A^*_{22}\hat{N}_y\frac{\partial\hat{N}_y}{\partial W_{ij}}\right]$$

$$+\frac{k^4 D_{11}}{2a^4}\frac{\partial}{\partial W_{ij}}\left[W_{11}^{\,2} + 81W_{31}^{\,2} + 625W_{13}^{\,2} + W_{33}^{\,2} + 81W_{51}^{\,2} + W_{15}^{\,2}\right]$$

$$+\frac{k^2(D_{12}+2D_{66})}{a^2b^2}\frac{\partial}{\partial W_{ij}}\left[W_{11}^{\,2} + 9W_{31}^{\,2} + 25W_{13}^{\,2} + 9W_{33}^{\,2} + 81W_{51}^{\,2} + 25W_{15}^{\,2}\right]$$

$$+\frac{D_{22}}{2b^4}\frac{\partial}{\partial W_{ij}}\left[W_{11}^{\,2} + W_{31}^{\,2} + W_{13}^{\,2} + 81W_{33}^{\,2} + 81W_{51}^{\,2} + 625W_{15}^{\,2}\right]$$

$$+\frac{8A^*_{11}}{b^4}\frac{\partial}{\partial W_{ij}}\left[2k_6^2 + 32k_7^2 + 162k_8^2 + 512k_9^2 + 1250k_{10}^2 + k_{11}^2 + k_{12}^2 + k_{13}^2\right.$$

$$\left. + k_{14}^2 + 16(k_{15}^2 + k_{16}^2 + k_{17}^2 + k_{18}^2) + 81(k_{19}^2 + k_{20}^2 + k_{21}^2) + 256(k_{22}^2 + k_{23}^2)\right]$$

$$+\frac{8k^2(A^*_{66}+2A^*_{12})}{a^2b^2}\frac{\partial}{\partial W_{ij}}\left[k_{11}^2 + 4k_{12}^2 + 9k_{13}^2 + 16k_{14}^2 + 4k_{15}^2 + 16k_{16}^2\right.$$

$$\left. + 36k_{17}^2 + 64k_{18}^2 + 9k_{19}^2 + 36k_{20}^2 + 81k_{21}^2 + 16k_{22}^2 + 64k_{23}^2\right]$$

$$+\frac{8A^*_{22}}{a^4}\frac{\partial}{\partial W_{ij}}\left[2k_1^2 + 32k_2^2 + 162k_3^2 + 512k_4^2 + 1250k_5^2 + k_{11}^2 + 16k_{12}^2 + 81k_{13}^2\right.$$

$$\left. + 256k_{14}^2 + k_{15}^2 + 16k_{16}^2 + 81k_{17}^2 + 256k_{18}^2 + k_{19}^2 + 16k_{20}^2 + 81k_{21}^2 + k_{22}^2 + 16k_{23}^2\right]$$

$$(i,j) = \{(1,1), (3,1), (1,3), (3,3), (5,1), (1,5)\}$$

where k_i 's (i= 1,2,...,23) are

$$k_1 = \frac{a^2}{32k^2A^*_{22}b^2}(W_{11}{}^2 - 2W_{11}W_{31} - 2W_{31}W_{13} + 9W_{33}{}^2 - 18W_{33}W_{51} + 25W_{15}{}^2)$$

$$k_2 = \frac{a^2}{64k^2A^*_{22}b^2}(W_{11}W_{31} - W_{11}W_{13} + 9W_{33}W_{51})$$

$$k_3 = \frac{a^2}{288k^2A^*_{22}b^2}(W_{31}{}^2 + 2W_{11}W_{13} + 9W_{51}{}^2)$$

$$k_4 = \frac{a^2}{256k^2A^*_{22}b^2}W_{31}W_{13} \quad , \quad k_5 = \frac{a^2}{800k^2A^*_{22}b^2}W_{13}{}^2$$

$$k_6 = \frac{k^2b^2}{32A^*_{11}a^2}(W_{11}{}^2 + 9W_{31}{}^2 + 25W_{13}{}^2 - 2W_{11}W_{33} - 18W_{31}W_{51} - 2W_{33}W_{15})$$

$$k_7 = \frac{k^2b^2}{64A^*_{11}a^2}(W_{11}W_{33} + 9W_{31}W_{51} - W_{11}W_{15})$$

$$k_8 = \frac{k^2b^2}{288A^*_{11}a^2}(W_{33}{}^2 + 2W_{11}W_{15} + 9W_{51}{}^2)$$

$$k_9 = \frac{k^2b^2}{256A^*_{11}a^2}W_{33}W_{15} \quad , \quad k_{10} = \frac{k^2b^2}{800A^*_{11}a^2}W_{15}{}^2$$

$$k_{11} = \frac{k^2(W_{11}W_{31} + 4W_{31}W_{13} + W_{11}W_{33} - 4W_{31}W_{33} - 9W_{13}W_{51} + 4W_{33}W_{15} - 9W_{51}W_{15})}{4[\frac{k^4b^2}{a^2}A^*_{22} + k^2(2A^*_{12} + A^*_{66}) + \frac{a^2}{b^2}A^*_{11}]}$$

$$k_{12} = \frac{k^2(-W_{11}W_{31} + 9W_{11}W_{13} + 25W_{31}W_{33} + 9W_{11}W_{51} - 49W_{13}W_{33} + 81W_{51}W_{15})}{16[16\frac{k^4b^2}{a^2}A^*_{22} + 4k^2(2A^*_{12} + A^*_{66}) + \frac{a^2}{b^2}A^*_{11}]}$$

$$k_{13} = \frac{k^2(-W_{11}W_{13} + 16W_{13}W_{33} + 9W_{31}W_{51})}{4[81\frac{k^4b^2}{a^2}A^*_{22} + 9k^2(2A^*_{12} + A^*_{66}) + \frac{a^2}{b^2}A^*_{11}]}$$

$$k_{14} = \frac{k^2(-W_{31}W_{13} + 81W_{13}W_{51})}{16[256\frac{k^4b^2}{a^2}A^*_{22} + 16k^2(2A^*_{12} + A^*_{66}) + \frac{a^2}{b^2}A^*_{11}]}$$

$$k_{15}=\frac{k^2(-W_{11}W_{33}+25W_{31}W_{33}+9W_{11}W_{51}+81W_{13}W_{51}+9W_{11}W_{15}-49W_{31}W_{15})}{16[\frac{k^4b^2}{a^2}A^*_{22}+4k^2(2A^*_{12}+A^*_{66})+16\frac{a^2}{b^2}A^*_{11}]}$$

$$k_{16}=\frac{k^2(-W_{31}W_{33}+4W_{13}W_{33}+4W_{31}W_{15}-9W_{13}W_{15})}{16[\frac{k^4b^2}{a^2}A^*_{22}+k^2(2A^*_{12}+A^*_{66})+\frac{a^2}{b^2}A^*_{11}]}$$

$$k_{17}=\frac{k^2(-49W_{13}W_{33}-9W_{31}W_{51}+169W_{13}W_{15})}{16[81\frac{k^4b^2}{a^2}A^*_{22}+36k^2(2A^*_{12}+A^*_{66})+16\frac{a^2}{b^2}A^*_{11}]}$$

$$k_{18}=-\frac{9k^2W_{13}W_{51}}{64[16\frac{k^4b^2}{a^2}A^*_{22}+4k^2(2A^*_{12}+A^*_{66})+\frac{a^2}{b^2}A^*_{11}]}$$

$$k_{19}=\frac{k^2(-W_{11}W_{15}+16W_{31}W_{15}+9W_{33}W_{51})}{4[\frac{k^4b^2}{a^2}A^*_{22}+9k^2(2A^*_{12}+A^*_{66})+81\frac{a^2}{b^2}A^*_{11}]}$$

$$k_{20}=\frac{k^2(-49W_{31}W_{15}-9W_{33}W_{51}+169W_{13}W_{15})}{16[16\frac{k^4b^2}{a^2}A^*_{22}+36k^2(2A^*_{12}+A^*_{66})+81\frac{a^2}{b^2}A^*_{11}]}$$

$$k_{21}=-\frac{k^2W_{13}W_{15}}{9[\frac{k^4b^2}{a^2}A^*_{22}+k^2(2A^*_{12}+A^*_{66})+\frac{a^2}{b^2}A^*_{11}]}$$

$$k_{22}=\frac{k^2(-W_{33}W_{15}+81W_{15}W_{51})}{16[\frac{k^4b^2}{a^2}A^*_{22}+16k^2(2A^*_{12}+A^*_{66})+256\frac{a^2}{b^2}A^*_{11}]}$$

$$k_{23}=-\frac{9k^2W_{15}W_{51}}{64[\frac{k^4b^2}{a^2}A^*_{22}+4k^2(2A^*_{12}+A^*_{66})+16\frac{a^2}{b^2}A^*_{11}]}$$

APPENDIX - C

Large Deformation Plate Equations

The large deformation shear-deformable plate equations used in the formulation of the finite element program are

$$\frac{\partial N_1}{\partial x} + \frac{\partial N_6}{\partial y} = 0 \tag{c.1}$$

$$\frac{\partial N_6}{\partial x} + \frac{\partial N_2}{\partial y} = 0 \tag{c.2}$$

$$\frac{\partial Q_1}{\partial x} + \frac{\partial Q_2}{\partial y} = \Omega(w, N_i) \tag{c.3}$$

$$\frac{\partial M_1}{\partial x} + \frac{\partial M_6}{\partial y} - Q_1 = 0 \tag{c.4}$$

$$\frac{\partial M_6}{\partial x} + \frac{\partial M_2}{\partial y} - Q_2 = 0 \tag{c.5}$$

$$\Omega(w, N_i) = \frac{\partial w}{\partial x}\left(\frac{\partial N_1}{\partial x} + \frac{\partial N_6}{\partial y}\right) + \frac{\partial w}{\partial y}\left(\frac{\partial N_6}{\partial x} + \frac{\partial N_2}{\partial y}\right)$$

where N_i, Q_i, and M_i (i = 1, 2, 6) are the stress and moment resultants defined by

$$\begin{Bmatrix} \{N\} \\ \{M\} \end{Bmatrix} = \begin{bmatrix} [A] & [B] \\ [B]^T & [D] \end{bmatrix} \begin{Bmatrix} \{\varepsilon\} \\ \{\kappa\} \end{Bmatrix} \tag{c.6}$$

$$\begin{Bmatrix} Q_1 \\ Q_2 \end{Bmatrix} = \begin{bmatrix} A_{55} & A_{45} \\ A_{45} & A_{44} \end{bmatrix} \begin{Bmatrix} \varepsilon_{xz} \\ \varepsilon_{yz} \end{Bmatrix} \tag{c.7}$$

In deriving the nonlinear shear-deformable plate equations in terms of mid-plane displacements and rotations, the Karman's nonlinear strain-displacement relation (2.9) is used and the transverse shear strains ε_{xz} and ε_{yz} are defined by

$$\varepsilon_{xz} = \phi_x + \frac{\partial w}{\partial x} \quad , \quad \varepsilon_{yz} = \phi_y + \frac{\partial w}{\partial y} \tag{c.8}$$

and curvatures by

$$\kappa_x = \frac{\partial \phi_x}{\partial x} \quad , \quad \kappa_y = \frac{\partial \phi_y}{\partial y} \quad , \quad \kappa_{xy} = \frac{\partial \phi_x}{\partial y} + \frac{\partial \phi_y}{\partial x} \tag{c.9}$$

where ϕ_x and ϕ_y are the rotations in the xz and yz plane due to plate bending.

By introducing the relations (2.9), (c.8) and (c.9) into Eqns. (c.6) and (c.7), the stress and moment resultants (N_i, Q_i, and M_i) can be expressed in terms of the displacements and rotations (u, v, w, ϕ_x, ϕ_y). Then, the large deformation shear deformable plate equations (c.1) through (c.5) can be rewritten for the unknown independent displacements and rotations (u, v, w, ϕ_x, ϕ_y).

Variational Formulation

A typical element used for the variational formulation is shown in Fig. (31). The element domain Ω^e is bounded by Γ^e with unit normal $\hat{n}$. For the typical element, the following variational equations can be obtained by multiplying the nonlinear plate equations (after substituting the displacements and rotations into Eqns. c.1-c.5) by weighting functions, g_i (i = 1,...,5), and integrating over the domain of that element, Ω^e :

$$0 = \int_{\Omega^e} \{ \frac{\partial g_1}{\partial x} [A_{11}(\frac{\partial u}{\partial x} + \frac{1}{2} (\frac{\partial w}{\partial x})^2) + A_{12}(\frac{\partial v}{\partial y} + \frac{1}{2} (\frac{\partial w}{\partial y})^2)$$
$$+ A_{16}(\frac{\partial u}{\partial y} + \frac{\partial v}{\partial x} + \frac{\partial w}{\partial x} \frac{\partial w}{\partial y}) + B_{11} \frac{\partial \phi_x}{\partial x} + B_{12} \frac{\partial \phi_y}{\partial y} + B_{16}(\frac{\partial \phi_x}{\partial y} + \frac{\partial \phi_y}{\partial x})]$$

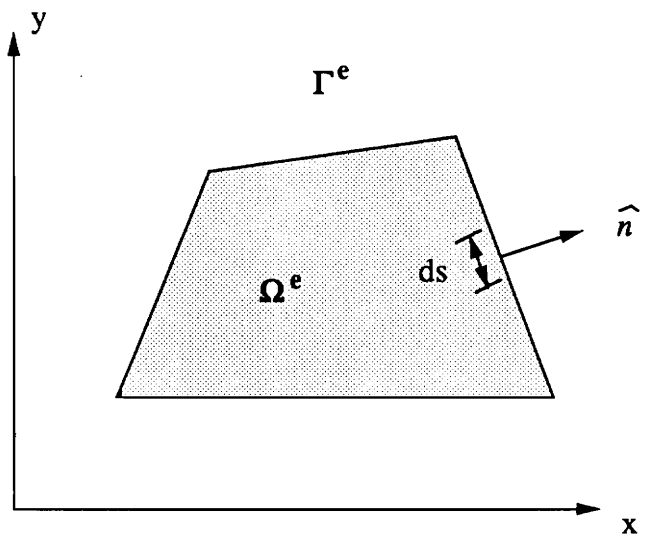

Fig. 31 Typical quadrilateral element

$$+\frac{\partial g_1}{\partial y}\left[A_{16}\left(\frac{\partial u}{\partial x}+\frac{1}{2}\left(\frac{\partial w}{\partial x}\right)^2\right)+A_{26}\left(\frac{\partial v}{\partial y}+\frac{1}{2}\left(\frac{\partial w}{\partial y}\right)^2\right)\right.$$

$$\left.+A_{66}\left(\frac{\partial u}{\partial y}+\frac{\partial v}{\partial x}+\frac{\partial w}{\partial x}\frac{\partial w}{\partial y}\right)+B_{16}\frac{\partial \phi_x}{\partial x}+B_{26}\frac{\partial \phi_y}{\partial y}+B_{66}\left(\frac{\partial \phi_x}{\partial y}+\frac{\partial \phi_y}{\partial x}\right)\right]\}dxdy$$

$$-\int_{\Gamma^e}\{g_1(N_1n_x+N_6n_y)\}dS \qquad (c.10)$$

$$0=\int_{\Omega^e}\{\frac{\partial g_2}{\partial x}\left[A_{16}\left(\frac{\partial u}{\partial x}+\frac{1}{2}\left(\frac{\partial w}{\partial x}\right)^2\right)+A_{26}\left(\frac{\partial v}{\partial y}+\frac{1}{2}\left(\frac{\partial w}{\partial y}\right)^2\right)\right.$$

$$\left.+A_{66}\left(\frac{\partial u}{\partial y}+\frac{\partial v}{\partial x}+\frac{\partial w}{\partial x}\frac{\partial w}{\partial y}\right)+B_{16}\frac{\partial \phi_x}{\partial x}+B_{26}\frac{\partial \phi_y}{\partial y}+B_{66}\left(\frac{\partial \phi_x}{\partial y}+\frac{\partial \phi_y}{\partial x}\right)\right]$$

$$+\frac{\partial g_2}{\partial y}\left[A_{12}\left(\frac{\partial u}{\partial x}+\frac{1}{2}\left(\frac{\partial w}{\partial x}\right)^2\right)+A_{22}\left(\frac{\partial v}{\partial y}+\frac{1}{2}\left(\frac{\partial w}{\partial y}\right)^2\right)\right.$$

$$\left.+A_{26}\left(\frac{\partial u}{\partial y}+\frac{\partial v}{\partial x}+\frac{\partial w}{\partial x}\frac{\partial w}{\partial y}\right)+B_{12}\frac{\partial \phi_x}{\partial x}+B_{22}\frac{\partial \phi_y}{\partial y}+B_{26}\left(\frac{\partial \phi_x}{\partial y}+\frac{\partial \phi_y}{\partial x}\right)\right]\}dxdy$$

$$-\int_{\Gamma^e}\{g_2(N_6n_x+N_2n_y)\}dS \qquad (c.11)$$

$$0=\int_{\Omega^e}\{\frac{\partial g_3}{\partial x}\left[A_{55}\left(\phi_x+\frac{\partial w}{\partial x}\right)+A_{45}\left(\phi_y+\frac{\partial w}{\partial y}\right)+A_{11}\left(\frac{\partial u}{\partial x}+\frac{1}{2}\left(\frac{\partial w}{\partial x}\right)^2\right)\frac{\partial w}{\partial x}\right.$$

$$+A_{12}\left(\frac{\partial v}{\partial y}+\frac{1}{2}\left(\frac{\partial w}{\partial y}\right)^2\right)\frac{\partial w}{\partial x}+A_{16}\left(\frac{\partial u}{\partial y}+\frac{\partial v}{\partial x}+\frac{\partial w}{\partial x}\frac{\partial w}{\partial y}\right)\frac{\partial w}{\partial x}$$

$$+A_{16}\left(\frac{\partial u}{\partial x}+\frac{1}{2}\left(\frac{\partial w}{\partial x}\right)^2\right)\frac{\partial w}{\partial y}+A_{26}\left(\frac{\partial v}{\partial y}+\frac{1}{2}\left(\frac{\partial w}{\partial y}\right)^2\right)\frac{\partial w}{\partial y}$$

$$+A_{66}\left(\frac{\partial u}{\partial y}+\frac{\partial v}{\partial x}+\frac{\partial w}{\partial x}\frac{\partial w}{\partial y}\right)\frac{\partial w}{\partial y}+B_{11}\frac{\partial \phi_x}{\partial x}\frac{\partial w}{\partial x}+B_{12}\frac{\partial \phi_y}{\partial y}\frac{\partial w}{\partial x}$$

$$+B_{16}\left(\frac{\partial \phi_x}{\partial y}+\frac{\partial \phi_y}{\partial x}\right)\frac{\partial w}{\partial x}+B_{16}\frac{\partial \phi_x}{\partial x}\frac{\partial w}{\partial y}+B_{26}\frac{\partial \phi_y}{\partial y}\frac{\partial w}{\partial y}$$

$$+B_{66}\left(\frac{\partial \phi_x}{\partial y}+\frac{\partial \phi_y}{\partial x}\right)\frac{\partial w}{\partial y}\left.\right]+\frac{\partial g_3}{\partial x}\left[A_{45}\left(\phi_x+\frac{\partial w}{\partial x}\right)+A_{44}\left(\phi_y+\frac{\partial w}{\partial y}\right)\right.$$

$$+A_{16}\left(\frac{\partial u}{\partial x}+\frac{1}{2}\left(\frac{\partial w}{\partial x}\right)^2\right)\frac{\partial w}{\partial x}+A_{26}\left(\frac{\partial v}{\partial y}+\frac{1}{2}\left(\frac{\partial w}{\partial y}\right)^2\right)\frac{\partial w}{\partial x}$$

$$+A_{66}\left(\frac{\partial u}{\partial y}+\frac{\partial v}{\partial x}+\frac{\partial w}{\partial x}\frac{\partial w}{\partial y}\right)\frac{\partial w}{\partial x}+A_{12}\left(\frac{\partial u}{\partial x}+\frac{1}{2}\left(\frac{\partial w}{\partial x}\right)^2\right)\frac{\partial w}{\partial y}$$

$$+A_{22}\left(\frac{\partial v}{\partial y}+\frac{1}{2}\left(\frac{\partial w}{\partial y}\right)^2\right)\frac{\partial w}{\partial y}+A_{26}\left(\frac{\partial u}{\partial y}+\frac{\partial v}{\partial x}+\frac{\partial w}{\partial x}\frac{\partial w}{\partial y}\right)\frac{\partial w}{\partial y}$$

$$+B_{16}\frac{\partial \phi_x}{\partial x}\frac{\partial w}{\partial x}+B_{26}\frac{\partial \phi_y}{\partial y}\frac{\partial w}{\partial x}+B_{66}\left(\frac{\partial \phi_x}{\partial y}+\frac{\partial \phi_y}{\partial x}\right)\frac{\partial w}{\partial x}+B_{12}\frac{\partial \phi_x}{\partial x}\frac{\partial w}{\partial y}$$

$$+B_{22}\frac{\partial \phi_y}{\partial y}\frac{\partial w}{\partial y}+B_{26}\left(\frac{\partial \phi_x}{\partial y}+\frac{\partial \phi_y}{\partial x}\right)\frac{\partial w}{\partial y}\Big]-g_3q_z\Big\}dxdy$$

$$-\int_{\Gamma^e} g_3\{(Q_1+N_1\frac{\partial w}{\partial x}+N_6\frac{\partial w}{\partial y})n_x+(Q_2+N_6\frac{\partial w}{\partial x}+N_2\frac{\partial w}{\partial y})n_y\}dS \qquad (c.12)$$

$$0=\int_{\Omega^e}\Big\{\frac{\partial g_4}{\partial x}\Big[B_{11}\left(\frac{\partial u}{\partial x}+\frac{1}{2}\left(\frac{\partial w}{\partial x}\right)^2\right)+B_{12}\left(\frac{\partial v}{\partial y}+\frac{1}{2}\left(\frac{\partial w}{\partial y}\right)^2\right)$$

$$+B_{16}\left(\frac{\partial u}{\partial y}+\frac{\partial v}{\partial x}+\frac{\partial w}{\partial x}\frac{\partial w}{\partial y}\right)+D_{11}\frac{\partial \phi_x}{\partial x}+D_{12}\frac{\partial \phi_y}{\partial y}+D_{16}\left(\frac{\partial \phi_x}{\partial y}+\frac{\partial \phi_y}{\partial x}\right)\Big]$$

$$+\frac{\partial g_4}{\partial y}\Big[B_{16}\left(\frac{\partial u}{\partial x}+\frac{1}{2}\left(\frac{\partial w}{\partial x}\right)^2\right)+B_{26}\left(\frac{\partial v}{\partial y}+\frac{1}{2}\left(\frac{\partial w}{\partial y}\right)^2\right)$$

$$+B_{66}\left(\frac{\partial u}{\partial y}+\frac{\partial v}{\partial x}+\frac{\partial w}{\partial x}\frac{\partial w}{\partial y}\right)+D_{16}\frac{\partial \phi_x}{\partial x}+D_{26}\frac{\partial \phi_y}{\partial y}$$

$$+D_{66}\left(\frac{\partial \phi_x}{\partial y}+\frac{\partial \phi_y}{\partial x}\right)\Big]+g_4\Big[A_{55}\left(\phi_x+\frac{\partial w}{\partial x}\right)+A_{45}\left(\phi_y+\frac{\partial w}{\partial y}\right)'\Big]\Big\}dxdy$$

$$-\int_{\Gamma^e}\{g_4(M_1n_x+M_6n_y)\}dS \qquad (c.13)$$

$$0=\int_{\Omega^e}\Big\{\frac{\partial g_5}{\partial x}\Big[B_{16}\left(\frac{\partial u}{\partial x}+\frac{1}{2}\left(\frac{\partial w}{\partial x}\right)^2\right)+B_{26}\left(\frac{\partial v}{\partial y}+\frac{1}{2}\left(\frac{\partial w}{\partial y}\right)^2\right)$$

$$+B_{66}\left(\frac{\partial u}{\partial y}+\frac{\partial v}{\partial x}+\frac{\partial w}{\partial x}\frac{\partial w}{\partial y}\right)+D_{16}\frac{\partial \phi_x}{\partial x}+D_{26}\frac{\partial \phi_y}{\partial y}+D_{66}\left(\frac{\partial \phi_x}{\partial y}+\frac{\partial \phi_y}{\partial x}\right)\Big]$$

$$+\frac{\partial g_5}{\partial y}\Big[B_{12}\left(\frac{\partial u}{\partial x}+\frac{1}{2}\left(\frac{\partial w}{\partial x}\right)^2\right)+B_{22}\left(\frac{\partial v}{\partial y}+\frac{1}{2}\left(\frac{\partial w}{\partial y}\right)^2\right)$$

$$+B_{26}\left(\frac{\partial u}{\partial y}+\frac{\partial v}{\partial x}+\frac{\partial w}{\partial x}\frac{\partial w}{\partial y}\right)+D_{12}\frac{\partial \phi_x}{\partial x}+D_{22}\frac{\partial \phi_y}{\partial y}$$

$$+D_{26}\left(\frac{\partial \phi_x}{\partial y}+\frac{\partial \phi_y}{\partial x}\right)\Big]+g_5\Big[A_{45}\left(\phi_x+\frac{\partial w}{\partial x}\right)+A_{44}\left(\phi_y+\frac{\partial w}{\partial y}\right)'\Big]\Big\}dxdy$$

$$- \int_{\Gamma^e} \{g_5(M_6 n_x + M_2 n_y)\} dS \qquad (c.14)$$

The above equations (c.10 through c.14) complete the variational formulation of the large deformation plate equations (Eqns. c.1-c.5).

Finite Element Formulation

In the finite element formulation, the primary degrees of freedom (u, v, w, ϕ_x, ϕ_y) are approximated in terms of nodal displacements and interpolation functions as following expressions :

$$\begin{aligned} u &\equiv \sum_{j=1}^{n} U_j \psi_j(x,y) \\ v &\equiv \sum_{j=1}^{n} V_j \psi_j(x,y) \\ w &\equiv \sum_{j=1}^{n} W_j \psi_j(x,y) \\ \phi_x &\equiv \sum_{j=1}^{n} \Phi_{xj} \psi_j(x,y) \\ \phi_y &\equiv \sum_{j=1}^{n} \Phi_{yj} \psi_j(x,y) \end{aligned} \qquad (c.15)$$

where U_j,..., Φ_{yj} denote the nodal values of the primary degrees of freedom and $\psi_j(x,y)$ and n are the interpolation functions and the number of nodes in a typical element, respectively.

Using the definitions (Eqn. c.15) and replacing the weighting functions $g_i (i = 1,..,5)$ by the interpolation functions ψ_j, the variational statements (Eqns. c.10 through c.14) can be rewritten in terms of the element stiffness matrix, nodal displacements, and force vector as

$$\sum_{j=1}^{n} K_{ij}^{11} U_j + \sum_{j=1}^{n} K_{ij}^{12} V_j + \sum_{j=1}^{n} K_{ij}^{14} \Phi_{xj} + \sum_{j=1}^{n} K_{ij}^{15} \Phi_{yj} - F_i^1 = 0 \qquad (c.16)$$

$$\sum_{j=1}^{n} K_{ij}^{21} U_j + \sum_{j=1}^{n} K_{ij}^{22} V_j + \sum_{j=1}^{n} K_{ij}^{24} \Phi_{xj} + \sum_{j=1}^{n} K_{ij}^{25} \Phi_{yj} - F_i^2 = 0 \qquad (c.17)$$

$$\sum_{j=1}^{n} K_{ij}^{31} U_j + \sum_{j=1}^{n} K_{ij}^{32} V_j + \sum_{j=1}^{n} K_{ij}^{33} W_j + \sum_{j=1}^{n} K_{ij}^{34} \Phi_{xj} + \sum_{j=1}^{n} K_{ij}^{35} \Phi_{yj} - F_i^3 = 0 \qquad (c.18)$$

$$\sum_{j=1}^{n} K_{ij}^{41} U_j + \sum_{j=1}^{n} K_{ij}^{42} V_j + \sum_{j=1}^{n} K_{ij}^{43} W_j + \sum_{j=1}^{n} K_{ij}^{44} \Phi_{xj} + \sum_{j=1}^{n} K_{ij}^{45} \Phi_{yj} - F_i^4 = 0 \qquad (c.19)$$

$$\sum_{j=1}^{n} K_{ij}^{51} U_j + \sum_{j=1}^{n} K_{ij}^{52} V_j + \sum_{j=1}^{n} K_{ij}^{53} W_j + \sum_{j=1}^{n} K_{ij}^{54} \Phi_{xj} + \sum_{j=1}^{n} K_{ij}^{55} \Phi_{yj} - F_i^5 = 0 \qquad (c.20)$$

where the stiffness matrices K_{ij}^{kl} and force vector F_i^k are presented at the end of Appendix-B.

Combining the system of equations (c.16)-(c.20) results in the following matrix equation for a typical element :

$$\begin{bmatrix} [K^{11}] & [K^{12}] & [K^{13}] & [K^{14}] & [K^{15}] \\ [K^{21}] & [K^{22}] & [K^{23}] & [K^{24}] & [K^{25}] \\ [K^{31}] & [K^{32}] & [K^{33}] & [K^{34}] & [K^{35}] \\ [K^{41}] & [K^{42}] & [K^{43}] & [K^{44}] & [K^{45}] \\ [K^{51}] & [K^{52}] & [K^{53}] & [K^{54}] & [K^{55}] \end{bmatrix} \begin{Bmatrix} \{U\} \\ \{V\} \\ \{W\} \\ \{\Phi_x\} \\ \{\Phi_y\} \end{Bmatrix} = \begin{Bmatrix} \{F^1\} \\ \{F^2\} \\ \{F^3\} \\ \{F^4\} \\ \{F^5\} \end{Bmatrix} \qquad (c.21)$$

or

$$[\, K(\Delta)\,]\{\,\Delta\,\} \;=\; \{\,F\,\} \qquad (c.22)$$

where $\{\Delta\} = \{\,\{U\},\{V\},\{W\},\{\Phi_x\},\{\Phi_y\}\,\}^T$.

The element stiffness matrix $[K(\Delta)]$ in the above expression contains geometrical nonlinear terms in addition to the usual linear terms. Thus, the solution of the nonlinear problem (c.22) is reached by an incremental and iterative procedure. In the computer program, the Newton-Rhapson iterative method [77] is used for the solution of the nonlinear equation (c.22).

Solution Procedure

In the Newton-Rhapson iteration technique, the basic equation is expressed in the form

$$\{\,R\,\} \equiv [\, K(\Delta)\,]\{\,\Delta\,\} - \{\,F\,\} \;=\; 0 \qquad (c.23)$$

where $\{R\}$ denotes residual vector.

Assuming that the solution is known at the r-th iteration, for any given load step, the residual vector $\{ R \}$ is expanded in Taylor's series about $\{ \Delta \}_r$:

$$0 = \{ R \}_r + [\frac{\partial \{R\}}{\partial \{\Delta\}}]_r (\{\Delta\}_{r+1} - \{\Delta\}_r) + \ldots\ldots \qquad (c.24)$$

If higher order terms are truncated, the above equation can be written as

$$\{ R \}_r + [K_T](\{\Delta\}_{r+1} - \{\Delta\}_r) = 0 \qquad (c.25)$$

where $[K_T]$ is the tangent stiffness matrix defined by

$$[K_T] = [\frac{\partial \{R\}}{\partial \{\Delta\}}]_r \qquad (c.26)$$

The residual at the r-th iteration can be obtained from (c.23) as

$$\{ R \}_r = [K] \{ \Delta \}_r - \{ F \} \qquad (c.27)$$

Substituting (c.27) into (c.26), the solution at the (r+1)th iteration can be obtained from the following equation

$$[K_T] \{ \Delta \}_{r+1} = ([K_T] - [K]) \{ \Delta \}_r + \{ F \} \qquad (c.28)$$

The iteration terminates if the following convergence criterion is satisfied

$$\{ \frac{\sum_{i=1}^{N} (\Delta_i^r - \Delta_i^{r+1})^2}{\sum_{i=1}^{N} (\Delta_i^r)^2} \}^{1/2} \leq \varepsilon_{Tol} \qquad (c.29)$$

where N is the total number of degrees of freedom and ε_{Tol} is the convergence tolerance.

Once the displacement is obtained, the stresses and strains are calculated for each layer at the Gauss points of each element.

Element Stiffness, Tangent Stiffness Matrix and Force Vector

The coefficients of element stiffness matrix K_{ij}^{rt} and force vector F_i^r are

$$K_{ij}^{11} = \int_{\Omega^e} \{ A_{11} \frac{\partial \psi_i}{\partial x} \frac{\partial \psi_j}{\partial x} + A_{16}(\frac{\partial \psi_i}{\partial x} \frac{\partial \psi_j}{\partial y} + \frac{\partial \psi_i}{\partial y} \frac{\partial \psi_j}{\partial x}) + A_{66} \frac{\partial \psi_i}{\partial y} \frac{\partial \psi_j}{\partial y} \} dxdy$$

$$K_{ij}^{12} = \int_{\Omega^e} \{ A_{16} \frac{\partial \psi_i}{\partial x} \frac{\partial \psi_j}{\partial x} + A_{12} \frac{\partial \psi_i}{\partial x} \frac{\partial \psi_j}{\partial y} + A_{66} \frac{\partial \psi_i}{\partial y} \frac{\partial \psi_j}{\partial x} + A_{26} \frac{\partial \psi_i}{\partial y} \frac{\partial \psi_j}{\partial y} \} dxdy$$

$$K_{ij}^{13} = \int_{\Omega^e} \frac{1}{2} \{ [A_{11} \frac{\partial \psi_i}{\partial x} \frac{\partial \psi_j}{\partial x} + A_{16} \frac{\partial \psi_i}{\partial x} \frac{\partial \psi_j}{\partial y} + A_{16} \frac{\partial \psi_i}{\partial y} \frac{\partial \psi_j}{\partial x} + A_{66} \frac{\partial \psi_i}{\partial y} \frac{\partial \psi_j}{\partial x}] \frac{\partial w}{\partial x} + [A_{16} \frac{\partial \psi_i}{\partial x} \frac{\partial \psi_j}{\partial x} + A_{12} \frac{\partial \psi_i}{\partial x} \frac{\partial \psi_j}{\partial y} + A_{66} \frac{\partial \psi_i}{\partial y} \frac{\partial \psi_j}{\partial x} + A_{26} \frac{\partial \psi_i}{\partial y} \frac{\partial \psi_j}{\partial y}] \frac{\partial w}{\partial y} \} dxdy$$

$$K_{ij}^{14} = \int_{\Omega^e} \{ B_{11} \frac{\partial \psi_i}{\partial x} \frac{\partial \psi_j}{\partial x} + B_{16}(\frac{\partial \psi_i}{\partial x} \frac{\partial \psi_j}{\partial y} + \frac{\partial \psi_i}{\partial y} \frac{\partial \psi_j}{\partial x}) + B_{66} \frac{\partial \psi_i}{\partial y} \frac{\partial \psi_j}{\partial y} \} dxdy$$

$$K_{ij}^{15} = \int_{\Omega^e} \{ B_{16} \frac{\partial \psi_i}{\partial x} \frac{\partial \psi_j}{\partial x} + B_{12} \frac{\partial \psi_i}{\partial x} \frac{\partial \psi_j}{\partial y} + B_{66} \frac{\partial \psi_i}{\partial y} \frac{\partial \psi_j}{\partial x} + B_{26} \frac{\partial \psi_i}{\partial y} \frac{\partial \psi_j}{\partial y} \} dxdy$$

$$F_i^1 = \int_{\Gamma^e} \{ \psi_i (N_1 n_x + N_6 n_y) \} dS$$

$$K_{ij}^{21} = K_{ji}^{12}$$

$$K_{ij}^{22} = \int_{\Omega^e} \{ A_{66} \frac{\partial \psi_i}{\partial x} \frac{\partial \psi_j}{\partial x} + A_{26}(\frac{\partial \psi_i}{\partial x} \frac{\partial \psi_j}{\partial y} + \frac{\partial \psi_i}{\partial y} \frac{\partial \psi_j}{\partial x}) + A_{66} \frac{\partial \psi_i}{\partial y} \frac{\partial \psi_j}{\partial y} \} dxdy$$

$$K_{ij}^{23} = \int_{\Omega^e} \frac{1}{2} \{ [A_{16} \frac{\partial \psi_i}{\partial x} \frac{\partial \psi_j}{\partial x} + A_{66} \frac{\partial \psi_i}{\partial x} \frac{\partial \psi_j}{\partial y} + A_{12} \frac{\partial \psi_i}{\partial y} \frac{\partial \psi_j}{\partial x} + A_{26} \frac{\partial \psi_i}{\partial y} \frac{\partial \psi_j}{\partial x}] \frac{\partial w}{\partial x}$$
$$+ [A_{66} \frac{\partial \psi_i}{\partial x} \frac{\partial \psi_j}{\partial x} + A_{26}(\frac{\partial \psi_i}{\partial x} \frac{\partial \psi_j}{\partial y} + \frac{\partial \psi_i}{\partial y} \frac{\partial \psi_j}{\partial x}) + A_{22} \frac{\partial \psi_i}{\partial y} \frac{\partial \psi_j}{\partial y}] \frac{\partial w}{\partial y} \} dxdy$$

$$K_{ij}^{24} = \int_{\Omega^e} \{ B_{16} \frac{\partial \psi_i}{\partial x} \frac{\partial \psi_j}{\partial x} + B_{66} \frac{\partial \psi_i}{\partial x} \frac{\partial \psi_j}{\partial y} + B_{12} \frac{\partial \psi_i}{\partial y} \frac{\partial \psi_j}{\partial x} + B_{26} \frac{\partial \psi_i}{\partial y} \frac{\partial \psi_j}{\partial y} \} dxdy$$

$$K_{ij}^{25} = \int_{\Omega^e} \{ B_{66} \frac{\partial \psi_i}{\partial x} \frac{\partial \psi_j}{\partial x} + B_{26}(\frac{\partial \psi_i}{\partial x} \frac{\partial \psi_j}{\partial y} + \frac{\partial \psi_i}{\partial y} \frac{\partial \psi_j}{\partial x}) + B_{22} \frac{\partial \psi_i}{\partial y} \frac{\partial \psi_j}{\partial y} \} dxdy$$

$$F_i^2 = \int_{\Gamma^e} \{ \psi_i (N_6 n_x + N_2 n_y) \} dS$$

$$K_{ij}^{31} = \int_{\Omega^e} \{ [A_{11} \frac{\partial \psi_i}{\partial x} \frac{\partial \psi_j}{\partial x} + A_{16}(\frac{\partial \psi_i}{\partial x} \frac{\partial \psi_j}{\partial y} + \frac{\partial \psi_i}{\partial y} \frac{\partial \psi_j}{\partial x}) + A_{66} \frac{\partial \psi_i}{\partial y} \frac{\partial \psi_j}{\partial y}] \frac{\partial w}{\partial x}$$
$$+ [A_{16} \frac{\partial \psi_i}{\partial x} \frac{\partial \psi_j}{\partial x} + A_{66} \frac{\partial \psi_i}{\partial x} \frac{\partial \psi_j}{\partial y} + A_{12} \frac{\partial \psi_i}{\partial y} \frac{\partial \psi_j}{\partial x} + A_{26} \frac{\partial \psi_i}{\partial y} \frac{\partial \psi_j}{\partial y}] \frac{\partial w}{\partial y} \} dxdy$$

$$K_{ij}^{32} = \int_{\Omega^e} \{ [A_{16} \frac{\partial \psi_i}{\partial x} \frac{\partial \psi_j}{\partial x} + A_{12} \frac{\partial \psi_i}{\partial x} \frac{\partial \psi_j}{\partial y} + A_{66} \frac{\partial \psi_i}{\partial y} \frac{\partial \psi_j}{\partial x} + A_{26} \frac{\partial \psi_i}{\partial y} \frac{\partial \psi_j}{\partial y}] \frac{\partial w}{\partial x}$$
$$+ [A_{66} \frac{\partial \psi_i}{\partial x} \frac{\partial \psi_j}{\partial x} + A_{26}(\frac{\partial \psi_i}{\partial x} \frac{\partial \psi_j}{\partial y} + \frac{\partial \psi_i}{\partial y} \frac{\partial \psi_j}{\partial x}) + A_{22} \frac{\partial \psi_i}{\partial y} \frac{\partial \psi_j}{\partial y}] \frac{\partial w}{\partial y} \} dxdy$$

$$K_{ij}^{33} = \int_{\Omega^e} \{ A_{55} \frac{\partial \psi_i}{\partial x} \frac{\partial \psi_j}{\partial x} + A_{45}(\frac{\partial \psi_i}{\partial x} \frac{\partial \psi_j}{\partial y} + \frac{\partial \psi_i}{\partial y} \frac{\partial \psi_j}{\partial x}) + A_{44} \frac{\partial \psi_i}{\partial y} \frac{\partial \psi_j}{\partial y}$$
$$+ \frac{1}{2} [(A_{11} \frac{\partial \psi_i}{\partial x} \frac{\partial \psi_j}{\partial x} + A_{16}(\frac{\partial \psi_i}{\partial x} \frac{\partial \psi_j}{\partial y} + \frac{\partial \psi_i}{\partial y} \frac{\partial \psi_j}{\partial x}) + A_{66} \frac{\partial \psi_i}{\partial y} \frac{\partial \psi_j}{\partial y}) \frac{\partial^2 w}{\partial x^2}$$
$$+ (2A_{16} \frac{\partial \psi_i}{\partial x} \frac{\partial \psi_j}{\partial x} + (A_{12} + A_{66})(\frac{\partial \psi_i}{\partial x} \frac{\partial \psi_j}{\partial y} + \frac{\partial \psi_i}{\partial y} \frac{\partial \psi_j}{\partial x})$$
$$+ 2A_{26} \frac{\partial \psi_i}{\partial y} \frac{\partial \psi_j}{\partial y}) \frac{\partial w}{\partial x} \frac{\partial w}{\partial y} + (A_{66} \frac{\partial \psi_i}{\partial x} \frac{\partial \psi_j}{\partial x} + A_{26}(\frac{\partial \psi_i}{\partial x} \frac{\partial \psi_j}{\partial y} + \frac{\partial \psi_i}{\partial y} \frac{\partial \psi_j}{\partial x})$$

$$+ A_{22}\frac{\partial\psi_i}{\partial y}\frac{\partial\psi_j}{\partial y})\frac{\partial^2 w}{\partial y^2}]\}dxdy$$

$$K_{ij}^{34} = \int_{\Omega^e}\{A_{55}\frac{\partial\psi_i}{\partial x}\psi_j + A_{45}\frac{\partial\psi_i}{\partial y}\psi_j + [B_{11}\frac{\partial\psi_i}{\partial x}\frac{\partial\psi_j}{\partial x} + B_{16}(\frac{\partial\psi_i}{\partial x}\frac{\partial\psi_j}{\partial y} + \frac{\partial\psi_i}{\partial y}\frac{\partial\psi_j}{\partial x})$$
$$+ B_{66}\frac{\partial\psi_i}{\partial y}\frac{\partial\psi_j}{\partial y}]\frac{\partial w}{\partial x} + [B_{16}\frac{\partial\psi_i}{\partial x}\frac{\partial\psi_j}{\partial x} + B_{66}\frac{\partial\psi_i}{\partial x}\frac{\partial\psi_j}{\partial y} + B_{12}\frac{\partial\psi_i}{\partial y}\frac{\partial\psi_j}{\partial x}$$
$$+ B_{26}\frac{\partial\psi_i}{\partial y}\frac{\partial\psi_j}{\partial y}]\frac{\partial w}{\partial y}\}dxdy$$

$$K_{ij}^{35} = \int_{\Omega^e}\{A_{45}\frac{\partial\psi_i}{\partial x}\psi_j + A_{44}\frac{\partial\psi_i}{\partial y}\psi_j + [B_{16}\frac{\partial\psi_i}{\partial x}\frac{\partial\psi_j}{\partial x} + B_{12}\frac{\partial\psi_i}{\partial x}\frac{\partial\psi_j}{\partial y} + B_{66}\frac{\partial\psi_i}{\partial y}\frac{\partial\psi_j}{\partial x}$$
$$+ B_{26}\frac{\partial\psi_i}{\partial y}\frac{\partial\psi_j}{\partial y}]\frac{\partial w}{\partial x} + [B_{66}\frac{\partial\psi_i}{\partial x}\frac{\partial\psi_j}{\partial x} + B_{26}(\frac{\partial\psi_i}{\partial x}\frac{\partial\psi_j}{\partial y} + \frac{\partial\psi_i}{\partial y}\frac{\partial\psi_j}{\partial x})$$
$$+ B_{22}\frac{\partial\psi_i}{\partial y}\frac{\partial\psi_j}{\partial y}]\frac{\partial w}{\partial y}\}dxdy$$

$$F_i^3 = \int_{\Omega^e}\psi_i q_z dxdy - \int_{\Gamma^e}\psi_i\{(Q_1 + N_1\frac{\partial w}{\partial x} + N_6\frac{\partial w}{\partial y})n_x + (Q_2 + N_6\frac{\partial w}{\partial x} + N_2\frac{\partial w}{\partial y})n_y\}dS$$

$$K_{ij}^{41} = K_{ji}^{14} \qquad , \qquad K_{ij}^{42} = K_{ji}^{24}$$

$$K_{ij}^{43} = \int_{\Omega^e}\{A_{55}\psi_i\frac{\partial\psi_j}{\partial x} + A_{45}\psi_i\frac{\partial\psi_j}{\partial y} + \frac{1}{2}[B_{11}\frac{\partial\psi_i}{\partial x}\frac{\partial\psi_j}{\partial x} + B_{16}(\frac{\partial\psi_i}{\partial x}\frac{\partial\psi_j}{\partial y} + \frac{\partial\psi_i}{\partial y}\frac{\partial\psi_j}{\partial x})$$
$$+ B_{66}\frac{\partial\psi_i}{\partial y}\frac{\partial\psi_j}{\partial y}]\frac{\partial w}{\partial x} + \frac{1}{2}[B_{16}\frac{\partial\psi_i}{\partial x}\frac{\partial\psi_j}{\partial x} + B_{12}\frac{\partial\psi_i}{\partial x}\frac{\partial\psi_j}{\partial y} + B_{66}\frac{\partial\psi_i}{\partial y}\frac{\partial\psi_j}{\partial x}$$
$$+ B_{26}\frac{\partial\psi_i}{\partial y}\frac{\partial\psi_j}{\partial y}]\frac{\partial w}{\partial y}\}dxdy$$

$$K_{ij}^{44} = \int_{\Omega^e}\{A_{55}\psi_i\psi_j + D_{11}\frac{\partial\psi_i}{\partial x}\frac{\partial\psi_j}{\partial x} + D_{16}(\frac{\partial\psi_i}{\partial x}\frac{\partial\psi_j}{\partial y} + \frac{\partial\psi_i}{\partial y}\frac{\partial\psi_j}{\partial x}) + D_{66}\frac{\partial\psi_i}{\partial y}\frac{\partial\psi_j}{\partial y}\}dxdy$$

$$K_{ij}^{45} = \int_{\Omega^e}\{A_{45}\psi_i\psi_j + D_{16}\frac{\partial\psi_i}{\partial x}\frac{\partial\psi_j}{\partial x} + D_{12}\frac{\partial\psi_i}{\partial x}\frac{\partial\psi_j}{\partial y} + D_{66}\frac{\partial\psi_i}{\partial y}\frac{\partial\psi_j}{\partial x} + D_{26}\frac{\partial\psi_i}{\partial y}\frac{\partial\psi_j}{\partial y}\}dxdy$$

$$F_i^4 = \int_{\Gamma^e} \{\psi_i(M_1 n_x + M_6 n_y)\} dS$$

$$K_{ij}^{51} = K_{ji}^{15} \quad , \quad K_{ij}^{52} = K_{ji}^{25}$$

$$K_{ij}^{53} = \int_{\Omega^e} \{ A_{45}\psi_i \frac{\partial \psi_j}{\partial x} + A_{44}\psi_i \frac{\partial \psi_j}{\partial y} + \frac{1}{2}[B_{16} \frac{\partial \psi_i}{\partial x}\frac{\partial \psi_j}{\partial x} + B_{66}\frac{\partial \psi_i}{\partial x}\frac{\partial \psi_j}{\partial y} + B_{12}\frac{\partial \psi_i}{\partial y}\frac{\partial \psi_j}{\partial x}$$
$$+ B_{26}\frac{\partial \psi_i}{\partial y}\frac{\partial \psi_j}{\partial y}]\frac{\partial w}{\partial x} + \frac{1}{2}[B_{66}\frac{\partial \psi_i}{\partial x}\frac{\partial \psi_j}{\partial x} + B_{26}(\frac{\partial \psi_i}{\partial x}\frac{\partial \psi_j}{\partial y} + \frac{\partial \psi_i}{\partial y}\frac{\partial \psi_j}{\partial x})$$
$$+ B_{22}\frac{\partial \psi_i}{\partial y}\frac{\partial \psi_j}{\partial y}]\frac{\partial w}{\partial y} \} dxdy$$

$$K_{ij}^{54} = K_{ji}^{45}$$

$$K_{ij}^{55} = \int_{\Omega^e} \{ A_{44}\psi_i\psi_j + D_{66}\frac{\partial \psi_i}{\partial x}\frac{\partial \psi_j}{\partial x} + D_{26}(\frac{\partial \psi_i}{\partial x}\frac{\partial \psi_j}{\partial y} + \frac{\partial \psi_i}{\partial y}\frac{\partial \psi_j}{\partial x}) + D_{22}\frac{\partial \psi_i}{\partial y}\frac{\partial \psi_j}{\partial y} \} dxdy$$

$$F_i^5 = \int_{\Gamma^e} \{\psi_i(M_6 n_x + M_2 n_y)\} dS$$

The coefficients of the tangent stiffness matrix $[K_T]$ are

$$K_{ij}^{11}{}_T = K_{ij}^{11} \quad , \quad K_{ij}^{12}{}_T = K_{ij}^{12} \quad , \quad K_{ij}^{13}{}_T = 2K_{ij}^{13} \quad , \quad K_{ij}^{14}{}_T = K_{ij}^{14} \quad , \quad K_{ij}^{15}{}_T = K_{ij}^{15}$$

$$K_{ij}^{21}{}_T = K_{ij}^{21} \quad , \quad K_{ij}^{22}{}_T = K_{ij}^{22} \quad , \quad K_{ij}^{23}{}_T = 2K_{ij}^{23} \quad , \quad K_{ij}^{24}{}_T = K_{ij}^{24} \quad , \quad K_{ij}^{25}{}_T = K_{ij}^{25}$$

$$K_{ij}^{31}{}_T = K_{ij}^{31} \quad , \quad K_{ij}^{32}{}_T = K_{ij}^{32} \quad , \quad K_{ij}^{34}{}_T = K_{ij}^{34} \quad , \quad K_{ij}^{35}{}_T = K_{ij}^{35}$$

$$K_{ij}^{33}{}_T = \int_{\Omega^e} \{ \frac{\partial \psi_i}{\partial x}\frac{\partial \psi_j}{\partial x}[A_{11}\frac{\partial u}{\partial x} + A_{16}\frac{\partial u}{\partial y} + A_{16}\frac{\partial v}{\partial x} + A_{12}\frac{\partial v}{\partial y} + \frac{3}{2}A_{11}(\frac{\partial w}{\partial x})^2$$
$$+ A_{16}\frac{\partial w}{\partial x}\frac{\partial w}{\partial y} + (\frac{A_{12}}{2} + A_{66})(\frac{\partial w}{\partial y})^2 + A_{55} + B_{11}\frac{\partial \phi_x}{\partial x} + B_{16}\frac{\partial \phi_x}{\partial y} + B_{16}\frac{\partial \phi_y}{\partial x}$$

$$+B_{12}\frac{\partial\phi_y}{\partial y}\Big]+\Big(\frac{\partial\psi_i}{\partial x}\frac{\partial\psi_j}{\partial y}+\frac{\partial\psi_i}{\partial y}\frac{\partial\psi_j}{\partial x}\Big)\Big[A_{16}\frac{\partial u}{\partial x}+A_{66}\frac{\partial u}{\partial y}+A_{66}\frac{\partial v}{\partial x}$$

$$+A_{26}\frac{\partial v}{\partial y}+\frac{3}{2}A_{16}\Big(\frac{\partial w}{\partial x}\Big)^2+(A_{12}+2A_{66})\frac{\partial w}{\partial x}\frac{\partial w}{\partial y}+\frac{3}{2}A_{26}\Big(\frac{\partial w}{\partial y}\Big)^2+A_{45}+B_{16}\frac{\partial\phi_x}{\partial x}$$

$$+B_{66}\frac{\partial\phi_x}{\partial y}+B_{66}\frac{\partial\phi_y}{\partial x}+B_{26}\frac{\partial\phi_y}{\partial y}\Big]+\frac{\partial\psi_i}{\partial y}\frac{\partial\psi_j}{\partial y}\Big[A_{12}\frac{\partial u}{\partial x}+A_{26}\frac{\partial u}{\partial y}$$

$$+A_{26}\frac{\partial v}{\partial x}+A_{22}\frac{\partial v}{\partial y}+\Big(\frac{A_{12}}{2}+A_{66}\Big)\Big(\frac{\partial w}{\partial x}\Big)^2+A_{26}\frac{\partial w}{\partial x}\frac{\partial w}{\partial y}+\frac{3}{2}A_{22}\Big(\frac{\partial w}{\partial y}\Big)^2$$

$$+A_{44}+B_{12}\frac{\partial\phi_x}{\partial x}+B_{26}\frac{\partial\phi_x}{\partial y}+B_{26}\frac{\partial\phi_y}{\partial x}+B_{22}\frac{\partial\phi_y}{\partial y}\Big]\Big\}dxdy$$

$$K_{ij}^{41}{}_T=K_{ij}^{41}\quad,\quad K_{ij}^{42}{}_T=K_{ij}^{42}\quad,\quad K_{ij}^{43}{}_T=2K_{ij}^{43}\quad,\quad K_{ij}^{44}{}_T=K_{ij}^{44}\quad,\quad K_{ij}^{45}{}_T=K_{ij}^{45}$$

$$K_{ij}^{51}{}_T=K_{ij}^{51}\quad,\quad K_{ij}^{52}{}_T=K_{ij}^{52}\quad,\quad K_{ij}^{53}{}_T=2K_{ij}^{53}\quad,\quad K_{ij}^{54}{}_T=K_{ij}^{54}\quad,\quad K_{ij}^{55}{}_T=K_{ij}^{55}$$

APPENDIX - D

The total potential energy of the expression (3.2) is

$$\Pi = \frac{ab}{2A^*_{11}}\left[\frac{\Delta_x}{a} - \frac{\pi^2}{8a^2}(W_{11}^2 + 4W_{21}^2)\right]^2 + \frac{\pi^4 ab}{8}\left[\frac{D_{11}}{a^4}(W_{11}^2 + 16W_{21}^2)\right. \qquad (d.1)$$

$$+ \frac{2(D_{12} + 2D_{66})}{a^2b^2}(W_{11}^2 + 4W_{21}^2) + \frac{D_{22}}{b^4}(W_{11}^2 + W_{21}^2) + \frac{16A^*_{11}}{b^4}(2b_{02}^2 + b_{12}^2 + b_{32}^2)$$

$$\left. + \frac{4(2A^*_{12} + A^*_{66})}{a^2b^2}(b_{12}^2 + 9b_{32}^2) + \frac{A^*_{22}}{a^4}(2b_{10}^2 + 32b_{20}^2 + 162b_{30}^2 + 512b_{40}^2 + b_{12}^2 + 81b_{32}^2)\right]$$

where

$$b_{10} = -\frac{a^2}{4b^2A^*_{22}} W_{11}W_{21}$$

$$b_{20} = \frac{a^2}{32b^2A^*_{22}} W_{11}^2$$

$$b_{30} = \frac{a^2}{36b^2A^*_{22}} W_{11}W_{21}$$

$$b_{40} = \frac{a^2}{128b^2A^*_{22}} W_{21}^2$$

$$b_{02} = \frac{b^2}{32a^2A^*_{11}}(W_{11}^2 + 4W_{21}^2)$$

$$B_{12} = \frac{9W_{11}W_{21}}{4\left[\frac{b^2}{a^2}A^*_{22} + 4(2A^*_{12} + A^*_{66}) + \frac{16a^2}{b^2}A^*_{11}\right]}$$

$$b_{32} = -\frac{W_{11}W_{21}}{4\left[81\frac{b^2}{a^2}A^*_{22} + 36(2A^*_{12} + A^*_{66}) + \frac{16a^2}{b^2}A^*_{11}\right]}$$

APPENDIX - E

A symmetric laminate of thickness t has a stacking sequence as shown in Fig. (32) such that the combined thickness of (i)-th and ($i+1$)-st layers is fixed as a constant while the individual thicknesses of (i)-th and ($i+1$)-st layers can vary by keeping z_i in the range of $z_{i+1} \leq z_i \leq z_{i-1}$. For a certain plate aspect ratio or fiber direction of (i)-th and ($i+1$)-st layers, it can be shown that the buckling load of the laminate is independent of the relative thicknesses of (i)-th and ($i+1$)-st layers. In Section 2.7, the buckling load of a laminate with freely shifting y-normal edges is found to be

$$\hat{N}_{xcr} = \pi^2 a^2 \left[k^2 \frac{D_{11}}{a^4} + \frac{2(D_{12} + 2D_{66})}{a^2 b^2} + \frac{1}{k^2} \frac{D_{22}}{b^4} \right] \qquad (e.1)$$

where k is the number of half waves in the loading direction corresponding to the critical mode.

In the above expression, the bending stiffnesses $D_{ij}(i,j = 1,2,6)$ can be expressed in terms of five material invariants and integrals that depend on the plate stacking sequence [47] as

$$\begin{aligned} D_{11} &= \frac{U_1 t^3}{12} + U_2 V_1 + U_3 V_3 \\ D_{22} &= \frac{U_1 t^3}{12} - U_2 V_1 + U_3 V_3 \\ D_{12} &= \frac{U_4 t^3}{12} - U_3 V_3 \\ D_{66} &= \frac{U_5 t^3}{12} - U_3 V_3 \end{aligned} \qquad (e.2)$$

where V_1 and V_3 are given as

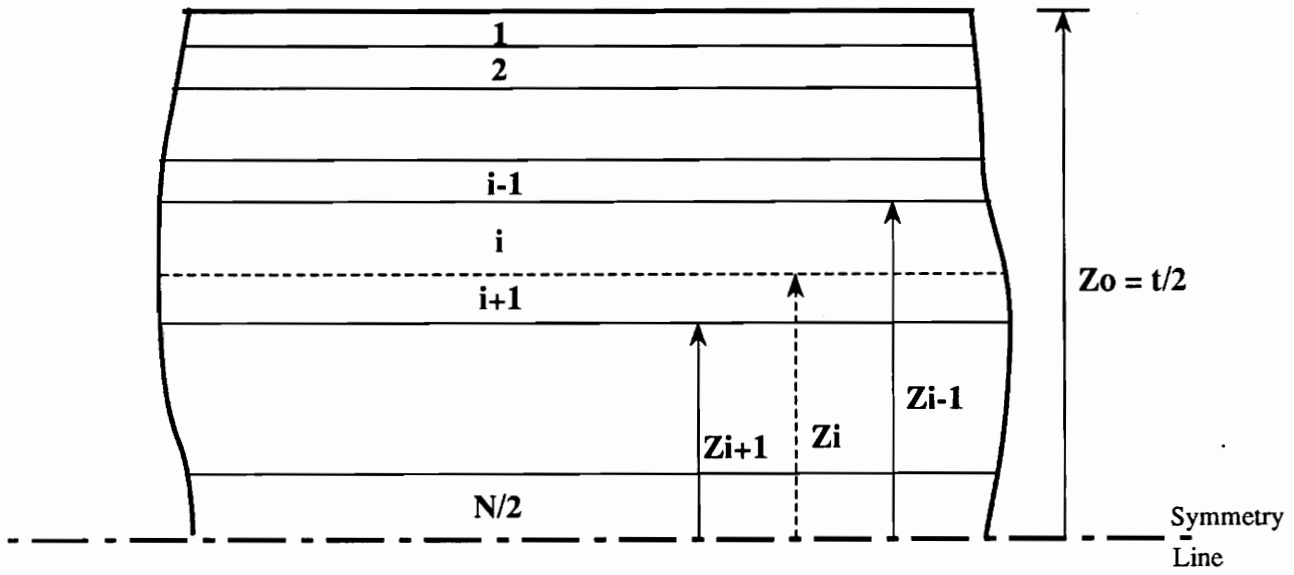

Fig. 32 Symmetric laminate stacking sequence

$$V_1 = \int_{-t/2}^{t/2} z^2 \cos 2\theta dz = \frac{2}{3} \sum_{k=1}^{N/2} \cos 2\theta_k (z_k^3 - z_{k-1}^3) \qquad (e.3)$$

$$V_3 = \int_{-t/2}^{t/2} z^2 \cos 4\theta dz = \frac{2}{3} \sum_{k=1}^{N/2} \cos 4\theta_k (z_k^3 - z_{k-1}^3)$$

and the material invariants are

$$U_1 = \frac{1}{8}(3Q_{11} + 3Q_{22} + 2Q_{12} + 4Q_{66})$$

$$U_2 = \frac{1}{2}(Q_{11} - Q_{22})$$

$$U_3 = \frac{1}{8}(Q_{11} + Q_{22} - 2Q_{12} - 4Q_{66}) \qquad (e.4)$$

$$U_4 = \frac{1}{8}(Q_{11} + Q_{22} + 6Q_{12} - 4Q_{66})$$

$$U_5 = \frac{1}{8}(Q_{11} + Q_{22} - 2Q_{12} + 4Q_{66})$$

If the laminate has a stacking sequence as shown in Fig. (32), the expression (e.3) can be written as

$$V_1 = \alpha + \frac{2}{3} \cos 2\theta_i (z_i^3 - z_{i-1}^3) + \frac{2}{3} \cos 2\theta_{i+1} (z_{i+1}^3 - z_i^3) \qquad (e.5)$$

$$V_3 = \beta + \frac{2}{3} \cos 4\theta_i (z_i^3 - z_{i-1}^3) + \frac{2}{3} \cos 4\theta_{i+1} (z_{i+1}^3 - z_i^3)$$

where the constants α and β are independent of z_i as given below

$$\alpha = \frac{2}{3} \sum_{k=1}^{N/2} \cos 2\theta_k (z_k^3 - z_{k-1}^3) \quad , \quad \beta = \frac{2}{3} \sum_{k=1}^{N/2} \cos 4\theta_k (z_k^3 - z_{k-1}^3) \quad , \quad (k \neq i \text{ and } k \neq i+1)$$

If $\theta_i = 0°$ and $\theta_{i+1} = 90°$, the bending stiffnesses D_{ij} can be expressed by substituting the above expression into (e.2) as

$$D_{11} = \frac{U_1 t^3}{12} + U_2[\alpha + \frac{2}{3}(-z_{i+1}^3 + 2z_i^3 - z_{i-1}^3)] + U_3[\beta + \frac{2}{3}(z_{i+1}^3 - z_{i-1}^3)]$$

$$D_{22} = \frac{U_1 t^3}{12} - U_2[\alpha + \frac{2}{3}(-z_{i+1}^3 + 2z_i^3 - z_{i-1}^3)] + U_3[\beta + \frac{2}{3}(z_{i+1}^3 - z_{i-1}^3)] \quad (e.6)$$

$$D_{12} = \frac{U_4 t^3}{12} - U_3[\beta + \frac{2}{3}(z_{i+1}^3 - z_{i-1}^3)]$$

$$D_{66} = \frac{U_5 t^3}{12} - U_3[\beta + \frac{2}{3}(z_{i+1}^3 - z_{i-1}^3)]$$

Then, the buckling load parameter in the expression (e.1) can be written as

$$\hat{N}_{xcr} = \pi^2 a^2 [\gamma + \frac{2}{3} U_2 (\frac{k^2}{a^4} - \frac{1}{k^2 b^4})(-z_{i+1}^3 + 2z_i^3 - z_{i-1}^3)] \quad (e.7)$$

where γ is an independent function of the thicknesses of the 0° and 90° layers as given in the following

$$\gamma = [\frac{k^2}{a^4} U_1 + 2\frac{(U_4 + 2U_5}{a^2 b^2} + \frac{U_1}{k^2 b^2}]\frac{t^3}{12} + (\frac{k^2}{a^4} - \frac{1}{k^2 b^4})\alpha U_2$$
$$+ (\frac{k^2}{a^4} - \frac{6}{a^2 b^2} + \frac{1}{k^2 b^4})[\beta + \frac{2}{3}(z_{i+1}^3 - z_{i-1}^3)]$$

The buckling load in the expression (e.7) is completely independent of the thicknesses of the 0° and 90° layers if the following condition is satisfied,

$$\frac{a}{b} = k \quad (e.8)$$

The condition (e.8) implies that if a plate aspect ratio is equal to the number of half waves in the loading direction corresponding to the critical mode, the 0° and 90° layers can be regarded to be one design variable. A square plate which buckles into a single half sine wave, for instance, clearly satisfies the above condition, and therefore, the thicknesses of the 0° and 90° layers can be treated as one design variable.

Furthermore, if $\theta_i = \theta^*$ and $\theta_{i+1} = -\theta^*$, the bending stiffnesses (e.2) can be expressed as

$$D_{11} = \frac{U_1 t^3}{12} + U_2[\alpha + \frac{2}{3}\cos 2\theta^*(z_{i+1}^3 - z_{i-1}^3)] + U_3[\beta + \frac{2}{3}\cos 4\theta^*(z_{i+1}^3 - z_{i-1}^3)]$$

$$D_{22} = \frac{U_1 t^3}{12} - U_2[\alpha + \frac{2}{3}\cos 2\theta^*(z_{i+1}^3 - z_{i-1}^3)] + U_3[\beta + \frac{2}{3}\cos 4\theta^*(z_{i+1}^3 - z_{i-1}^3)] \quad (e.9)$$

$$D_{12} = \frac{U_4 t^3}{12} - U_3[\beta + \frac{2}{3}\cos 4\theta^*(z_{i+1}^3 - z_{i-1}^3)]$$

$$D_{66} = \frac{U_5 t^3}{12} - U_3[\beta + \frac{2}{3}\cos 4\theta^*(z_{i+1}^3 - z_{i-1}^3)]$$

It can be readily seen from the above expression that the buckling load (e.1) is independent of z_i. Thus, the thicknesses of the θ_i and θ_{i+1} layers can be also treated as one design variable regardless of a plate aspect ratio.

Vita

The author was born to Kyung Cheol Shin and Pum Ok Lee on December 22, 1961 in Kwangju, Korea. After receiving his education in Kwangju, he entered Seoul National University, Seoul, Korea and received his B.S. and M.S. degrees in civil engineering in 1983 and 1985, respectively. After fulfilling his military duty, he was married to Eunjean Jahng in August 1986. Since being admitted in September 1986 by Virginia Polytechnic Institute and State University, Blacksburg, Virginia, he has been working towards the degree of Doctor of Philosophy in Engineering Mechanics. He is on leave to work as a composite structural engineer in Daejeon, Korea. The author has a three-year-old son, Manseop.